

Metal-Semiconductor Contacts for Schottky Diode Fabrication

by

Mark D. Barlow

Submitted in Partial Fulfillment of the Requirements

for the Degree of

Master of Science in Engineering

in the

Electrical and Computer Engineering

Program

YOUNGSTOWN STATE UNIVERSITY

December 2007

Metal-Semiconductor Contacts for Schottky Diode Fabrication

Mark D. Barlow

I hereby release this thesis to the public. I understand that this thesis will be made available from the OhioLINK ETD Center and the Maag library Circulation Desk for public access. I also authorize the University or other individuals to make copies of this thesis as needed for scholarly research.

Signature:

Mark D. Barlow, Student

Date

Approvals:

Dr. Frank X. Li, Thesis Advisor

Date

Dr. Tom N. Oder, Committee Member

Date

Dr. Salvatore Pansino, Committee Member

Date

Dr. Philip C. Munro, Committee Member

Date

Peter J. Kasvinsky, Dean of School of Graduate Studies & Research

Date

ABSTRACT

This research demonstrates several methods to produce high voltage Schottky contact diodes. How contact construction and process temperatures affect turn-on voltage Schottky barrier height, on-resistance, and reverse breakdown voltage are studied. The performance of varied contact terminal construction types and temperature processes used to fabricate Schottky diodes were evaluated. The diodes are constructed of nickel metal mechanical (pressure) contacts and plasma sputter deposited nickel metal contacts on silicon carbide (SiC). Current-voltage characterizations were used to study the differences in performance verses geometric construction types, sputter deposition temperature, and annealing temperatures. The configurations studied were needle points, spheres, and planar metal-semiconductor contacts varying in interface areas that ranged from 0.58×10^{-4} to 6.2×10^{-4} cm². Planar Schottky contacts 500 μ m in diameter sputter deposited at 27°C and 600°C are exposed to a range of temperatures in ultra pure nitrogen atmosphere. These Schottky contacts were studied to gain insight into mechanical contacts, plasma sputter deposited contacts, and temperature processes.

Viva Ad Infinitum

Donald Mark Barlow: Naval Radioman and Locomotive Engineer

TABLE OF CONTENTS

ABSTRACT	iii
DEDICATION	iv
TABLE OF CONTENTS	v
LIST OF FIGURES	vii
LIST OF SYMBOLS	x
CHAPTER ONE	1
INTRODUCTION	1
1.1 THEORY AND OPERATION OF SCHOTTKY DIODES	2
1.2 SURVEY OF SCHOTTKY DIODES STRUCTURES	9
CHAPTER TWO	12
SCHOTTKY DIODE RESEARCH	12
2.1 HIGH VOLTAGE CONTACT TERMINAL EVALUATION AND TESTING	13
2.2 CORONA CURRENT VERSES CONTACT TERMINAL GEOMETRY	17
2.3 FINITE ELEMENT ELECTRIC FIELD ANALYSIS	19
2.4 SIMILAR DEVELOPMENTS IN SCHOTTKY CONTACT TERMINALS	22
CHAPTER THREE	24
SCHOTTKY CONTACT DIODE FABRICATION	24
3.1 FABRICATION: PREPARING SiC SUBSTRATE AND OHMIC CONTACTS.....	25
3.2 FABRICATION: MECHANICAL SCHOTTKY CONTACTS	27
3.3 FABRICATION: PLANAR PLASMA SPUTTER DEPOSIT CONTACTS.....	28
3.4 INSPECTION & MODELING OF THE SCHOTTKY CONTACT TERMINALS	31
CHAPTER FOUR	40
EFFECTS OF VARIED DIODE CONTACT GEOMETRIES	40
4.1 TESTING METHODS FOR I-V CHARACTERIZATION	43
4.2 VARIED CONTACT GEOMETRIES FORWARD BIAS MEASUREMENTS.....	44
4.3 ANALYSIS OF VARIED CONTACT GEOMETRIES IN FORWARD BIAS	46
4.4 MEASUREMENT AND ANALYSIS OF THE CONTACTS IN REVERSE BIAS.....	48

CHAPTER FIVE.....	52
EFFECTS OF TEMPERATURE PROCESSES	52
5.1 FORWARD BIAS I-V MEASUREMENTS ACROSS TEMPERATURES	53
5.2 ANALYSIS OF TEMPERATURE EFFECTS IN FORWARD BIAS	57
5.3 REVERSE BIAS I-V MEASUREMENT FOR TEMPERATURE PROCESSES	59
CHAPTER SIX.....	62
CONCLUSION.....	62
6.1 CONCLUSIONS ON VARIED FABRICATION TEMPERATURE PROCESSES	63
6.2 CONCLUSIONS ON VARIED CONTACT TERMINAL GEOMETRY.....	66
6.3 RECOMMENDATIONS FOR FURTHER STUDIES	67
REFERENCES	68
APPENDIX	70
APPENDED CHAPTER FOUR ANALYSIS	70
1. NEEDLE POINT CONTACT	70
2. SMALL SPHERE CONTACT (0.82MM DIA.)	72
3. LARGE SPHERE CONTACT (1.71MM DIA.)	74
4. PLANAR CONTACT (0.125MM DIA.)	76
5. LARGE PLANAR CONTACT (0.5MM DIA.)	78
APPENDED CHAPTER FIVE ANALYSIS	80
1. NO ANNEALING	80
2. 200°C ANNEAL	82
3. 300°C ANNEAL	83
4. 400°C ANNEAL	84
5. 500°C ANNEAL	85
6. 600°C ANNEAL	87

LIST OF FIGURES

Figure 1	Nickel coated spherical (1.71mm dia.) mechanical (pressure) contact.	1
Figure 2	Nickel planar contact plasma sputter deposited (500 μ m dia.).	1
Figure 3	Metal and semiconductor before contact; Schottky barrier height.	3
Figure 4	Metal and semiconductor in contact; built-in potential.	3
Figure 5	Mirrored electric dipole potentials of the contact depletion region.	4
Figure 6	Band diagram showing the forward bias current through the diode.	6
Figure 7	Band diagram showing the reverse bias diode with built-in potential.	6
Figure 8	Ni on SiC Schottky diode Ar implantation; and I-V curve sketch.	9
Figure 9	Schottky contact with and without oxide layer edge guard.	10
Figure 10	Diodes with different guard ring configurations for improved V_{RB} .	11
Figure 11	Difference found between discharge terminals of varied geometry.	13
Figure 12	A spherical discharge terminal is shown suspended above a plane.	14
Figure 13	Setup used to induce corona discharge around a metal electrode.	15
Figure 14	Test rig for corona onset with test electrode beneath water plate.	15
Figure 15	Effective contact diameter (ECD) and corona discharge terminals.	16
Figure 16	Corona currents for various high voltage terminal geometries tested.	18
Figure 17	Corona currents for planar terminals increase with contact periphery.	18
Figure 18	Electnet simulation of planar corona discharge terminal.	20
Figure 19	Electnet simulation of sphere (16 mm dia.) corona terminal.	21
Figure 20	Large Sphere (50mm dia.) simulation with corona photo.	21
Figure 21	Spherical contact on diamond substrate characterization.	22
Figure 22	Oxide ramp field plate termination on SiC with Ni Schottky contact.	23
Figure 23	Diode contacts to be tested and diagram of the SiC substrate.	24
Figure 24	5x5mm samples and sputter diagram of ohmic metal contact.	26
Figure 25	Rapid thermal processor, temperature profile, & HF acid preparation.	26
Figure 26	Plasma arc process and electro-erode/plate process.	27
Figure 27	Spherical contacts in various stages of construction.	28
Figure 28	Spin coater, hot plate, mask aligner, and dot pattern after developer.	29
Figure 29	Plasma sputter deposit process with chamber and sputter targets.	29

Figure 30	High temperature plasma sputter deposit process with shadow mask.	30
Figure 31	Youngstown State University laboratories and personnel.	31
Figure 32	SEM & optical microscope photos of the needle point contact.	32
Figure 33	SEM & optical microscope photos of the small spherical contact.	32
Figure 34	SEM & optical microscope photos of the large spherical contact.	32
Figure 35	SEM & optical microscope photos of 125 μ m planar contact.	33
Figure 36	Optical microscope photos 27 $^{\circ}$ C deposit planar contact.	33
Figure 37	Optical microscope photos 600 $^{\circ}$ C deposit planar contact.	33
Figure 38	Contact radius R_a , calculated Radius R_h , and the error margin.	35
Figure 39	SEM analysis of mechanical Schottky contacts.	36
Figure 40	Elecnet simulation of electric field surrounding 1.71mm dia. contact.	38
Figure 41	Elecnet simulation of electric field surrounding 0.82mm dia. contact.	38
Figure 42	Elecnet simulation of electric field surrounding needle point contact.	39
Figure 43	Simulation of electric field surrounding planar 0.5mm dia. contact.	39
Figure 44	I-V curves zoomed to nano amps scale to show turn-on voltage.	42
Figure 45	I-V curves zoomed to micro amps scale to show resistance.	42
Figure 46	Test rig for the mechanical contacts and the Keithley curve tracer.	43
Figure 47	Planar contacts on copper substrate with test probe.	43
Figure 48	I-V measurements of diode for various construction geometries.	45
Figure 49	Ideality and SBH for varied contact terminal constructions.	47
Figure 50	Contact resistance for the varied contact terminal constructions.	47
Figure 51	Reverse bias breakdown with the Keithley/Labview curve tracer.	49
Figure 52	Tektronix 576 I-V curve tracer attached to the probe station.	49
Figure 53	Tektronix 576 I-V curve tracer attached to the custom diode test rig.	49
Figure 54	Breakdown needle point, small sphere (left) and large sphere (right).	50
Figure 55	Summary of the mechanical contact reverse breakdown data.	50
Figure 56	Breakdown 0.125mm (left) and 0.5mm planar contacts (right).	51
Figure 57	Summary of the planar and large sphere contact reverse breakdown.	51
Figure 58	Thermal profile set for the Rapid Thermal Processor (RTP).	52
Figure 59	27 $^{\circ}$ C deposited nickel contact and 600 $^{\circ}$ C deposited nickel contacts.	53
Figure 60	I-V data no annealing for samples YSU111 and YSU112.	53

Figure 61	I-V data for 200°C, 300°C and 400°C for samples YSU111 and YSU112.	54
Figure 62	Discolored 27°C and 600°C deposit contact respectively after 500°C.	55
Figure 63	Data for 27°C and 600°C deposited contacts respectively post 500°C.	55
Figure 64	Color change of 27°C and 600°C unaffected contacts post 600°C.	56
Figure 65	I-V data for the 27°C and 600°C deposited contacts post 600°C.	56
Figure 66	Resistance vs anneal temperature for 27°C & 600°C deposit contacts.	57
Figure 67	SBH and ideality vs anneal temperature for 27°C deposit contacts.	58
Figure 68	SBH and ideality vs anneal temperature for 600°C deposit contacts.	58
Figure 69	Breakdown 27°C and 600°C deposited contacts -325V and -200V.	59
Figure 70	Breakdown voltage for 27°C and 600°C contacts no annealing.	59
Figure 71	Breakdown voltages planar 27°C and 600°C contacts -325V.	60
Figure 72	Breakdown voltages for 27°C and 600°C contacts post 300°C.	60
Figure 73	Oscillographs 27°C contact -600V breakdown, 600°C contact -325V.	61
Figure 74	Breakdown voltages for 27°C and 600°C contacts post 600°C.	61
Figure 75	Initial measurements and anticipated changes due to thermal process.	63
Figure 76	Initial measurements and actual changes due to thermal process.	63
Figure 77	Changes in resistance of the samples over the annealing process.	64
Figure 78	Changes in SBH and reverse breakdown voltage with annealing.	65
Figure 79	Simulation with a questionable volume of depletion region.	66
Figure 80	Untested design concept for spherical metal–semiconductor contacts.	67
Table 1	Summery of 27°C vs. 600°C sputter deposit contacts vs. anneal temp.	64
Table 2	Summery of data collected on Schottky contact diode terminal types.	66

LIST OF SYMBOLS

E_G	Energy of the band gap (eV)
E_f	Energy of the Fermi level (eV)
E_c	Energy level of the conduction band in (eV)
E_{fi}	Energy of the Fermi level for an intrinsic semiconductor (eV)
E_v	Energy level of the valence band (eV)
V_{BI}	Built-in voltage potential (eV)
Φ_B	Schottky barrier height (eV)
Φ_m	Work function of the material (eV)
Φ_s	Work function of the semiconductor (eV)
χ	Electron affinity (eV)
k	Boltzmann's constant ($m^2 \text{ kg s}^{-2} \text{ K}^{-1}$)
T	Temperature (Kelvin)
N_a	Acceptor doping concentration (holes/cm ³)
N_d	Donor doping concentration (electrons/cm ³)
n_i	Intrinsic carrier concentration of the semiconductor (charge/cm ³)
q	Charge of the electron (Coulombs)
ϵ_o	Free space permittivity (F/m)
ϵ	Combine permittivity of the material (F/m)
I_f	Forward current through the diode (Amps)
I_o	Initial current of the diode (Amps)
I_r	Reverse current through the diode (mille Amps)
A	Area of metal semiconductor interface (cm ²)
A^*	Richardson's constant ($A \text{ m}^{-2} \text{ K}^{-2}$)
n	Ideality factor (Dimensionless)
ϵ_m	Permittivity of the material (F/m)
W	Width of the semiconductor layer (cm)

W_{idth}	Width of the depletion region (μm)
R_s	Series on resistance of the diode (Ohms)
R_{on}	Series resistance inherent to the semiconductor (Ohms)
ΔV	Change in voltage (Volts)
ΔI	Change in current (Amps)
V_{RB}	Reverse breakdown voltage (Volts)
E_c	Critical breakdown voltage of the material (V/m)
V_a	Applied voltage (Volts)
Q	Charge (Coulombs)
σ	Charge density (C/m^3)
d	Electrode separation distance (m)
R	Radius of curvature for an electrode terminal (m)
ECD	Effective contact diameter (mm)
E_Δ	Electric field gradient (V/m)
V_c	Corona voltage (Volts)
I_c	Corona current (Amps)
kV	Kilo Volts
E^*	Young's Modulus (Pascal)
ν	Poisons Ratio (Dimensionless)
F	Force (Newton)
R_h	Mechanical Contact radius (μm)
A_c	Area of mechanical Contact (cm^2)

CHAPTER ONE

INTRODUCTION

This work presents the development performed on several innovative methods to manufacture Schottky diodes on SiC. These methods feature several mechanical contacts including a spherical metal contact terminal (Figure 1) implemented to reduce electric field stress at edge terminations, and planar metal contacts (Figure 2) deposited at 27°C and 600°C with varied temperature processes. I-V characteristics of these diodes will be recorded and the performance of these devices will be evaluated.

Background information on the operation of Schottky diodes, technical problems, and fabrication techniques that address those problems will be provided. The analysis of electric field stress around high voltage terminals and Schottky contact terminals will be evaluated. Details of fabrication, testing methods, and modeling of working diode devices will then be presented. Finally the results will be reviewed and conclusions will be made concerning the contact terminal data and work that may be preformed in the future.

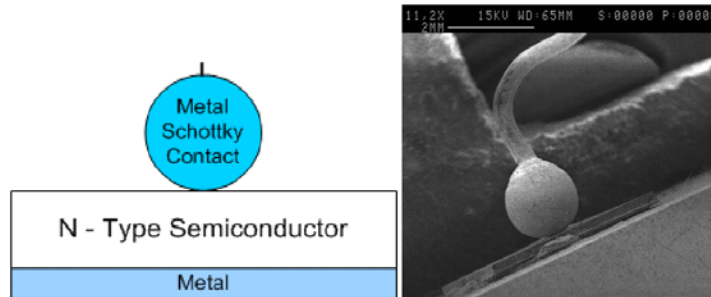


Figure 1: Nickel coated spherical (1.71mm dia.) mechanical (pressure) contact

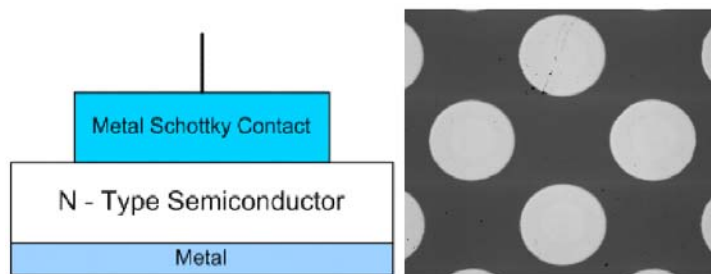


Figure 2: Nickel planar contact plasma sputter deposited (500µm dia.)

1.1 Theory and Operation of Schottky Diodes

The point contact diode is one of the earliest solid state semiconductor devices constructed. This type of diode is made when metal makes contact with a semiconductor surface. The point contact diode was later studied by Walter H. Schottky circa 1938 who formulated a theory as to why the diode worked; subsequently this device was named the Schottky diode to honor his contributions. Due to the fabrication simplicity of this device, the Schottky diode makes an excellent choice for testing experimental processes in semiconductor manufacturing.

The semiconductor material for this study will be 4H-silicon carbide with n-type doping. The nickel metal that composes the other half of this device (a conductor) always has an abundance of free electron charge carriers. The metal also has a work function Φ_m the energy it takes to remove an electron from the atom to the vacuum level potential. The attributes of both metal and semiconductor while separated are illustrated in Figure 3. The potential energy needed to inject charge carriers from the metal into the semiconductor material is the Schottky barrier height measured in electron volts (eV). The Schottky barrier height value is the energy it takes to remove an electron from the metal minus the energy required to detach an electron from the n-type semiconductor material (electron affinity) creating electron flow from the semiconductor to the metal. The Schottky barrier height may be computed for a Schottky diode by the following equation 1.1. The electron affinity for silicon carbide is 4.17 eV while the work function for the metal can vary if inter-metallic compounds are formed at the Schottky diode junction [3].

$$\Phi_B = \Phi_m - \chi \quad (1.1)$$

The Schottky barrier height (often referred to as SBH) is a fixed amount of energy drop across the diode, this value is unique to the combination of metal and semiconductor, ideally this does not vary with forward voltage biasing or current flow. However the phenomenon of SBH lowering may occur in reverse bias due to electric field crowding [4].

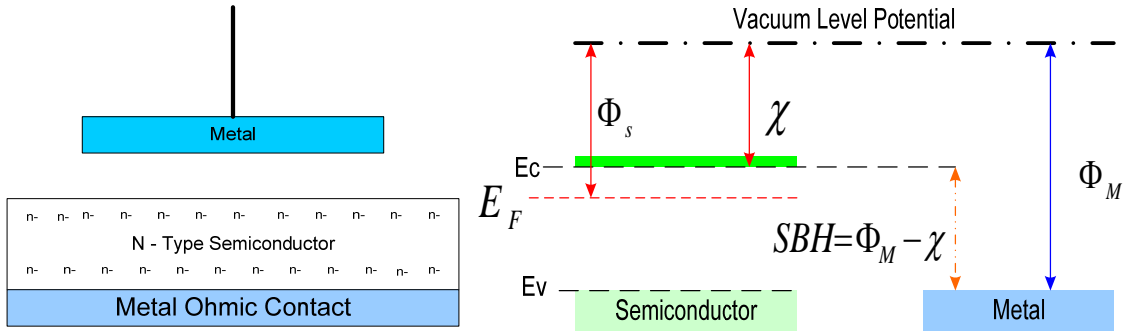


Figure 3: Metal and semiconductor before contact; band diagram Schottky barrier height.

When the metal contacts the semiconductor there is an imbalance of Fermi energy states in the two materials and the charges migrate to reach equilibrium levels. To simplify this matter, some of the electrons in the n-type semiconductor migrate into the metal leaving behind a region of material with no free charge carriers. This area is called the depletion region, and the energy it takes to cross this region is known as the built-in potential. This concept is illustrated in Figure 4.

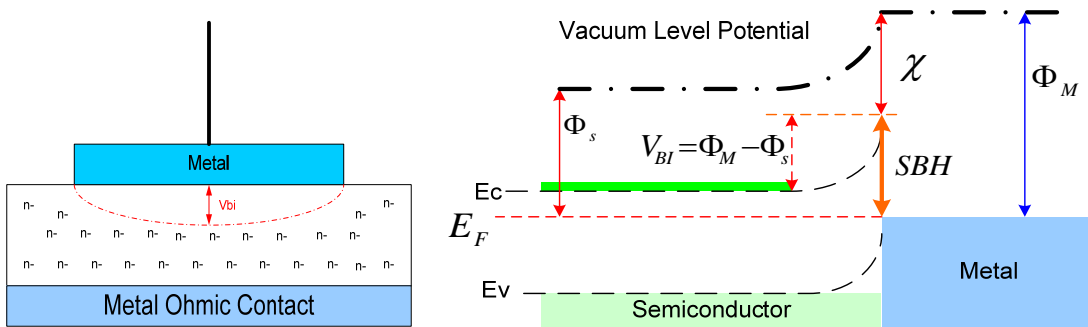


Figure 4: Metal and semiconductor in contact; band diagram of built-in potential.

The built-in potential V_{BI} also referred to as equilibrium contact potential (occurring when the Fermi levels have reached a balance) is the mechanism that prevents any further charge movement from the semiconductor conduction band to the metal. This built-in potential V_{BI} is the difference in the work function of the metal and the work function of the semiconductor.

$$V_{BI} = \Phi_m - \Phi_s \quad (1.2)$$

The built-in potential V_{BI} , the applied voltage, and the doping concentration play a large role in the width of the depletion region. This depletion region is absent of charge carriers in the semiconductor essentially behaving as a layer of insulation. The width of this depletion region is related to both the built-in potential and doping concentration. Where V_a is the applied biasing voltage with N_a and N_d being the acceptor/donor carrier concentrations, it is theorized that electrons (donors) in the n-material migrate into the metal and have a mirrored electric positive (acceptor) potential in the semiconductor opposite the depletion region. So that $N_a = N_d$ and the equation of 1.3 for pn junctions may be used to model the Schottky diode [5].

$$W_{idth} = \sqrt{\frac{2\epsilon \cdot (V_{BI} - V_a)}{q} \left(\frac{N_a + N_d}{N_a \cdot N_d} \right)} \quad (1.3)$$

The below illustration of Figure 5 helps to show why the doping concentration N_a may be considered equal to N_d because of the mirrored electric field in the metal [4]. This depletion width can be manipulated by applying voltage across the device which will allow for passage of or resistance to the flow of electricity. When a forward biasing voltage V_a is applied to the Schottky diode the work function of the semiconductor material Φ_s is reduced and thus the built-in potential is lowered as well.

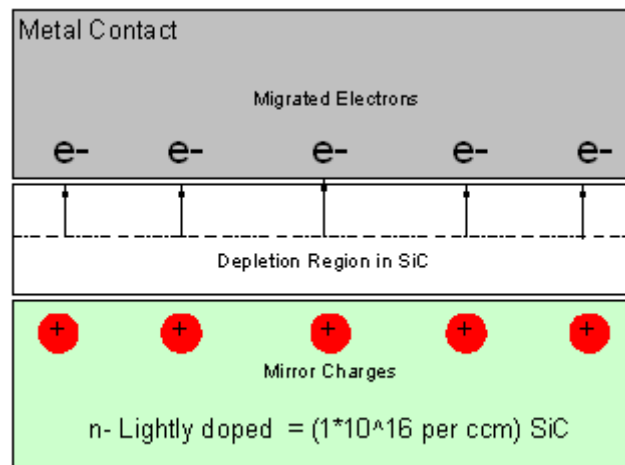


Figure 5: Mirrored electric dipole potentials of the Schottky contact depletion region.

The exponential current through the diode can be modeled by equation 1.4 below. The forward current I_F through the diode depends exponentially on the applied voltage V_a . The initial current I_o forms in the depletion region with both with currents both equal and opposite in equilibrium conditions, thus it can be factored out [5].

$$I_F = I_o \left(e^{\frac{qV_a}{kT}} - 1 \right) \quad (1.4)$$

Figure 6 shows an illustration of the conducting diode and the accompanying energy band diagram. During forward bias with the depletion region is reduced and the electrons migrate over the Schottky barrier and move from the n-type semiconductor material into the metal contact. From the energy band diagram the Fermi level of the semiconductor is raised by the value of the applied voltage. It should be noted that the metal at the bottom of the semiconductor has been prepared to be ohmic having a linear current voltage relationship and posses a very low value of resistance that does not play a role in the ideal analysis of the Schottky diode current [4].

During the reverse bias mode of the Schottky contact the applied voltage reinforces the built-in potential and creates a wider depletion region within the material. Because of the large negative value the applied voltage the forward current term tends to zero leaving just the reverse initial current that no longer has an opposing forward bias equilibrium current.

$$I_R = -I_o \quad (1.5)$$

The initial current I_o of the device under thermal equilibrium can be approximated by knowing the SBH of the diode given equation 1.1 along with the charge of the electron and the thermal voltage [5].

$$I_o \propto e^{\frac{-q\Phi_B}{kT}} \quad (1.6)$$

During reverse bias with the depletion region widens and the only electrons that migrate over the Schottky barrier, those that existed in thermal equilibrium of the initial current I_o . Figure 7 shows a reverse bias diode illustration and the band diagram of the Fermi level of the semiconductor lowered by the value of the applied voltage.

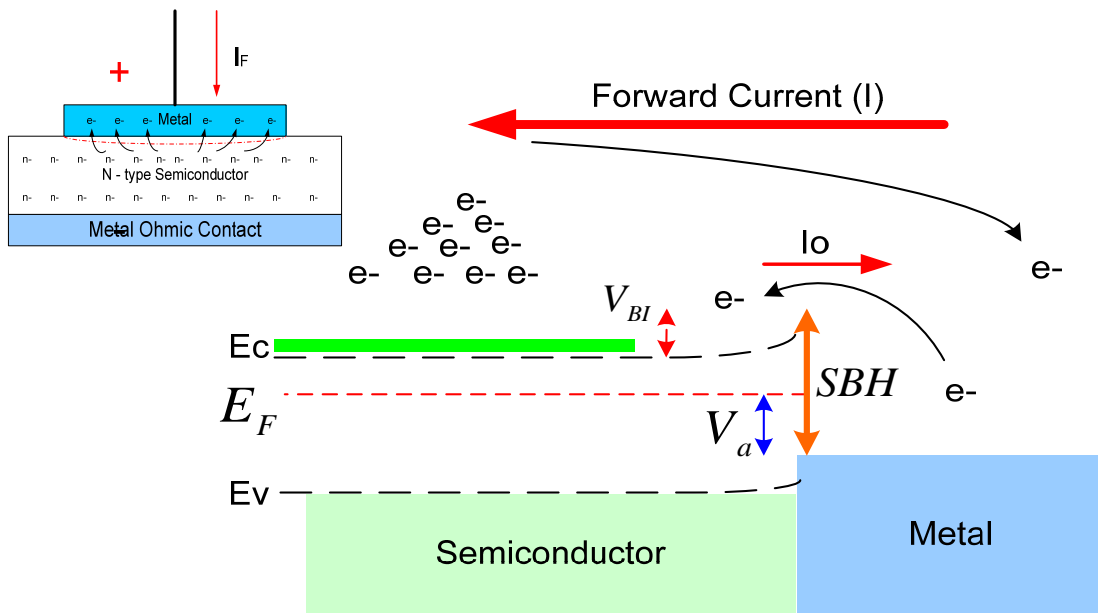


Figure 6: Schottky diode with energy band diagram showing the forward flow of electrical current through the diode.

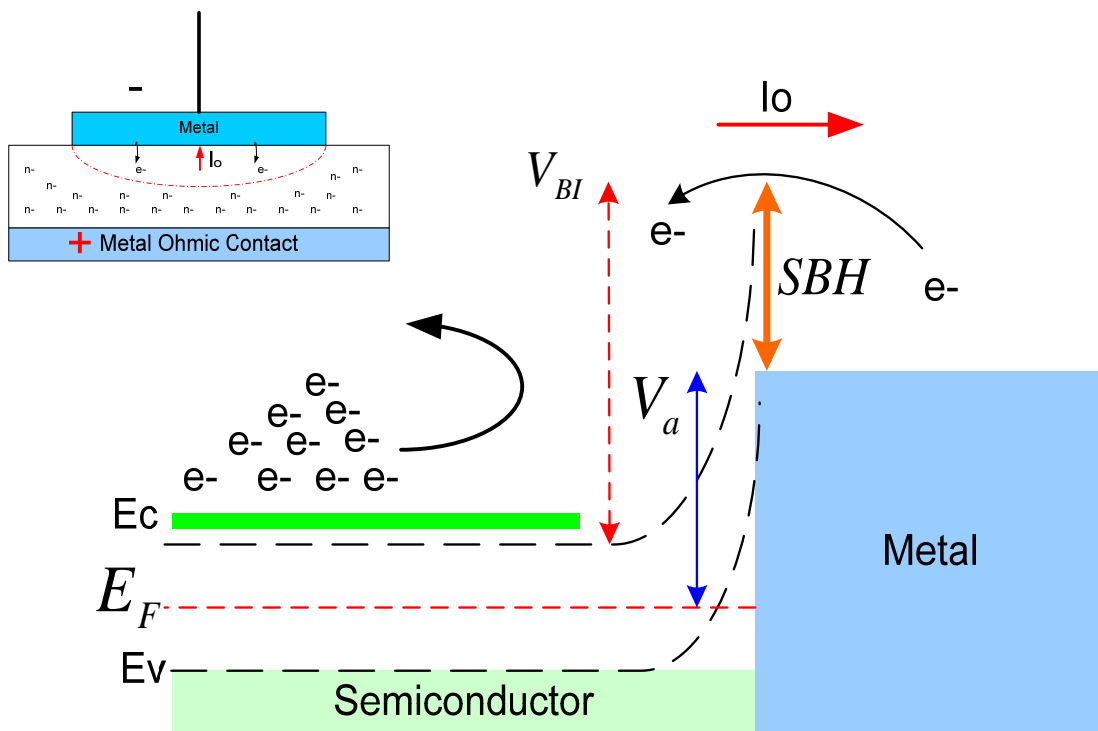


Figure 7: Schottky diode with energy band diagram showing the reverse bias V_a applied to the diode that increases the built-in potential.

Aspects that affect the magnitude of current through the ideal Schottky diode are the area (A) of the metal contacting the semiconductor, the temperature (T) of the material, and the Richardson's constant (A^*) for the material which is a relation of current density and temperature. With these values known for the material a more accurate and comprehensive formula for the Schottky diode contact current may be expressed by equation 1.7. This equation also accommodates deviation from ideal diode performance by a factor of n. This value is known as the ideality factor and for the ideal diode this value should be nearly equal to 1.

$$I_F = A \cdot A^* \cdot T^2 e^{\frac{-q\Phi_B}{kT}} \left(e^{\frac{qV_a}{nkT}} - 1 \right) \quad (1.7)$$

Now that a more accurate expression to describe the Schottky diode has been composed it is now necessary to discuss some of the aspects of the non ideal diode Schottky diode.

Various aspects of the material and fabrication will cause considerable deviation from the diode performance predicted by equation 1.7. Some of the ways in which variation from the ideal diode characteristics can occur are offset potentials and linearization due to resistance. While in the reverse direction carrier generation can cause a steadily increase current greater than that of I_o and conduction of electrical current in reverse bias will occur due to Zener and avalanche breakdown [5].

Current linearization due to ohmic resistance could be the cause of a poor quality ohmic contact or a poor quality Schottky contact interface. Both of these will contribute to a high series resistance within the diode. When large currents and voltages are applied to the diode the otherwise exponential I-V curve will become linear. At this point the linear part of the I-V curve may be evaluated with the help of equation 1.8 and the value for the total series resistance of the diode may be calculated by finding the change in voltage over the change in current [5].

$$R_s = \frac{\Delta V}{\Delta I} \quad (1.8)$$

In the reverse bias operation of a Schottky diode there are several mechanisms that create current flow through when the diode should be in a high resistance mode due the applied reverse polarity. Carrier generation in a neutral transition region occurs due to thermal activity and the nature of the semiconductor in regard to what carrier generation - recombination centers may be in the material. A significant aspect of the diode is the reverse breakdown voltage that occurs when the diode in the reverse bias mode begins to conduct electrical current exponentially. There are generally two mechanisms that contribute to reverse bias breakdown. These phenomenons are known as avalanche multiplication and quantum mechanical tunneling. Neither of these two breakdown methods will destroy the diode, however heating of the diode could occur due to the high currents due to voltage breakdown which could result in permanent device failure [8]. Avalanche breakdown is created by impact ionization occurring when a large electrical potential is applied across the device and high energy electrons cross the barrier and trigger other electron hole pairs to form. Zener breakdown is attributed to a mechanism known as quantum mechanical tunneling which effectively allows the charge to penetrate the barrier of forbidden region. The applied reverse voltage at which these mechanisms of breakdown will occur can be estimated by the following equation of 1.9 that relates the breakdown electric field for the material E_c with the doping concentration N_d [1].

$$V_{RB} \approx \frac{\epsilon_o \epsilon_m (E_c)^2}{2qN_d} \quad (1.9)$$

The best way to reduce currents resulting from the preceding phenomenon is to reduce the field intensity across the device. One of the most influential aspects to electric field intensity surrounding a Schottky contact is the physical shape of the metal in contact with the semiconductor forming the diode junction. Many techniques for design and construction of Schottky diode contacts implement varied contact geometries so that reverse breakdown voltages may be increased.

1.2 Survey of Schottky Diodes Structures

Many techniques have been tested in trying to improve Schottky contact diode characteristics. Based on layered nature of the photolithographic process most Schottky contacts are of a planar design. One of the problems encountered while utilizing planar contact geometries is the effects that occur at edge terminations. A common technique to prevent electric field stress at edge terminals is buffering the edges of the metal contact with insulator. Research conducted by Ravi Chilukuri and B.J. Baliga at North Carolina State University implemented the usage of low energy Argon (Ar) implantation into the 4H SiC epilayer for planar edge termination[9]. An illustration of the design for the Schottky diode is shown in Figure 8. The Argon ion implantations can be seen to the left and right of the Schottky diode contact.

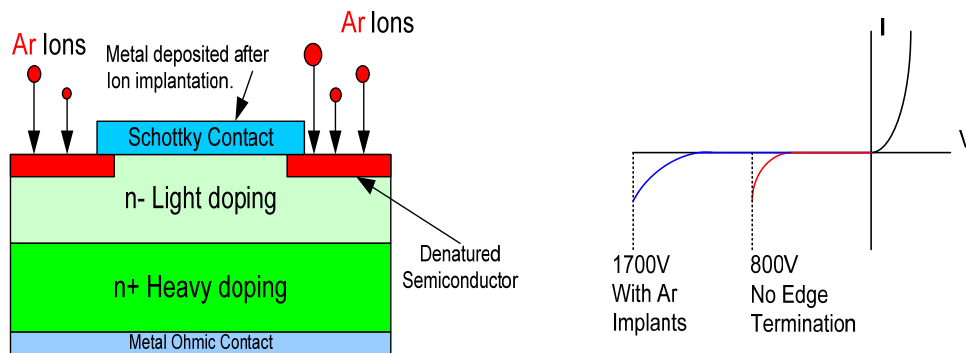


Figure 8: Nickel on SiC Schottky contact diode and I-V curve sketch of the performance difference obtainable by adding argon implantation edge termination to the diode design.

The diodes without edge termination were found to have a leakage current proportional to the diode diameter indicating a dominance of perimeter leakage where barrier height lowering occurred due to electric field crowding at the edge terminal. The Schottky diodes constructed with the use of low energy argon implantation for planar edge termination were found to result in breakdown voltages above 1 kV. This technique created a thin highly resistive layer at the edges of the planar metal contact where the doses of argon ions were implanted.

The quality of a Schottky contact and successful edge termination is measured by how closely the device can approach its theoretical breakdown voltage. The method discussed previously is a technique of buffering the edges with a highly resistive layer of denatured semiconductor. Another technique is to deposit a field plate insulator (typically a layer of oxide) over the semiconductor so that a Schottky contacts edge terminal may be protected by the field plate. This way fringing effects at the edge terminals are directed through the insulator field plate and not the semiconductor.

Research conducted by M.C. Tarplee, V.P. Madangalri, Q. Zhang, and T. Sudarshan developed design rules for optimizing field plate thickness and metal contact overlap [10]. The computer simulation performed by the group also showed that breakdown occurred directly underneath the corner of the unguarded Schottky contact. Electric field stress computer simulations allowed the team to make predictions as to what ratio of field plate thickness to metal contact overlap would be optimal. Figure 9 contrasts the diodes to show the benefit of oxide field plate termination. The concepts discussed in “Design Rules for Field Plate Edge Termination in SiC Schottky Diodes” provide a 4 step design process that may be used to optimize the oxide layer thickness and field plate overlap (X_o) when fabricating Schottky diodes [10].

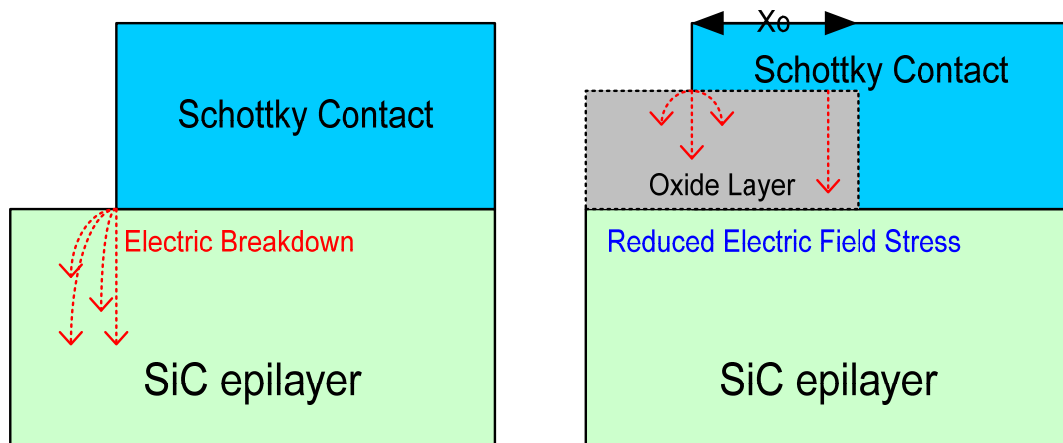


Figure 9: Schottky contact with and without oxide layer edge guard.

Another common technique to prevent electric field stress at edge terminations is guard rings. The importance of electric field distribution around a geometric design plays a major role in the development of ring guard terminations also referred to as field limiting rings FLR. Research performed by Seong-Jin Kim at Woosuk University studied the improvement of high voltage reverse breakdown characteristics of Schottky barrier diodes with ring guard terminations [7]. In this study no ring guard protection, a single guard ring protector, and multiple guarding protectors made from Aluminum (Al) were deposited by using electron beam deposition and thermal treatment upon the SiC substrate. The aluminum oxidized and formed Al silicide at the deposited locations becoming an insulator. The research based the dimensions for the FLR design on a two dimensional numerical device simulation using the SILVACO ATLAS simulator. The findings confirmed that the breakdown voltage characteristics were greatly dependant on the FLR width and spacing. When I-V curve analysis was performed on the device it was shown that the absence of ring guards had no effect on the forward conduction current. However the reverse leakage currents where greatly affected by the ring guard edge termination structure. Figure 10 illustrates the concept of ring guard termination similar to those discussed. Multiple ring guards could achieve breakdowns higher than -1.2kV

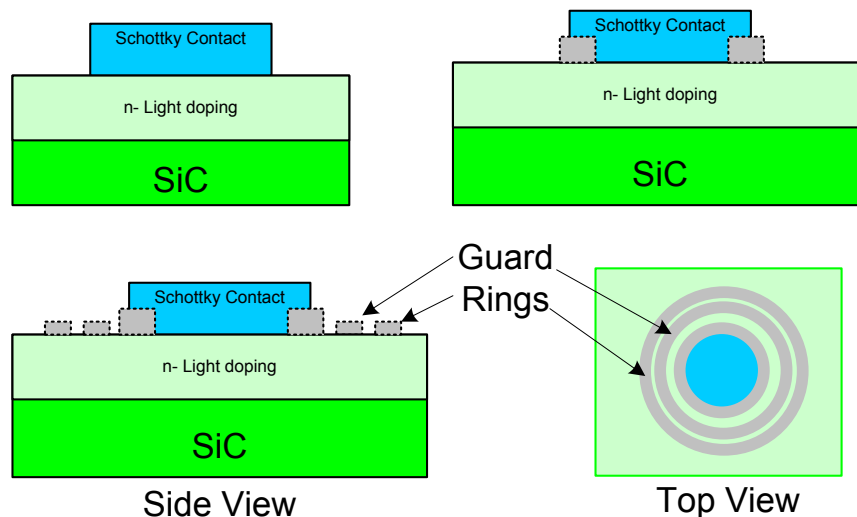


Figure 10: Diodes with different guard ring configurations for improved V_{RB} , one with no ring guard, a single guard ring, and multiple guard rings for improved breakdown characteristics.

CHAPTER TWO

SCHOTTKY DIODE RESEARCH

There are two techniques investigated during this research that are proposed to improve the quality of the metal-semiconductor Schottky diode junctions. By deviating from the standard planar contact a spherically shaped contact will be formed and mechanically contact the semiconductor. Adopting physical dimensions with large radii of curvature in high voltage applications is widely practiced in macro scale electrical systems. Several mechanical Schottky diode contacts were fabricated, characterized, and contrasted. This technique of varied mechanical contact geometry became of interest because it had the prospects of reducing planar edge termination electric field stress without the requirement of advanced diode fabrication equipment. Another potential benefit was the possibility to test some of the semiconductors parameters by quickly making a mechanical Schottky contact and avoiding the time consuming process of vacuum sputter deposition. Several well fabricated mechanical contacts with varied metals of interest could be swapped between various semiconductor materials and some parametric measurements could be taken in a short period of time. The sphere with the best electrical performance will then be compared with conventional planar contacts of similar dimensions that were fabricated by plasma sputter deposit.

The second technique to improve the quality of the Schottky diode devices will address the temperature aspects of planar Schottky contact diode construction. The focus of this research will be to fabricate the conventional 500 μ m planar contacts at high temperature and then heat treat the diodes. Two samples will be plasma sputter deposited one at room temperature 27°C and the other at 600°C. The two samples will be taken and annealed with a rapid thermal processor that will heat them to 200°C, 300°C, 400°C, 500°C, and 600°C. After each heat treatment the diodes will be removed from the rapid thermal processor and I-V characterization will be performed any changes in performance will be noted.

2.1 High Voltage Contact Terminal Evaluation and Testing

The way electrodes or insulators are shaped can greatly reduce the intensity of electric field stress surrounding a device. This technique is used to reduce electric breakdown at high voltages in large scale systems. These systems implement construction designs that feature physical dimensions with large radii of curvature. Possible advantages could result in applying these techniques to small scale devices such as metal contacts on semiconductors. Research conducted on the effects of discharge terminal geometry variation and breakdown voltage is a well developed topic for large scale devices. Figure 11 qualitatively shows the improvement of voltage breakdown with increased terminal size and was inspired by Los Alamos research based on data collected from discharge terminals placed in dry transformer oil at 25 °C. The electrode dimensions were 25 cm diameter spheres, 1.1 cm diameter spheres, and needle points [15].

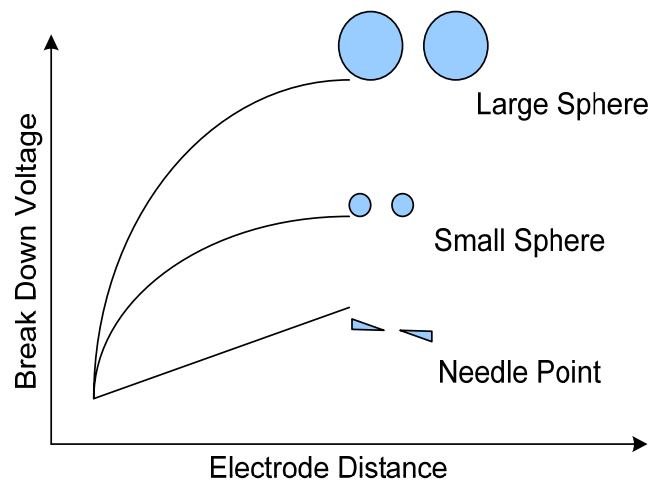


Figure 11: Qualitative difference found between discharge terminals of varied geometry.

In order to model the interaction of the electric fields for different geometries in of high voltage terminals and later semiconductor contacts a formula that relates the plane and sphere relationship to the electric field gradient was used and the related variables show in Figure 12. An interesting aspect for this geometric configuration is that the electric breakdown field is effectively divided in half from that of the sphere to sphere configuration.

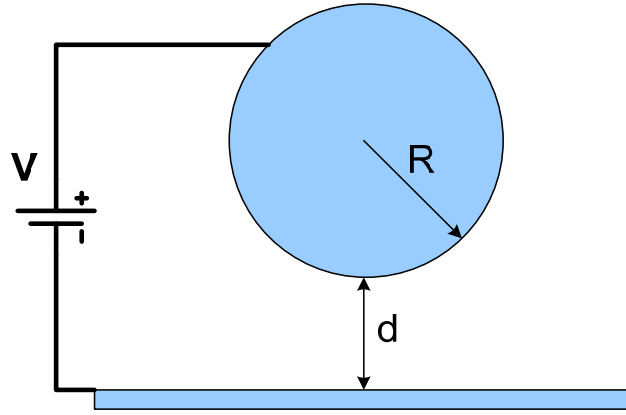


Figure 12: A spherical discharge terminal is shown suspended above a plane.

The equation that models the sphere to plane relationship of Figure 12 is expressed by the equation 2.1 which is used to estimate the performance of the corona discharge terminal experiments. The same will be later used to model electrical field stress surrounding Schottky contact terminals on the silicon carbide devices.

$$E_v = \left[\frac{d}{R} + 1 + \sqrt{\left(\frac{d}{R} + 1 \right)^2 + 8} \right] \times V / (4d) \quad (2.1)$$

The first of the experimental testing was done on corona discharge terminals. The benefit of this test was to insure the ability to model and predict contact terminal performance on a large scale and shift toward smaller scale electrodes. A high voltage 18kV transformer was utilized to elevate the various metal terminals to corona onset potentials. The 18kV potential transformer (PT) was controlled with a variable transformer that could be adjusted from 0 to 100%. A divide by 100 probe was connected across the high voltage terminals of the (PT) and readings were taken from 0 to 100% in decade increments for a total of 11 voltage measurements. The impedance of the divide by 100 probe was 10 mega ohms and it was removed while measuring corona current to reduce loading effects.

To measure the corona current a 20kΩ sensing resistor was placed in series with the transformer and the water plate discharge terminal test rig. A high impedance analog voltmeter was connected across the current sensing resistor. This type of volt meter was used because it was isolated from ground so that there would be no damage to the instrument. Figure 13 features the water plate discharge terminal test rig that is further illustrated and detailed in Figure 14.

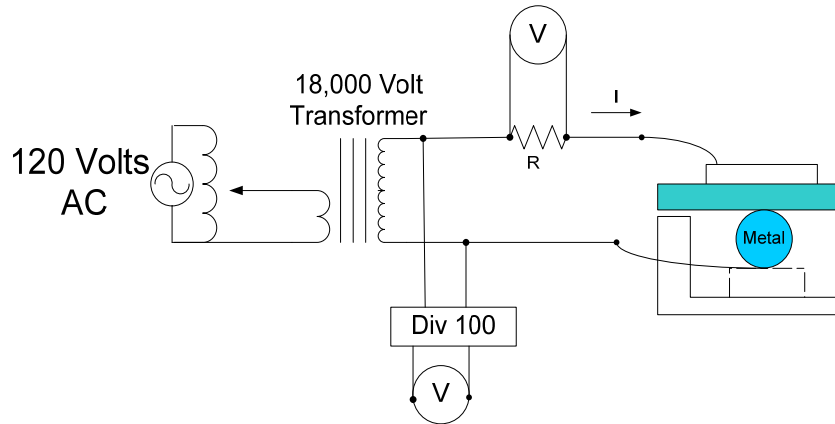


Figure 13: Experimental setup used to induce corona discharge around a metal electrode.

The metal electrode was placed under a glass plate (2mm in thickness) with pool of water on the opposite side. An electric potential difference was applied to the water and electrode. The water allowed for easy observation of corona discharge, while monitoring the corona current with the meter and observing that area of discharge beneath the water plate the various contact terminal geometries were evaluated.

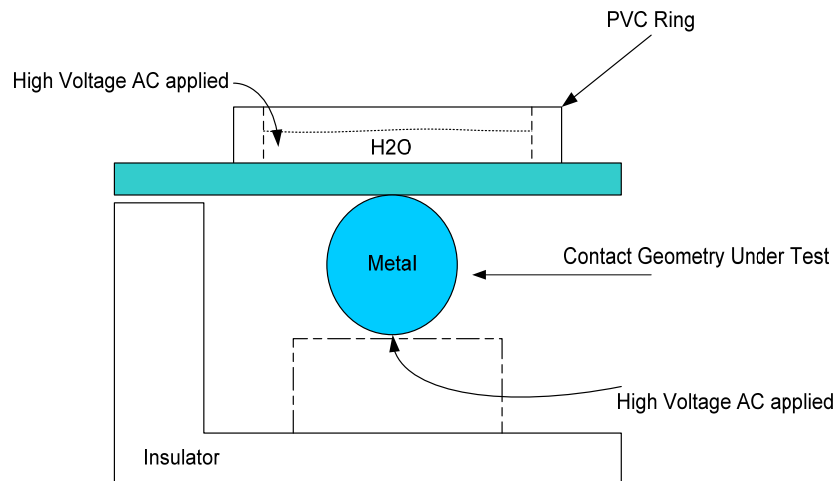


Figure 14: Test rig for corona onset occurring on the test electrode beneath water plate.

An initial problem in the evaluation of performance was to determine effective contact area of the discharge terminals on the glass substrate. To establish a method to compare spherical terminals with planar terminals an estimation formula for effective contact diameter (ECD) was based on a mean location for dominate corona discharge activity. The equation of 2.2 was a formula empirically developed to estimate the effective contact diameter.

$$ECD = 2 \times \frac{R}{\tan(60^\circ)} \quad (2.2)$$

For the effective contact diameter (ECD), the distance from the plane to the sphere's elevated surface was equal to 15% of the sphere's radius. This provided a method to determine the appropriate sized planar contacts to be used comparatively in the study. Figure 15 shows how the equation 2.7 was arrived at by showing the separation distance from sphere to plane of at the angle of 60 degrees which is equal to 15% of the initial R value. This 15% tolerance was arrived at by observation of the corona discharge. The photographs in Figure 15 show the two spherical discharge terminals (a) and (b) below them are photographs of their respective corona onsets (c) and (d). In photographs (c) and (d) an overlay of the effective contact diameters for the spheres has been drawn over top of the corona discharge. The written overlays point out 9.6mm ECD for the small sphere (c) and 30mm ECD for the large sphere (d) this by observation effectively approximates the centralization of the corona discharge activity.

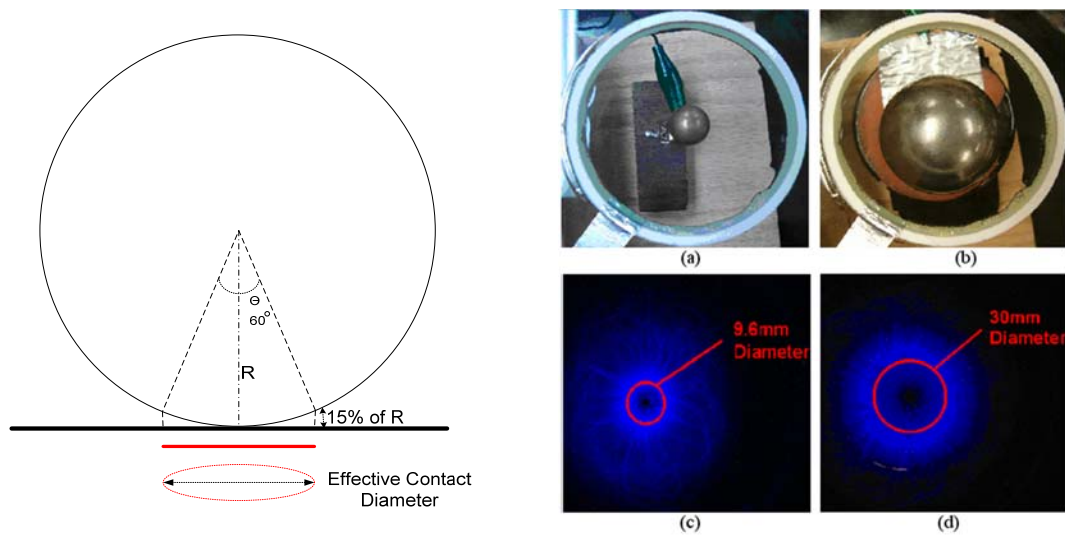


Figure 15: Effective contact diameter (ECD) and corona discharge terminals.

2.2 Corona Current verses Contact Terminal Geometry

Initially the data showed what appeared to be exponential growth of corona current I_c (in micro amps) with an increase in applied voltage V_c (in kilovolts) which was to be expected by the relation of equation 2.3 taken from corona air propulsion research [17].

$$I_c = 3 \cdot 10^{-5} e^{2V_c} \quad (2.3)$$

The observation was made that the spherical corona discharge terminals outperformed the planar contacts in the sense that they had lower corona leakage currents. The observation was made, in which the larger sphere that should possess a lower surface electric potential gradient had a larger corona leakage current than that of the smaller sphere. This deviation from the expected was proposed to be caused by the larger contact having more peripheral area for corona discharge to occur despite the reduced electric field. In addition to spheres, several types of circular planar contacts (9mm, 19mm, and 26mm diameters) were tested and compared with each other in order to see which construction would have the most corona leakage current. Figure 16 shows the results of the corona discharge experiments. Most corona leakage current occurred around the contact with the largest periphery of electric field stress. For any given voltage applied more corona current will onset around a larger planar contact terminal due to its increased perimeter. From these results it is anticipated that larger circular planar contacts on semiconductor devices will have a lowered breakdown voltage because the contact possesses a larger perimeter with an aggravated electric field condition at the edge terminal. The data shows that there is increased corona current in proportion to the periphery around the planar contact (Figure 17). Given the results of the water plate corona discharge experiments it is anticipated that the spherical contacts on semiconductor substrates may be advantageous over planar contacts. This corona discharge terminal experiment will also be modeled in the electric field simulation.

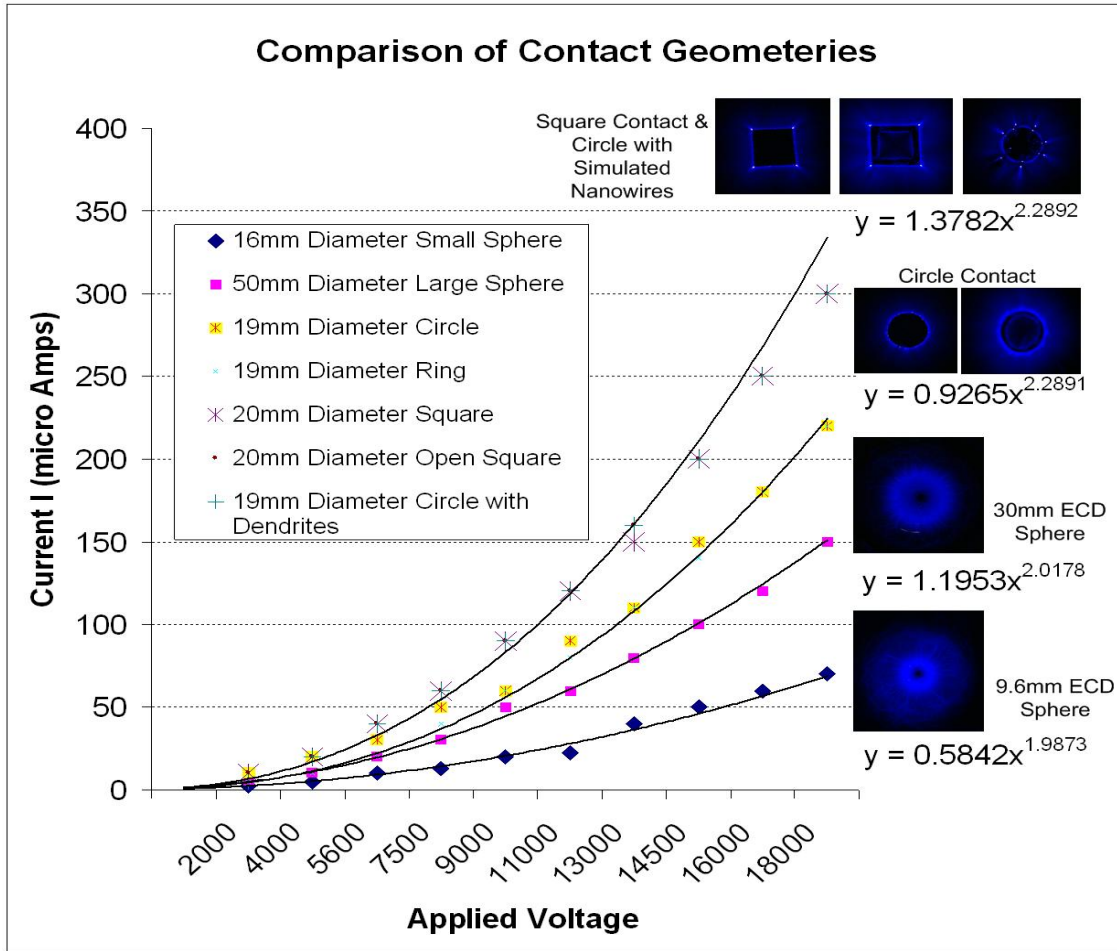


Figure 16: Corona currents plotted for various high voltage terminal geometries tested.

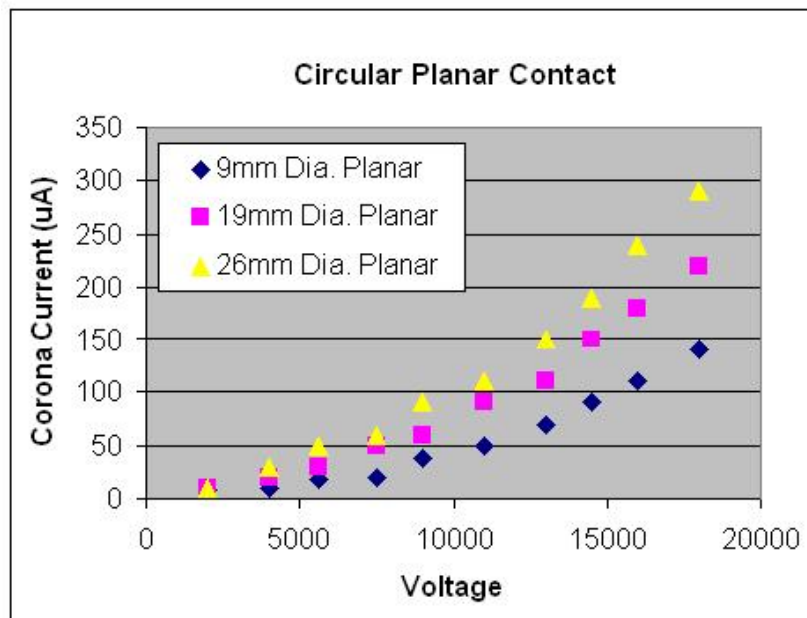


Figure 17: Corona currents for circular planar terminals increase with contact periphery.

2.3 Finite Element Electric Field Analysis

To model the corona discharge terminals the exact dimensions of the metal terminals and glass substrate were entered into the Infolytica Electnet electric field simulation software. The applied voltage of 18kV was set to the electrodes, the conductivity of all the metal corona electrodes simulated was set to that of Aluminum and electric permittivity of the surrounding air ($\epsilon = 1$) and glass (EP05 $\epsilon = 5$) were taken into account. The water plate that would have been above the sphere in the experiment is now positioned below; since it serves as a ground plane, the electrical parameters of the water were set to that of a perfect conductor. In the simulation featured in Figures 18, 19, 20 the maximum of the electric field scale represented in red is set to 3×10^6 V/m which is approximately the breakdown field for air. Therefore, the red area depicted in the Figures gives a good indication of where corona discharge will occur around the electrode. A photo of the corona onset confirms this and is shown in the upper left corner of the simulation.

Simulation helped to confirm that the larger sphere (50mm dia.) does have a reduced electric field at the surface (Figure 20). However, at the voltages applied more surface area was at corona potential than that of the smaller sphere (16mm dia.). Figure 19 features the simulation for the small spherical corona electrode with the perimeter of larger sphere positioned over top. From this it can be easily seen that the larger sphere has more area at the elevated potentials for discharge to occur relative to the smaller sphere.

Several planar contact terminals constructions were tested including square, circle, and square with center removed. The open square construction investigates the effect of contact area versus perimeter. It was found the square and the open square had the same amount of corona current indicating perimeter leakage was dominant in corona discharge experiments. Since the perimeter was the largest contributing factor for corona leakage only one simulation was run for all types of planar electrodes. All material parameters have been kept the same as in prior simulations with the thickness of the planar contact set to 0.1mm. Figure 18 shows the electric field stressing that occurs at the perimeter.

There were several benefits in performing the corona discharge terminal concept testing before contact terminal testing on semiconductors. The first was that testing confirmed plausible improvement due to spherical contacts. Secondly, this testing confirmed the ability to qualitatively examine electric field stress surrounding contact terminals by using the Electnet simulation software. Doing this testing as a precursor it helped to develop expectations of performance that could be easily examined on a large scale so the effects of small scale contacts could be more closely examined. Finally this testing aided in the experiment designs for semiconductor testing and demonstrated need for accurate measurement of metal semiconductor interface region.

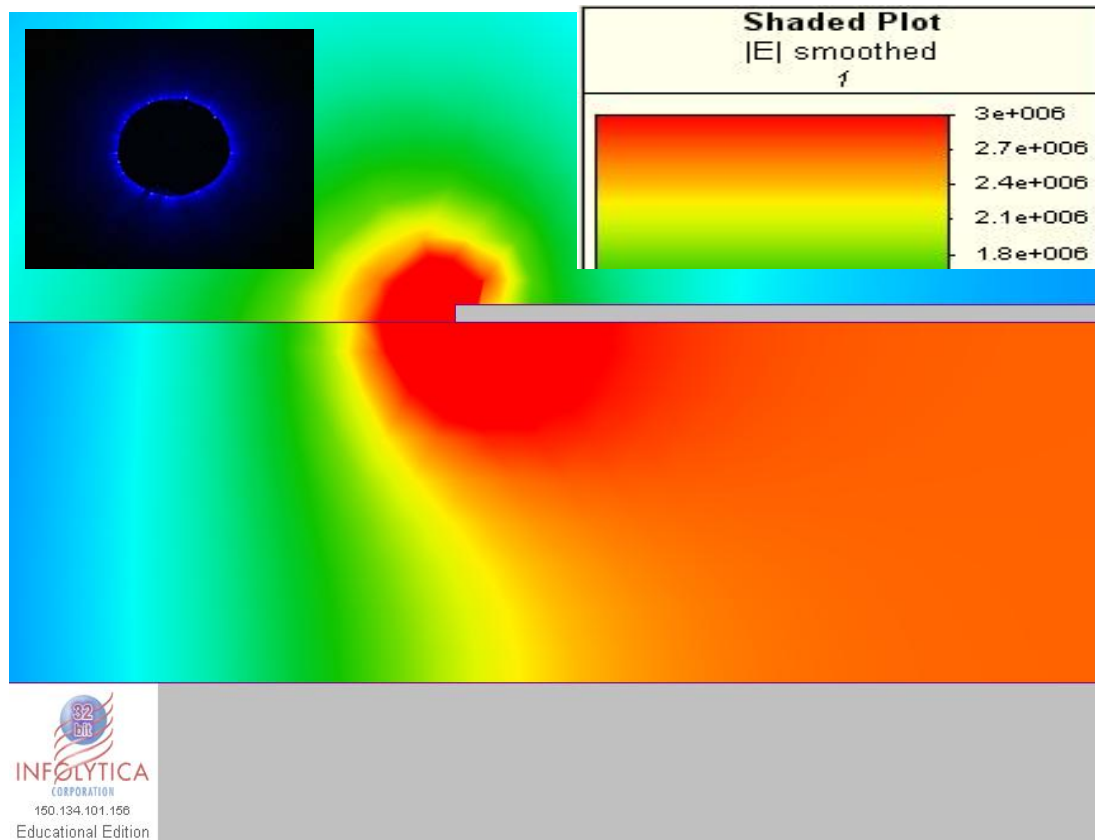


Figure 18: Electnet simulation of planar corona discharge terminal, with high electric field intensities at the perimeter.

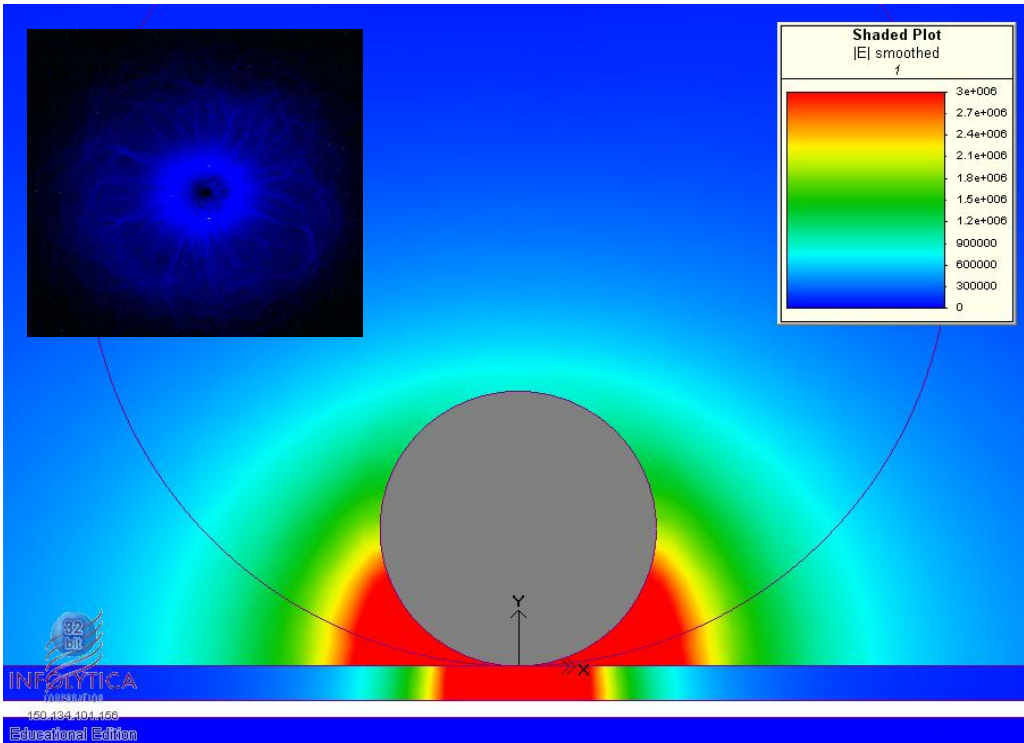


Figure 19: Sphere (16 mm dia.) with the large sphere's perimeter over lay comparison.

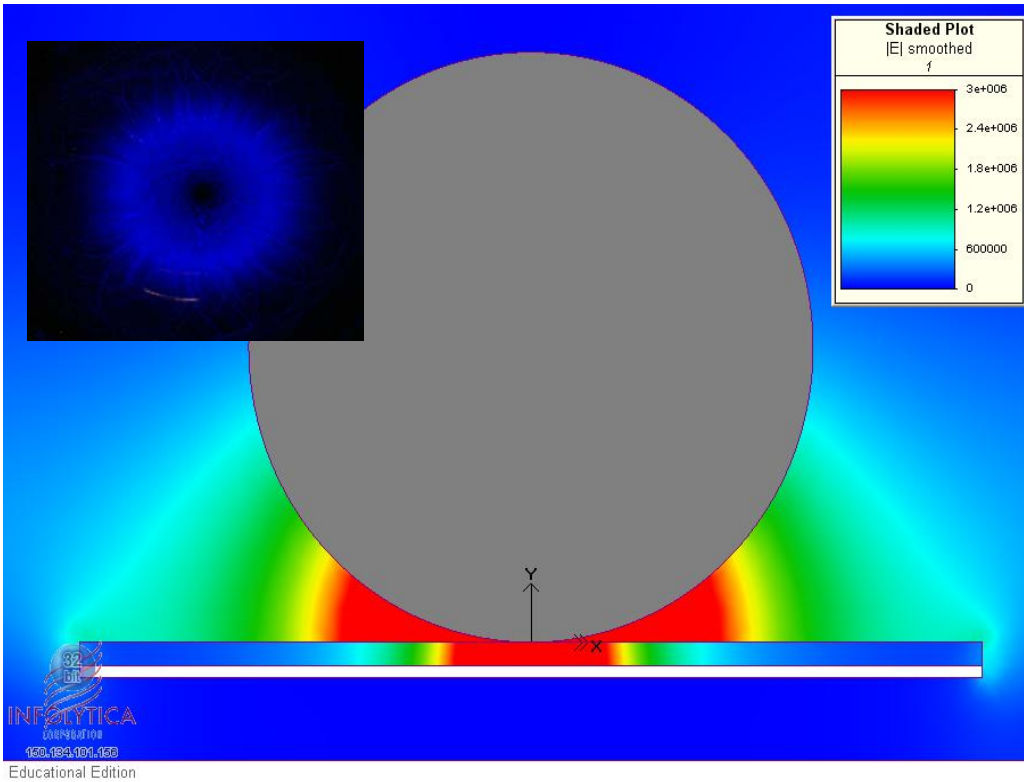


Figure 20: Large sphere (50mm dia.) simulation with the corresponding corona photo.

2.4 Similar Developments in Schottky Contact Terminals

Recent literature reveals several techniques were that are currently in use with semiconductor applications and are also similar the proposed research. A mechanical contact method that closely resembles this research conducted in regard to spherical contacts was implemented on diamond substrates in 2004. In this research gold metal pressure (mechanical) contacts were fabricated without edge termination. To better evaluate the high voltage reverse characteristics the contacts were spherically shaped and used in place of the conventional sputter contacts. The size of the spherically shaped mechanical contact was 1.2 mm in diameter. This research specified the contact area of the sphere on semiconductor only to be a “small interface” with the diamond substrate and it was not quantified. Though there was no edge termination the device was tested within a high breakdown dielectric fluid. The spherical contact when used on diamond with stood breakdown voltages up to -4kV with less than 1 nano ampere of reverse leakage current detected. The research group then performed finite element analysis on the sphere and found that electric field intensity surrounding the contact was on the order of 4 MV/cm [13]

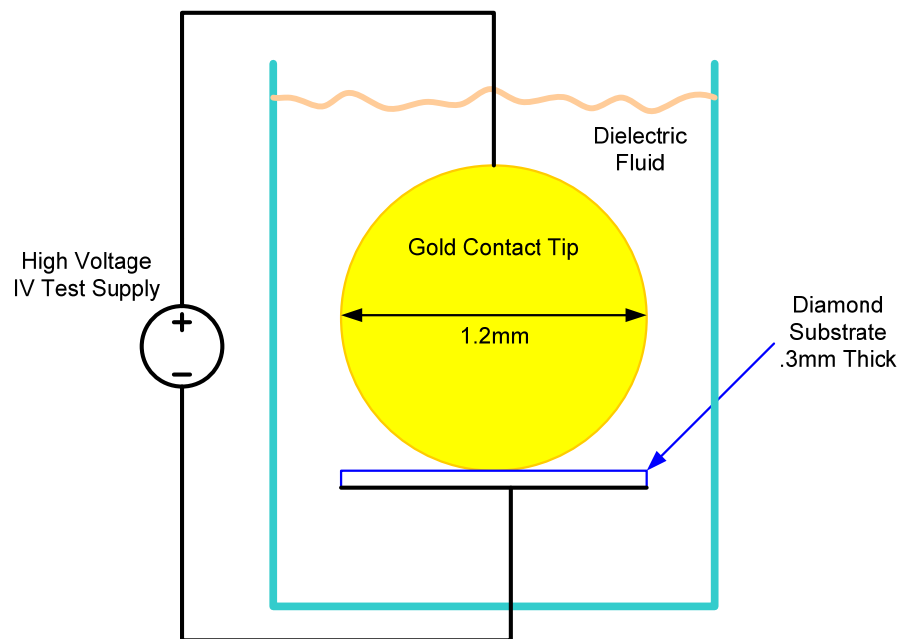


Figure 21: Spherical contact on diamond substrate characterization, test was performed in a container of dielectric fluid to reduce arcing flash over.

Another innovative tactic in reducing electrical field stress implemented was an oxide field plate overlap design in which the oxide layer is etched into the form of a ramp. The periphery of the Schottky contacts where edge terminal electric field crowding would occur, an oxide field plate with a ramped contour of a 5° incline has been added. The oxide layer was 1.1 μm thick with Ni metal contacts on n-type 6H SiC. The circular contact windows in the field plate termination have a diameter of 320 μm and were created with the use of a shadow mask. In order to obtain the ramp profile, multiple layers of oxide were over etched with acid solution [14]. Figure 22 illustrates the implementation of an oxide ramp to reduce electrical field stress at the edge termination of the contact. The research on these contacts was also conducted at high temperatures of 800°C, 900°C, and 1000°C.

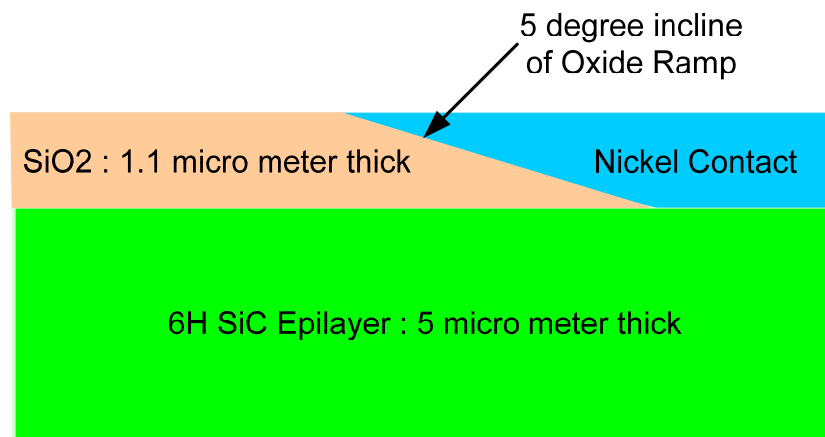


Figure 22: Oxide ramp field plate termination on SiC with Ni Schottky contact.

The exposure of the diode to high temperatures resulted in higher reversed bias leakage currents, until the diode became ohmic at 1000°C [14]. However, research performed by Q. Zhang and T.S. Sudarshan investigated the annealing of Schottky diodes up to 800°C and found benefits in both forward and reverse bias characteristics. It was found that annealing the diodes repaired leaky low barrier parasitic parallel diodes that may have been present due to various barrier inconsistencies [12]. From this prior research it is shown that both physical contact terminal design and temperature treatment play a crucial role in the development of better metal-semiconductor contact terminal design. Therefore, both of these parameters are studied in this research.

CHAPTER THREE

SCHOTTKY CONTACT DIODE FABRICATION

Six different kinds of Schottky contacts have been constructed. The 1.71mm diameter sphere, 0.85 diameter sphere, and a needle point contact fashioned from 0.82mm diameter wire. Three sets of circular planar contact terminals have been constructed, one set of 125 μ m in diameter and two sets of 0.5mm diameter Schottky contacts. These circular planar contacts will be fabricated with metal sputter deposition and one set of the 0.5mm contacts will have metal deposited at a temperature of 600°C. The semiconductor sample used for this research is n-type 4H SiC manufactured by Cree. The doping concentrations and layer thickness are featured below. The bottom of the 400 μ m SiC layer was coated with Ti/NiGa/Ti and heated to 950°C to form an ohmic contact. The effectiveness of the ohmic contact used in this research was based on a well established fabrication method. Figure 35 below shows an overview of the contacts tested and the general parameters of the SiC sample.

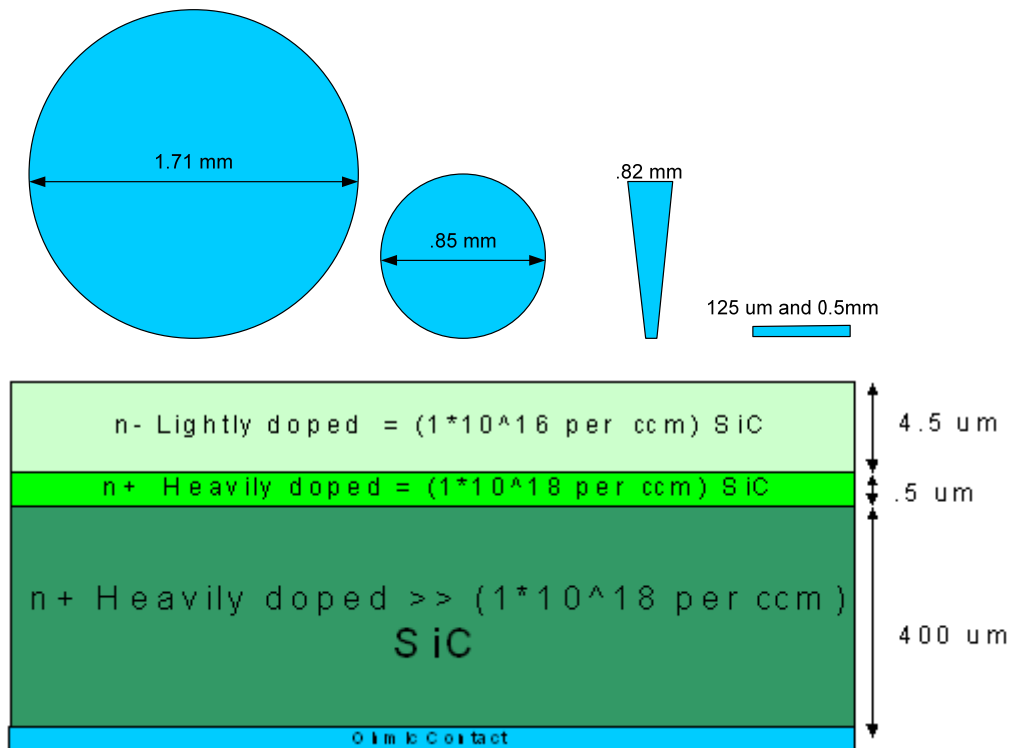


Figure 23: Overview of the diode contacts to be tested and a diagram of the SiC substrate.

3.1 Fabrication: Preparing SiC Substrate and Ohmic Contacts

The 4H n-type Silicon Carbide (SiC) samples used were manufactured by Cree; the wafer was assigned the following serial number XZ0799 – 05 X4NXXXX – 00S2. The sample wafer was sliced into 5 by 5 mm squares that are used in the experiments. Over the sample wafer there is a protective SiO₂ layer on top of the SiC epilayer.

The samples used were assigned a names based on YSUXX standard labeling nomenclature used at the Youngstown State University's Wide Bandgap Laboratory. Samples YSU 96, YSU 97, YSU 114 are used with the mechanical contact terminals. Sample YSU 113 was used to fabricate 125 μm diameter circular planar contacts. Lastly, samples YSU 111 and YSU 112 were used to fabricate planar 0.5 mm diameter contacts. YSU 111 was elevated to 600°C during metal plasma sputter deposition to study the effects of high temperature processes. Before the fabrication of Schottky diodes began, the backs of all these samples were polished with a fine grit sand paper to prepare the back surface for ohmic contacts.

The ohmic contact is the first step needed to make a functional diode. This provides a low resistance terminal attached to the back of the semiconductor so that the device may be biased with a voltage potential. After the back of the samples have been polished they were all boiled in acetone, rinsed in alcohol, and rinsed in de-ionized water. The samples were mounted to a sputter platform equipped with a film thickness monitor and suspended 10 cm above the sputter target. The vacuum metal sputter deposition chamber was then employed to coat the backs of the samples. The vacuum chamber was pumped down to a base pressure of 7.2×10^{-10} Torr, Argon was then allowed to flow into the chamber at a rate of 15.3 sccm and the pressure of the chamber during sputtering was held at 2 milli Torr. Titanium was sputtered with a current of 0.1 amperes and the Nickel Gallium was sputtered at 0.05 amperes, a pre-sputter time of 1 minute was allowed to clean surface oxides from the targets. The thickness of the metal sputtered was monitored with the film thickness monitor so that the correct amount of material could be deposited; the monitor was recalibrated for each new metal sputtered. A layer of 25 nm of Titanium, 70 nm of Nickel Gallium, and a final 10 nm of Titanium were deposited. Figure 24 shows the polished SiC samples and the metals sputtered for the ohmic contact.

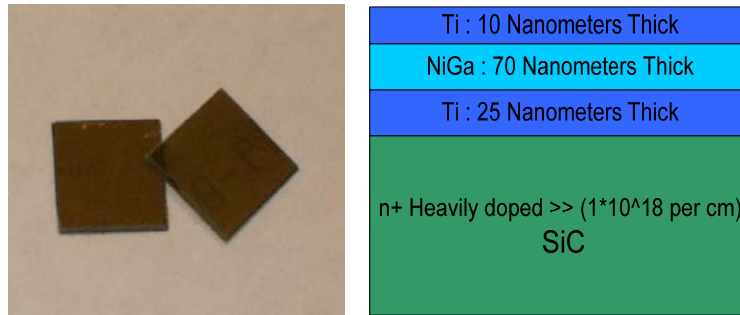


Figure 24: Polished 5x5mm samples and sputter diagram of ohmic metal contact.

The samples were again cleaned by boiling in acetone, rinsing alcohol and rinsing in water. Now the samples are ready to be heated in the Rapid Thermal Processor (RTP) at high temperatures so that the metals sputtered will diffuse into the semiconductor and form an ohmic contact terminal. The RTP was set to reach a temperature of 950°C and will hold this temperature for 2 minutes so that the metal adsorption into the material would occur and resistive contact will form. Ultra pure Nitrogen (N₂) an inert gas was fed into the annealing chamber so that no there will be no reaction with oxygen at the metallic surface of the ohmic contacts. The RTP and the thermal profile for annealing the samples is shown if Figure 25 as well as the surface oxide removal procedure.

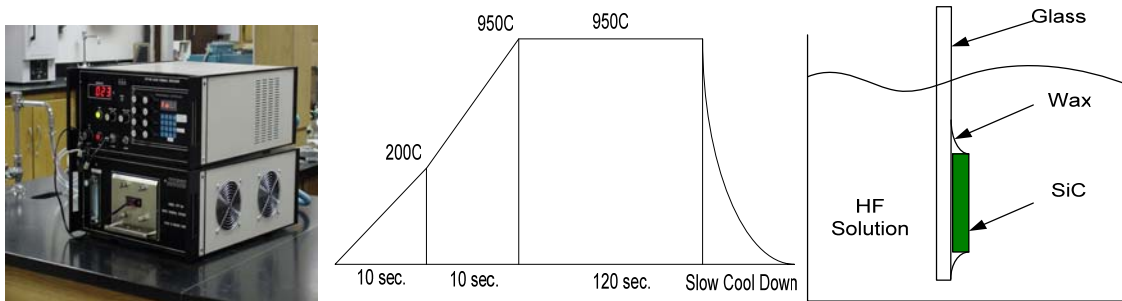


Figure 25: Rapid thermal processor, temperature verses time, and HF acid preparation.

The final step in preparing the test samples for Schottky diode fabrication was to remove the protective oxide (SiO₂) layer from the epilayer of the SiC. This was done by mounting the sample on a glass slide with wax (protecting the side with the metal ohmic contact) and soaking the sample in dilute 1:10 hydro fluoric acid (HF) for 3 minutes.

3.2 Fabrication: Mechanical Schottky Contacts

The mechanical Schottky contacts were fabricated during this research since a key point of interest was to investigate how the variation of contact terminal geometry will affect diode performance. The mechanical contacts were made in the form of spheres in anticipation of a performance advantage. The experimental process used to form the spherical mechanical contacts started by drawing a plasma arc from a copper wire. The heat of the arc would bead the copper into a ball termination at the end of the wire. Once a ball was formed a combination of electro-erosion and electroplating was used. A +12 volt potential was applied to the sphere termination it was dipped in a copper sulfate solution that eroded contours and oxides from the spheres surface. Following this the voltage was lowered to 1 volt and a clean layer of copper was electroplated onto the surface of the spherical contact. Photos of the plasma arc fabrication of the contacts and an illustration of the electro erosion process is shown in Figure 26. The needle point contacts to be discussed only used the electro-erosion/plating process no plasma arc.

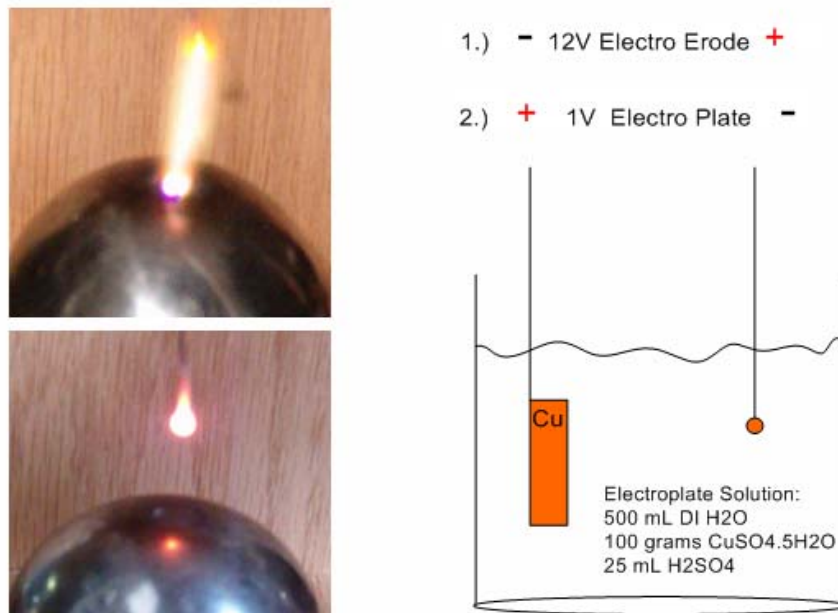


Figure 26: Plasma arc process formation of spheres and electro-erode/plate process.

Due to the experimental nature of the plasma arc and electro-erosion/plating method used to form the contacts there was a lack of control in creating consistent spheres. Many spherical and needle point contacts were fabricated and examined. The contacts that were of the best geometry and surface quality were selected for research purposes. Figure 27 shows a collection of spherical contacts that had been fabricated during this research. The mechanical contacts will all receive a coating of 2000 Å of nickel with the planar contacts during plasma sputter deposit.



Figure 27: Several dimensions of spherical contacts in various stages of construction.

3.3 Fabrication: Planar Plasma Sputter Deposit Contacts

The second type of Schottky contact construction was the 125µm planar contact. This diameter was chosen because it was close to the contact diameter of the largest spherical contact. The comparable contact area will lend itself for comparison of planar versus spherical contact performance. This 125µm contact was made by using the photolithographic process. The sample YSU 113 was again boiled in acetone, rinsed in alcohol, rinsed in de-ionized water, and blown dry. Photo resist AZ 5214 was applied to the sample and spin coated by rotating the sample 4000 RPM for 30 seconds. This allowed for a uniform distribution of photo resist across the sample. The sample was then removed from the spin coater and placed on the hot plate to bake the photo resist for 1 minute at 100°C. The sample was then placed in the mask aligner and a pattern with 125µm dots was placed over the sample YSU 113. Ultraviolet light was allowed shine through the pattern to expose the photo resist for 3 minutes. The sample was then removed from the mask aligner machine and the pattern in the photo resist was developed by soaking the sample in AZ 400 developer for 50 seconds. The equipment used in the preceding process is featured in Figure 28 which illustrates the spin coater, hot plate, mask aligner, and the final sample with photo resist applied.



Figure 28: Spin coater, hot plate, mask aligner, and dot pattern after soaked in developer.

The final step in fabrication of the spherical, needle point, and 125 μm diameter planar contacts is the metal sputter deposition which will apply a uniform coating of nickel to all of the contacts. The contacts were placed on a movable holder that had a film thickness monitor attached. The contact terminals and YSU113 were moved over the plasma and Nickel_{90%} Gallium_{10%} was sputtered to coat all of the contacts with 2000 \AA of the material. The vacuum chamber was initially pumped down to a base pressure of 8.9×10^{-7} Torr. Argon was then allowed to flow into the chamber at a rate of 15 SCCM and the pressure of the chamber during sputtering was held at 2 milli Torr. Nickel_{90%} Gallium_{10%} was sputtered at 0.075 amperes, a pre-sputter time of 1 min was allowed to clean surface oxides from the targets.

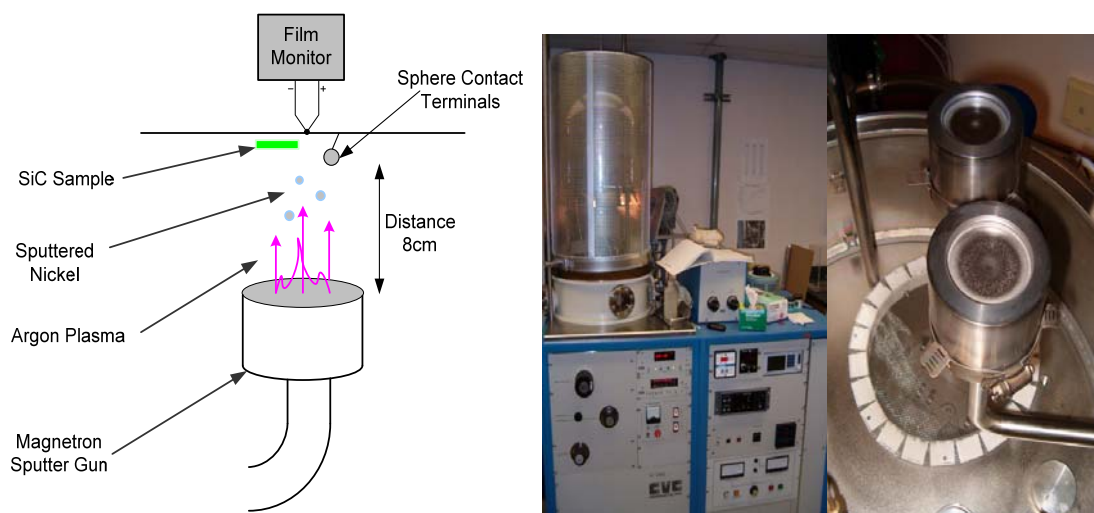


Figure 29: Plasma sputter deposit process with chamber and sputter targets shown.

The last contacts fabricated made with the use of a shadow mask, which has been placed in front of the SiC samples. Photolithography may not be used here because of the high temperatures at which one of the two samples will be deposited. At a deposition temperature of 600°C the photo resist would deform or melt away. The shadow mask is made from stainless steel and is perforated with 0.5 mm diameter holes. When the sample is sputtered with the metal (NiGa) the material will only be deposited on the SiC exposed by the perforations. To investigate temperature effects one sample YSU 112 was deposited with the shadow mask at room temperature 27°C. During the sputter process of sample YSU 112 the temperature was monitored and recorded to only rise up to 33°C. The other sample, YSU 111 was deposited at high temperature of 600°C using heat lamps. Investigated as to how the metal deposition temperature affected the forward and reverse bias characteristics of the diode will be studied. Though samples YSU111 and YSU112 were sputtered at different times and temperatures all other parameters of sputter deposition were held the same. The vacuum chamber was initially pumped down to a base pressure of 5.8×10^{-7} Torr for YSU 111 and 9.8×10^{-7} for YSU 112, argon was then allowed to flow into the chamber at a rate of 15 sccm and the pressure of the chamber during sputtering was held at 2 milli Torr. NiGa was sputtered at 0.075 amperes; a pre-sputter time of 1 min was allowed to clean surface oxides from the targets. The sputtering continued for 24 minutes allowing 439 Å of NiGa to be sputtered onto the substrates.

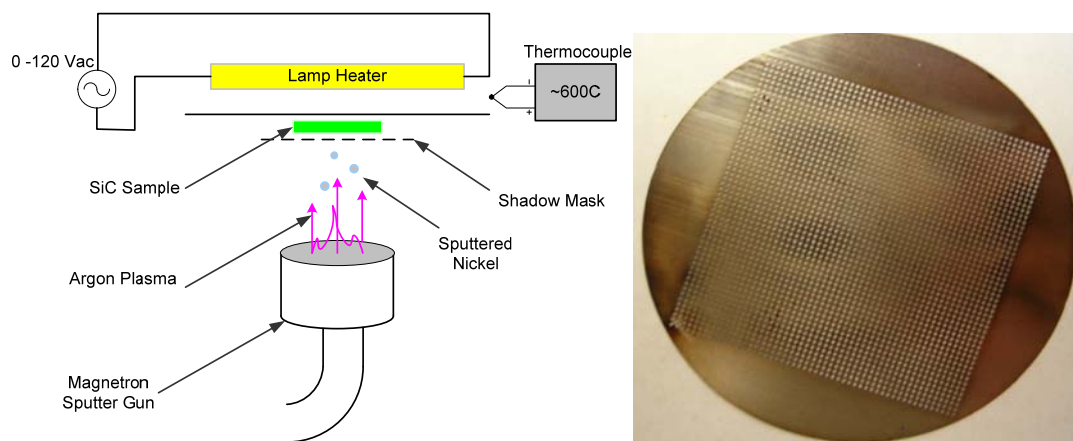


Figure 30: High temperature plasma sputter deposit process with shadow mask.

3.4 Inspection & Modeling of the Schottky Contact Terminals

At this point all Schottky contact diodes needed for the research have been constructed. These diodes are mounted to a copper substrate (this will facilitate testing) that was custom fabricated. The mechanical contacts will be supported by a custom designed insulation support structure that was fabricated on the three dimensional printer. Other resources that culminated in the production and testing of these Schottky diode devices were the Wide Band Gap Laboratory (general testing and fabrication) Electromagnetic Fields Instrumentation and Research Center (electric field simulation), Scanning Electron Microscope or SEM (metal semiconductor interface analysis), and the Electronics Maintenance Services (providing vital test equipment and technical support).

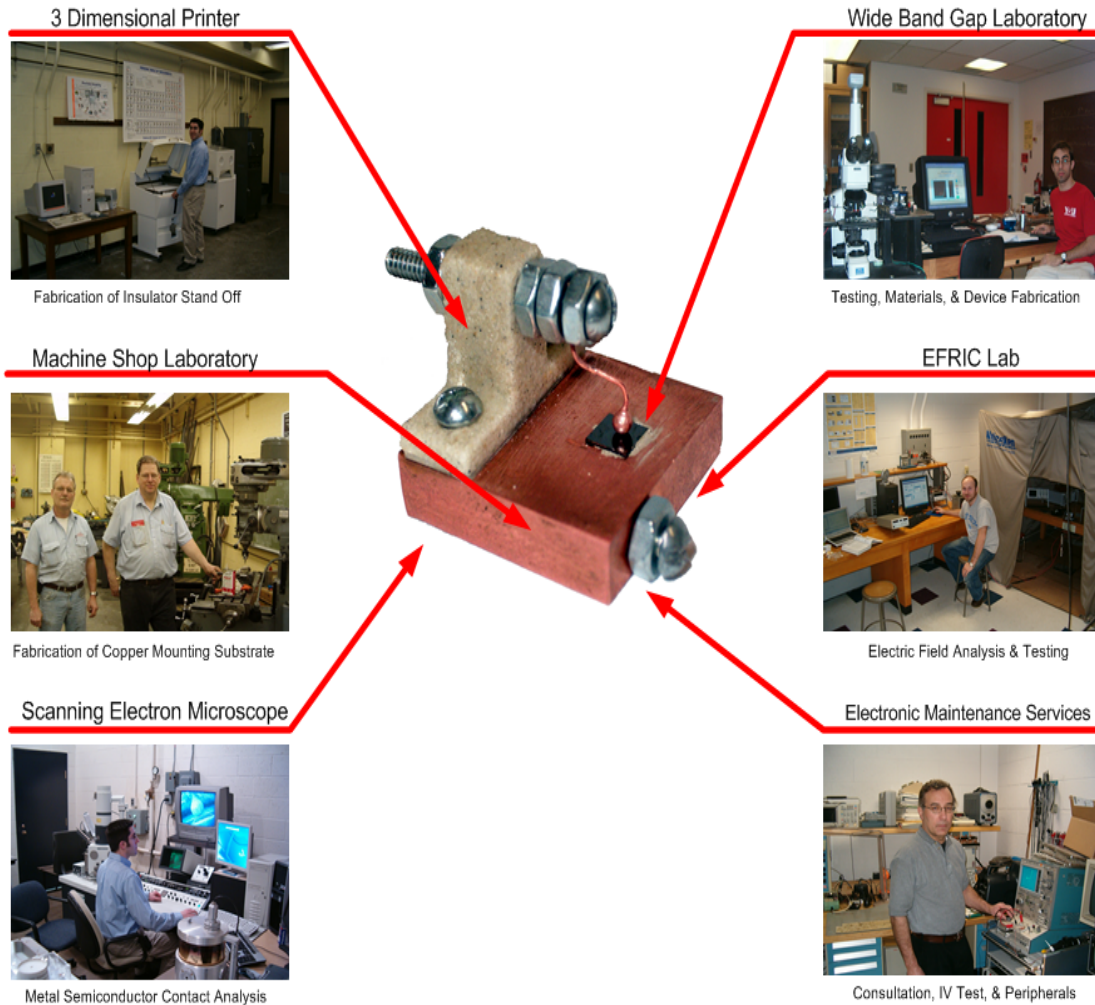


Figure 31: Youngstown State University laboratories and personnel surrounding the diode helped contributed to the construction and analysis of these devices.

The measurement of contact dimensions of the newly fabricated Schottky contact terminals is necessary for analysis and modeling. The first contact reviewed will be the needle point contact fabricated from 0.82mm diameter wire electro eroded to a fine point. The radius of curvature has been approximated with the optical microscope to be 0.2mm (Figure 32). The second contact terminal is the small sphere produced by the plasma arc electro erosion/plating method. It has 0.85mm diameter and a radius of 0.42mm (Figure33). The third contact terminal is the large sphere produced by the same plasma arc electro-erosion/plating method. It has 1.71mm diameter and a radius of 0.85mm (Figure 34). All contacts made from copper are sputter coated with 2000 Å of NiGa.

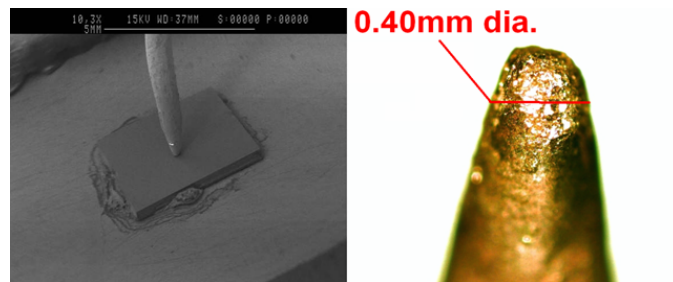


Figure 32: SEM & optical microscope photos of the needle point contact.

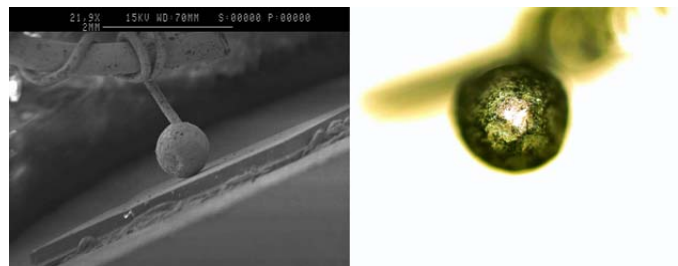


Figure 33: SEM & optical microscope photos of the small spherical contact.

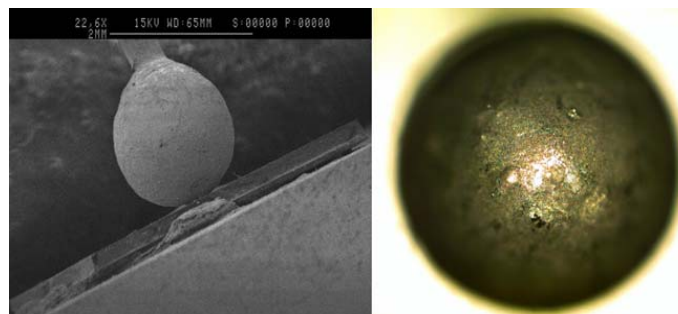


Figure 34: SEM & optical microscope photos of the large spherical contact.

The fourth diode constructed is the 125 μm planar contact terminal produced by photolithographic patterning and plasma sputter deposit. The circular planar contact of Figure 35 has 62.5 μm radius and a thickness of 2000 \AA of NiGa.

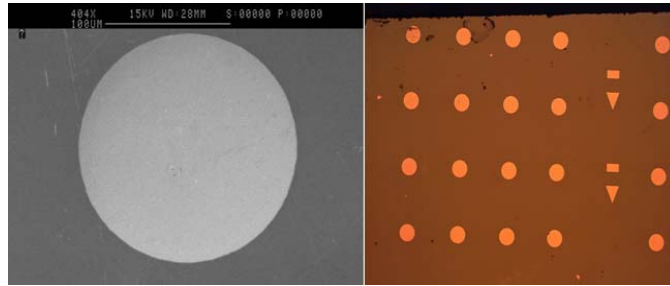


Figure 35: SEM & optical microscope photos of 125 μm planar contact.

The fifth and sixth diodes are the 0.5mm planar contact terminals produced by plasma sputtering metal vapor deposition through a shadow mask. The fifth contact is metal sputter coated with NiGa at room temperature (27 $^{\circ}\text{C}$) for 24 minutes resulted in a layer thickness of 439 \AA . While the sixth contact terminal was NiGa sputter coated on to the substrate at 600 $^{\circ}\text{C}$ for a period of 24 minutes resulting in approximately 439 \AA .

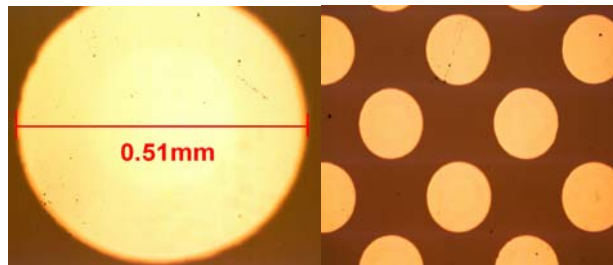


Figure 36: Optical microscope photos 27 $^{\circ}\text{C}$ deposit planar contact.

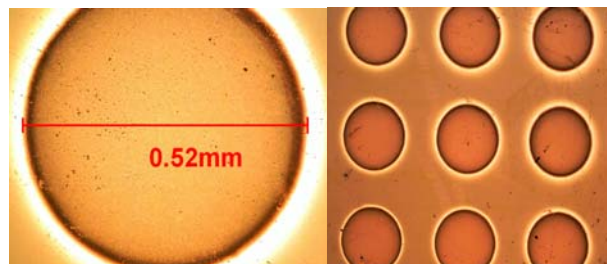


Figure 37: Optical microscope photos 600 $^{\circ}\text{C}$ deposit planar contact, note the halo effect caused at high temperature.

To calculate the amount of metal-semiconductor area for the spherical contact, a mathematical technique was employed that has been used in the analysis of sphere plane electrical contacts and contact creep effects [18-19]. The formula allows for R_h the radius of circular contact to be determined which allows for the contact area to be established as in equation 3.1

$$A_c = \pi(Rh)^2 \quad (3.1)$$

Equation 3.2 produces R_h the effective radius of circular contact for a sphere interfaced with a plane. Where F is the force applied to the contact, R_s is the radius of the spherical contact, and E^* is the combined Young's modulus for the SiC and Copper sphere material.

$$Rh = \sqrt[3]{\frac{3 \cdot F \cdot R_s}{4 \cdot E^*}} \quad (3.2)$$

The combined Young's Modulus for the two contacting materials is determined by equation 3.3 where ν_1 is the Poisson Ratio for copper (0.34) and E_1 is the Young's Modulus for copper (110 GPa) and ν_2 is the Poisson Ratio for SiC (0.192) and E_2 is the Young's Modulus for SiC (302.8 GPa). This yields a combined Young's Modulus value of 89.1 Giga Pascal (GPa) (Note: Pascal is equal to 1 N/ m²).

$$E^* = \left(\frac{1-\nu_1^2}{E_1} + \frac{1-\nu_2^2}{E_2} \right)^{-1} \quad (3.3)$$

The force applied to the contact terminal was mostly due to the weight of the contact and spring tension from that of the metal wire attached. The force exerted on the SiC substrate by the metal contact was crudely measured with the use of a scale by resting the contact on the scale surface as if it was the SiC substrate. Through this experiment the force exerted on the plate of the scale caused a reading of a weight equal to 100 grams was measured. With the use of $F=mg$ the force exerted was approximated to be on the order of 1 Newton. To find R_h the values of the combined Young's modulus, the force and the various contact radii were substituted into equation 3.2 to form equation 3.4.

$$R_h = \sqrt[3]{\frac{3 \cdot 1N \cdot R_s m}{4 \cdot 89.1 \cdot 10^9 N / m^2}} \quad (3.4)$$

The values of R_s will be 0.81 mm large sphere, 0.42mm small sphere, and 0.2 mm needle contact. Below Figure 38 illustrates the variable used in the above calculations to the left the calculated and observable contact areas are contrasted and the error term is illustrated. To the right in the Figure 52 a typical spherical contact is shown and the variable R_s is illustrated and the actual contact area to be solved for with equation 3.1 is shown at the base of the sphere.

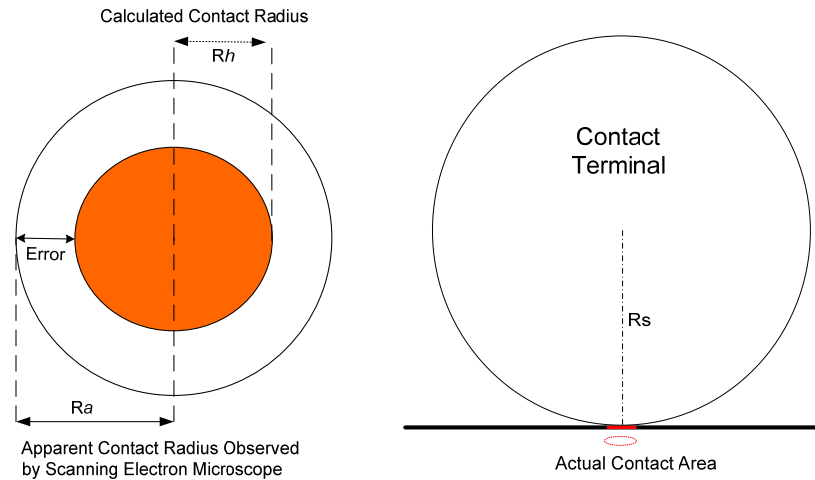


Figure 38: Apparent contact radius R_a , calculated Radius R_h , and the error margin.

To test the contact area equations it was necessary to make some observations to compare the observable contact area with that predicted. The mechanical contacts on silicon carbide were placed in the SEM and a side angle view was utilized to make an estimate of the contact area. The projected scale in the SEM image capture was utilized with a software tool known as Screen Calipers to measure the contact diameter. The screen caliper was calibrated to that of the SEM scale and the calipers were adjusted over the image of the contact until a best fit of estimation of contact diameter was reached. When the results of observed and predicted contacts were compared, an error term was found. Each of the SEM observations measured $30\mu\text{m}$ more than the estimate the predicted by the contact equations. Figure 53 shows the three mechanical contacts constructed and micrographed in the SEM. The screen caliper tool is used to estimate the diameter of contact. In the SEM photos deviation from the ideal geometry can be seen as well as some surface artifacts on the contact terminals.



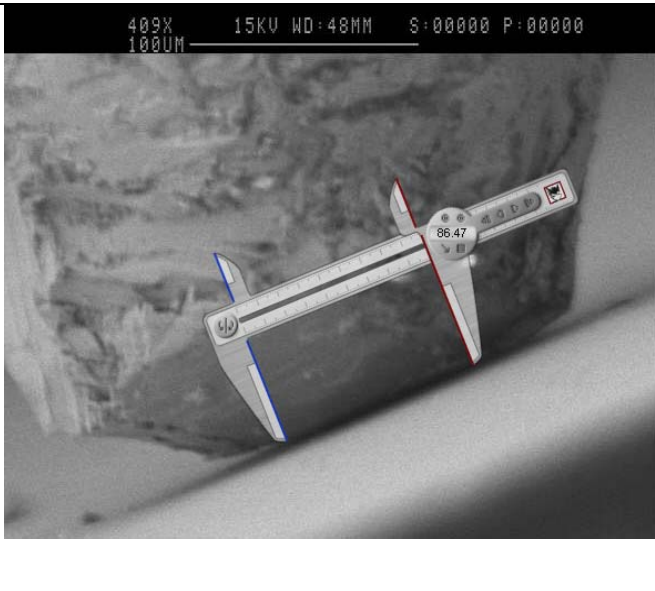
<p>Large Sphere</p> <p>Contact Diameter: 109.7μm</p> <p><u>Measured</u> Contact Radius: 54.85μm</p> <p><u>Calculated</u> Contact Radius: 19.2μm</p> <p>Error: 64%</p> <p>Difference: 35.65μm</p>	
<p>Small Sphere</p> <p>Contact Diameter: 95.65μm</p> <p><u>Measured</u> Contact Radius: 47.85μm</p> <p><u>Calculated</u> Contact Radius: 15.2 μm</p> <p>Error: 68%</p> <p>Difference: 32.65μm</p>	
<p>Needle Point</p> <p>Contact Diameter: 86.47μm</p> <p><u>Measured</u> Contact Radius: 43.25μm</p> <p><u>Calculated</u> Contact Radius: 11.89μm</p> <p>Error: 72%</p> <p>Difference: 31.36μm</p>	

Figure 39: SEM analysis of mechanical Schottky contacts, error term around 30 μm .

The same electric field simulation software that was used to model the corona discharge terminals has also been used to simulate the electrical field stresses that would exist around the mechanical Schottky diode contacts. The first simulation performed was on the large spherical contact terminal. The dimensions of the SiC (405 μ m thick by 5mm across) were entered into the simulation software. The ϵ_r relative electric permittivity of the SiC was set to $\epsilon_r=10$ and the conductivity of the mechanical contact terminal were set to that of Copper. The diameter of the sphere in the simulation was set to the directly measured value of 1.71mm. (Figure 40) The diameter of the small sphere in the simulation the measured value of 0.85mm. (Figure 41) The measurements of physical dimensions discovered with the use of the SEM were the parameters entered into the simulation for the needle point contact as well. (Figure 42) The measurements of the planar contacts diameter & physical dimensions were observed with an optical microscope and found to be 0.5mm in diameter. (Figure 43) This diameter was entered into the simulation and the thickness of the planar contact was set to 0.01mm the thinnest resolution that the simulation would practically allow. All contacts in the simulation had +10 volts of electric potential applied. The scale for this simulation and all of the proceeding simulations is 60kV/m or 60V/mm this scale was used because it showed the contrast in field reduction between the different types of contact geometries. From the simulations it can be shown that the largest sphere does have the greatest reduction in electric field intensity.

Because of the electric field at the perimeter the planar contacts in comparison with the other mechanical contact constructions there are more intense regions of electrical stress where breakdown can occur. It is anticipated that as a result of this electric field stress these contacts would exhibit higher amounts of reverse leakage current and premature breakdown. Since only the peripheral electric field edge effects were of interest only the 0.5mm diameter contact was simulated with the Electnet software. In comparison of the planar contact to that of the large spherical contact, a significant difference in performance should be noticeable due to the nature of the electric field surrounding these two geometries.

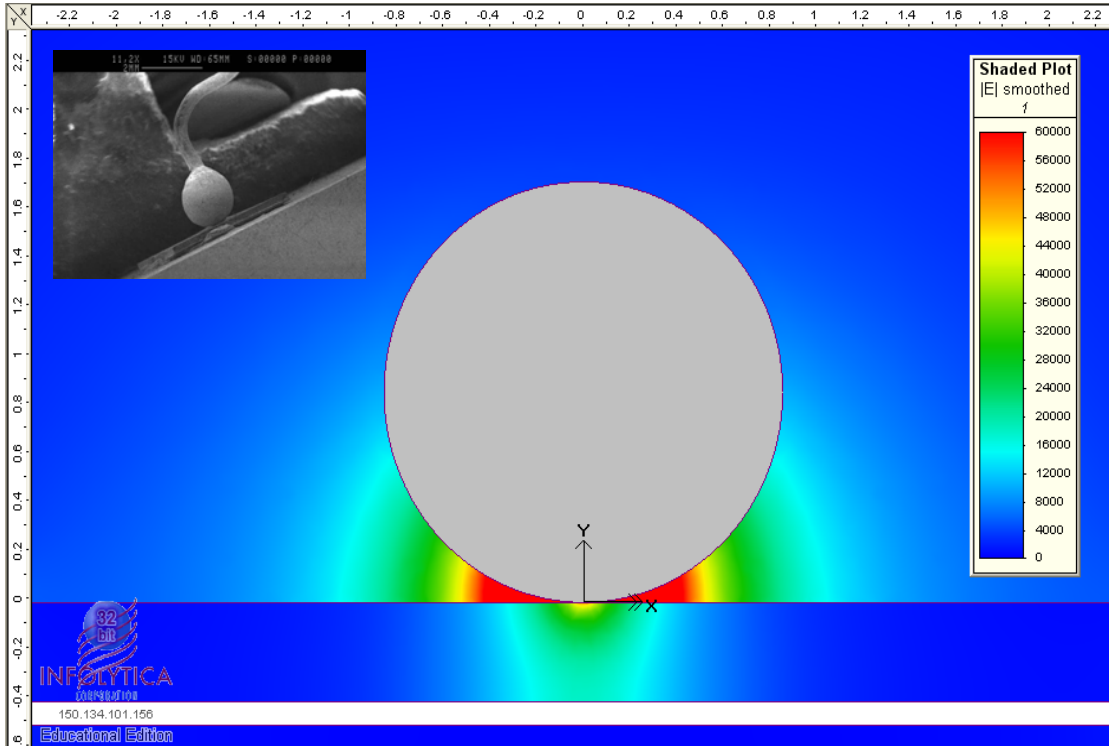


Figure 40: Elecnet simulation of electric field surrounding 1.71mm dia. contact.

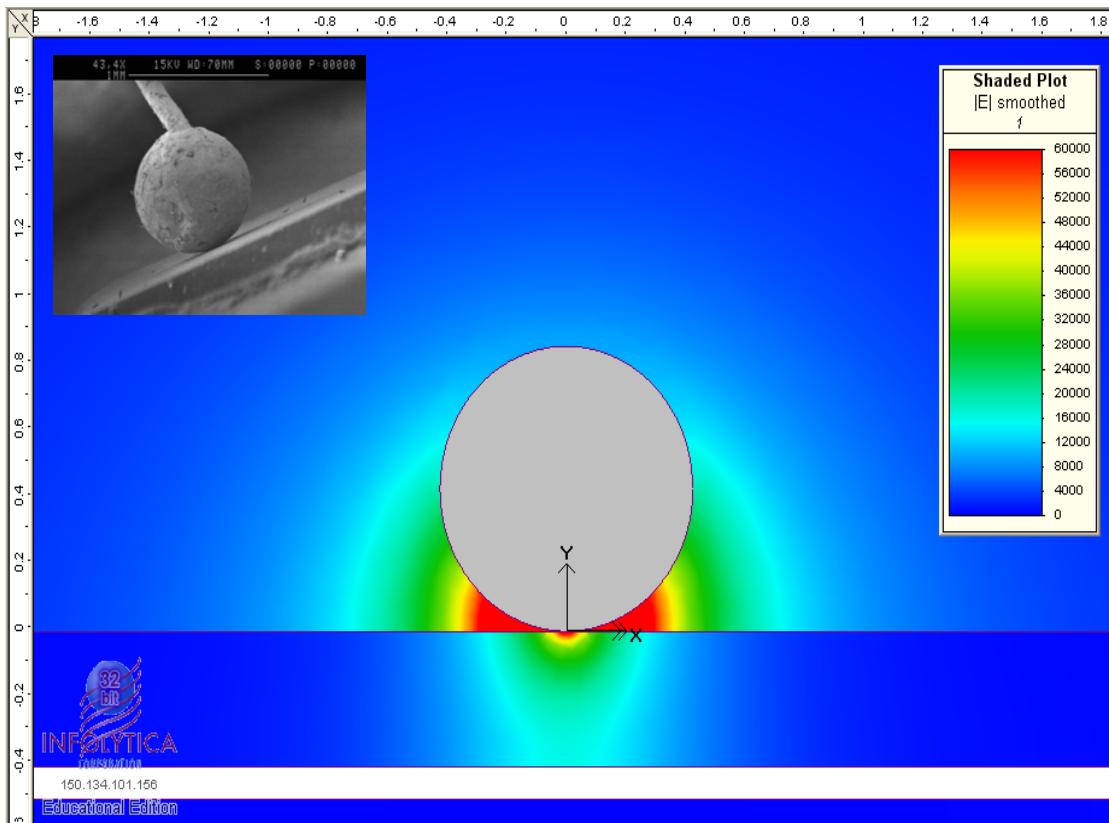


Figure 41: Elecnet simulation of electric field surrounding 0.82mm dia. contact.

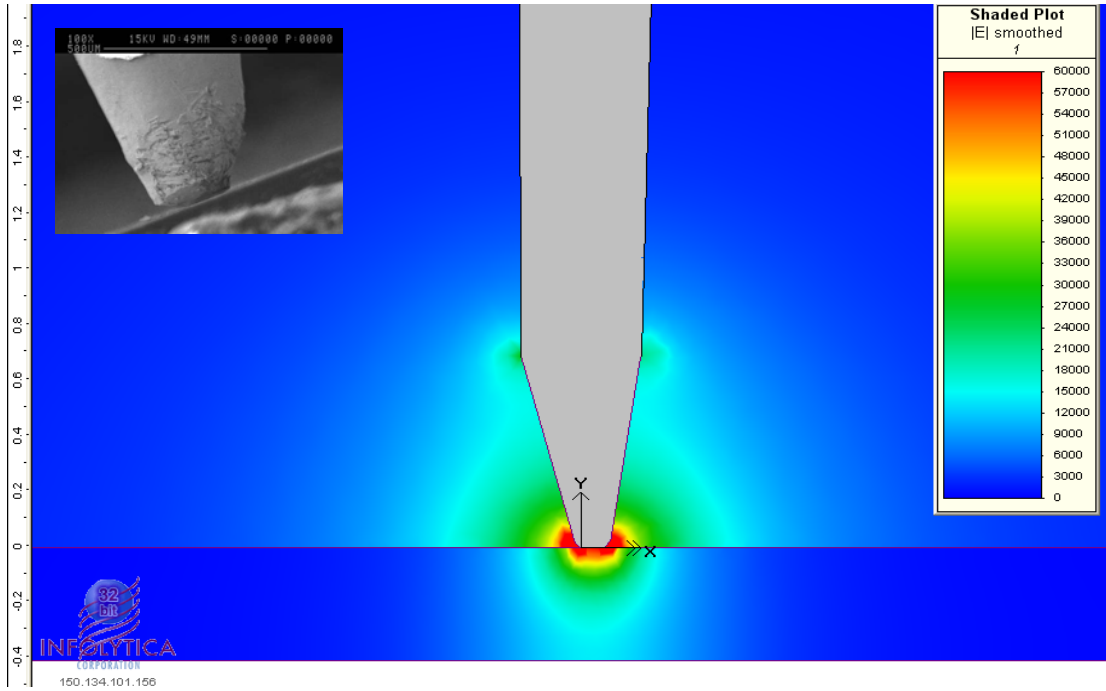


Figure 42: Elecnet simulation of electric field surrounding needle point contact.

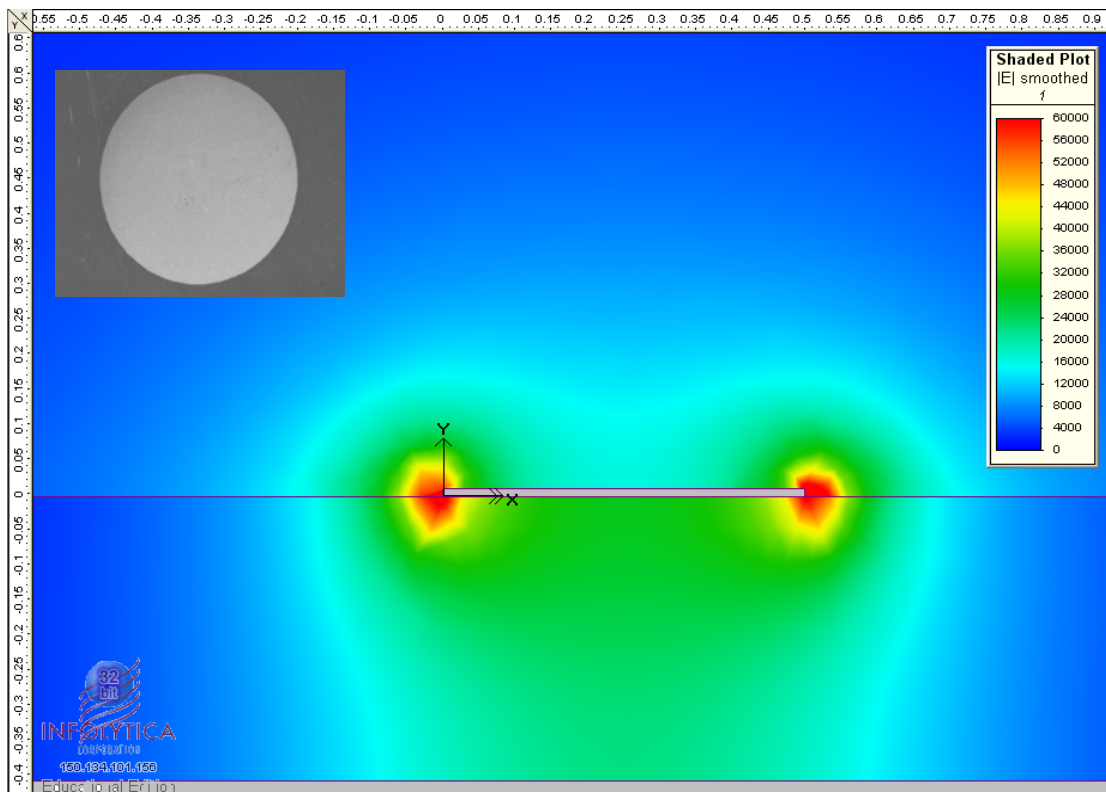


Figure 43: Elecnet simulation of electric field surrounding planar 0.5mm dia. contact.

CHAPTER FOUR

EFFECTS OF VARIED DIODE CONTACT GEOMETRIES

Five of the six different kinds of Schottky contact constructions were tested to investigate the variation of construction geometry on diode performance. A 1.71mm dia. sphere, 0.85mm dia. sphere, a needle point contact fashioned from 0.82mm dia. wire, a 0.125mm in diameter circular planar contact, and a 0.5mm dia. circular planar contact. All of these junctions were made at room temperature with no thermal effects investigated. In the forward bias regime of testing some predictions were made with the use of the Schottky diode equation and its auxiliary relationships. Typical Schottky Barrier Height values for metals on 4H - SiC may vary between values of 0.8eV to 1.7eV [22] and differences in SBH values measured have been found to vary in sample preparation procedures. The value used for the Schottky Barrier Height of Ni on 4H – SiC was determined by calculations found in referenced material. [6]:

$$\Phi_B = 1.63eV$$

The Schottky diode equation below will have the appropriate values of n, k, T, A*, A_c, Φ_B and q substituted to make some predictions as to diode performance.

$$I_F = A_c \cdot A^* \cdot T^2 e^{\frac{-q\Phi_B}{kT}} \left(e^{\frac{qV_a}{nKT}} - 1 \right)$$

I_F = Forward diode current as a function of applied voltage

V_a = Applied voltage

A_c = Area of metal in contact with semiconductor

q = Charge of the electron (**1.602176*10⁻¹⁹ Coulombs**)

T = Absolute Temperature in Kelvin (**Room Temp. 300K**)

k = Boltzmann Constant (**1.38065*10⁻²³ m²*kg/(s²*K)**)

n = Ideality Factor (**approx. = 1**)

A* = Richardson's constant for the specific material (**142 A/(cm²K²)**)

Φ_B = Barrier height of the metal semiconductor junction (**1.63eV**)

The equation of 4.1 below is the Schottky diode equation with the appropriate values substituted for the types of contact diodes constructed. The last variable of contact area varies with the types of contact geometry tested.

$$I_F = A_c \cdot 146 \cdot 300^2 e^{-63.0511} \left(e^{38.677 \cdot V_a} - 1 \right) \quad (4.1)$$

The following will represent the area of the mechanical contacts tested by use of the SEM measured contact radii, 43.25 μ m, 47.85 μ m, and 54.85 μ m, respectively. The area is shown in centimeters due to the nature of the Richardson's Constant (A*)

$$A_c = 5.8 \times 10^{-5} \text{ cm}^2 (\text{Needle})$$

$$A_c = 7.2 \times 10^{-5} \text{ cm}^2 (\text{Small_Sphere})$$

$$A_c = 9.4 \times 10^{-5} \text{ cm}^2 (\text{Lrg._Sphere})$$

Planar contact areas are calculated from equation 4.2 and the measured radii of 62.5um and 250um respectively:

$$A_c = 1.2 \times 10^{-4} \text{ cm}^2 (\text{Planar})$$

$$A_c = 6.2 \times 10^{-4} \text{ cm}^2 (\text{Lrg._Planar})$$

These values of contact area will be substituted into the equation of 4.1 to yield the graphs in Figures 44 and 45. The predicted I-V relationships resulting from 4.1 will be compared to that of the measured I-V experimental results.

Theoretically the only parameter changing from one Schottky diode to another is the contact area. Contact area affects the forward current of each diode tested. The needle point contact construction should experience the least forward current flow while the large 0.5mm diameter planar contact will experience the largest current flow due to the contact area. The values for voltages substituted into equation 4.1 are exactly the same values applied to diodes under testing. Notice that there is no resistance accounted for in the simulated modeling so it can be anticipated that there will be linear deviation from exponential current voltage relationship.

Figures 44 and 45 show the experimental results (dotted lines) in comparison with the theoretically predicted values (solid lines). The mechanical contacts are found to have turn-on voltages much lower than those predicted while the 0.125mm contact has a turn-on voltage that is much higher. Figure 45 is shown with the current scale adjusted to show how contact resistance has linearized the diode curves.

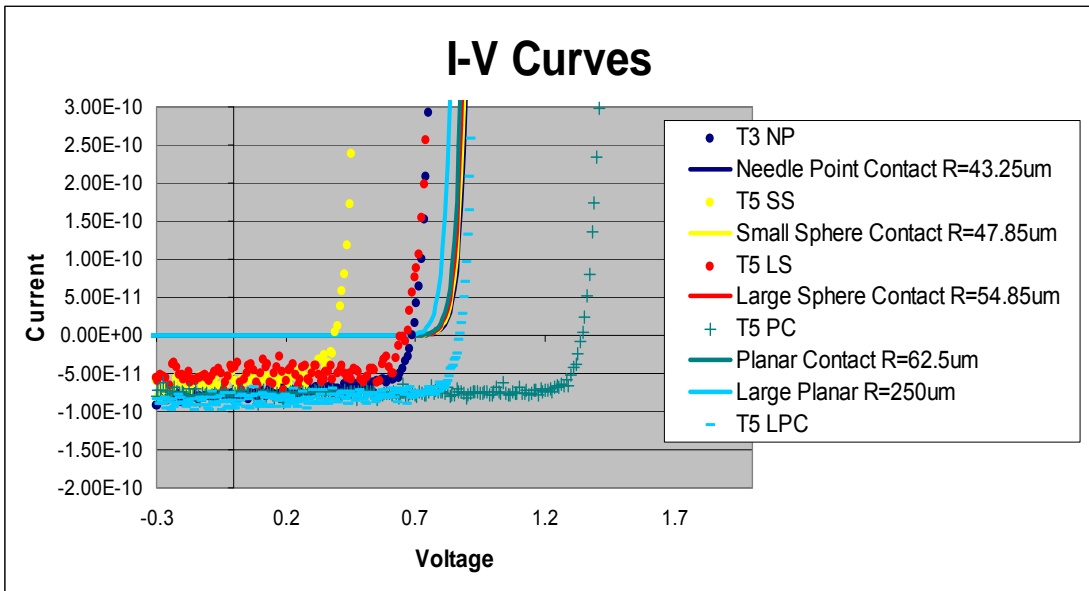


Figure 44: Experiment I-V curves zoomed to nano amps scale to show turn-on voltage.

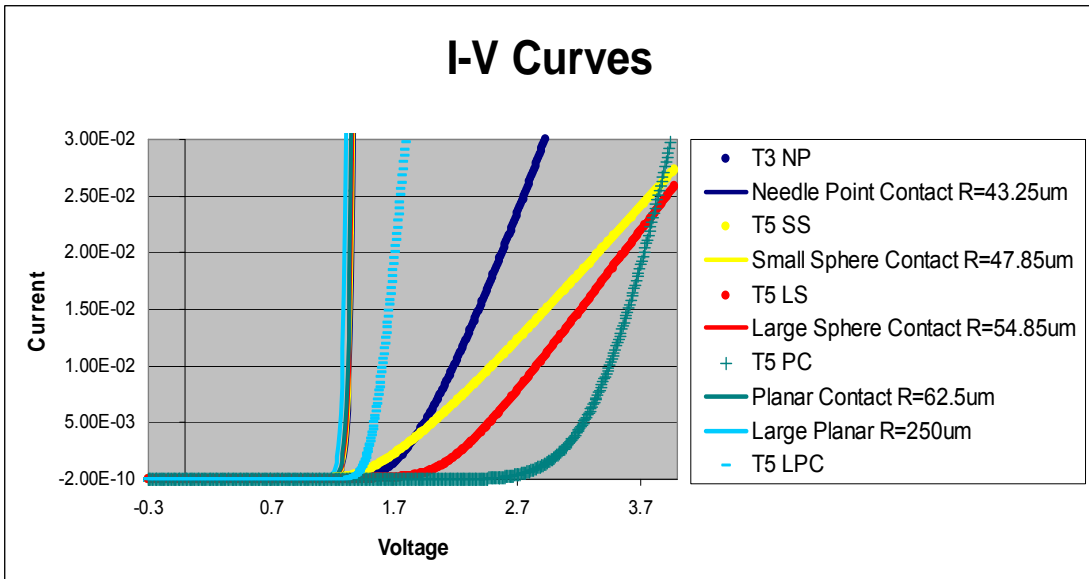


Figure 45: Experiment I-V curves zoomed to micro amps scale to show resistance.

4.1 Testing Methods for I-V Characterization

All forward bias I-V characterizations were taken with the use of the Keithley power supply that was interfaced to a PC running Labview. For each voltage applied a corresponding current measurement through the device was taken. In each measurement the mechanical Schottky contacts were attached to the Keithley by the bolt of the insulator terminal and the base of the copper substrate. Each test sample for a particular diode the mechanical contact was placed and the replaced on different parts of the SiC.

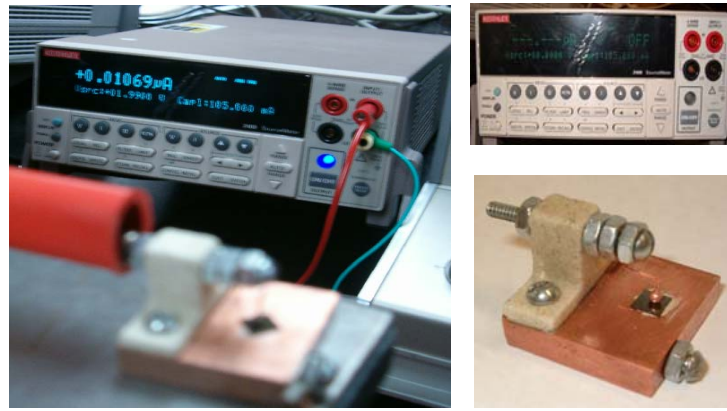


Figure 46: The test rig for the mechanical diode contacts and the Keithley curve tracer.

All planar contact plasma sputter deposited contacts were tested with a single gliding probe attached to the positive terminal of the Keithley and the copper substrate attached to the ground terminal. A different circular Schottky contact diode was selected for each test sample measured. The SiC sample is mounted to copper with silver paste.

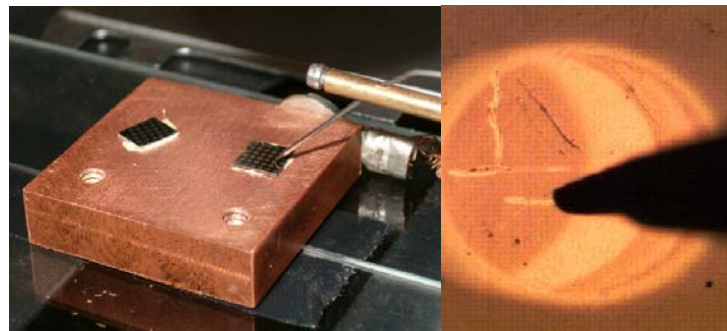


Figure 47: Planar plasma sputter deposit contacts on copper substrate with test probe.

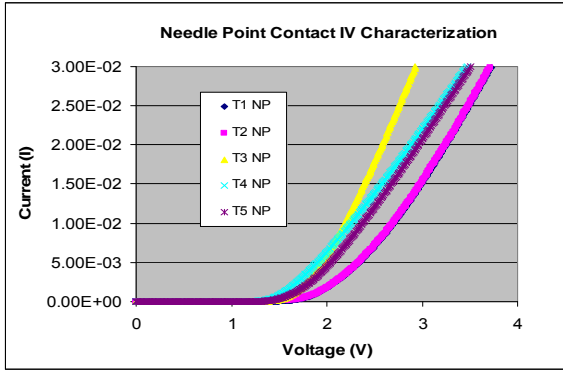
4.2 Varied Contact Geometries Forward Bias Measurements

The mechanical Schottky diode contact terminals with varied geometries of construction are tested and the I-V curves are shown in Figures 48. Immediately variation in contact resistance from test diode to test diode can be observed due to inconsistency of mechanical contact interface of metal with semiconductor. Each test sample was formed by placing the mechanical contact in a new area of the semiconductor. Though each mechanical contact tested shows variation in contact resistance a functional diode is formed on every attempt. The quality of the diode junction formed will be further investigated by examining the specific series on resistance, Schottky barrier height, and ideality factor.

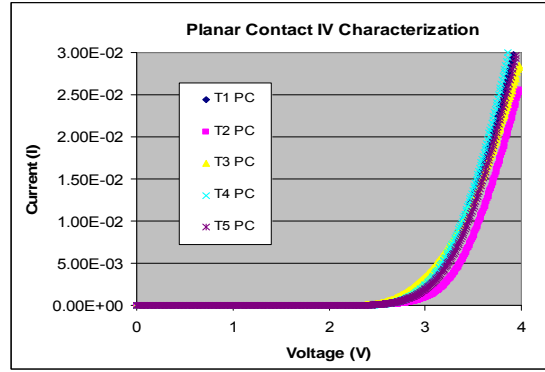
Improved methods to develop mechanical contact Schottky diodes might include systems to accurately maintain pressure and position for the mechanical contacts. All of these mechanical Schottky contact diodes tested were held in position by the nonconductive holding stand and the force exerted by the metal wire. It is anticipated from simulation that these types of mechanical contacts due to their unique shapes will have advantages in the reverse bias voltage regime by possessing higher breakdown voltages. It is also suggested by prior simulation that the planar contacts may have aggravated electric field stress at their peripheral edges.

The planar sputter deposited Schottky diode contact terminals with two varied diameters are tested and the I-V curves are shown in Figures 48 as well. The planar contacts are more consistent from test diode to test diode. A different contact was tested in each case to form the five data samples shown in the plots.

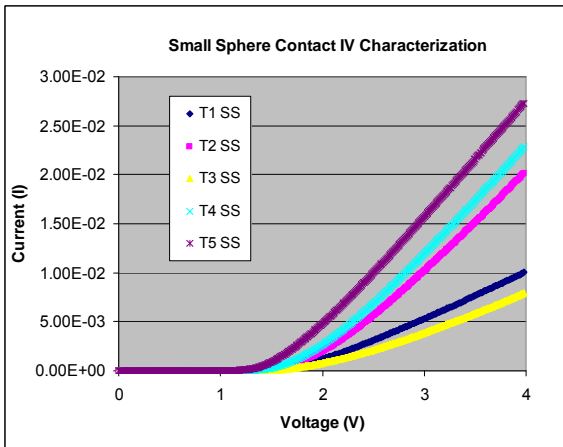
Figure 48.1 shows the data collected for the needle point contact terminal which forms a Schottky contact diode. Figure 48.3 shows the data points collected for the small sphere mechanical contact terminal ($R = 47.85\mu\text{m}$). Figure 48.5 shows the data points collected for the large sphere mechanical contact ($R = 54.85\mu\text{m}$). Figure 48.2 shows the data points collected for the planar sputter deposited metal contacts ($R = 62.5\mu\text{m}$). Figure 48.4 shows the data points collected for the large planar sputter deposited metal contacts ($R = 250\mu\text{m}$). Five separate diodes were tested and curves recorded in all cases.



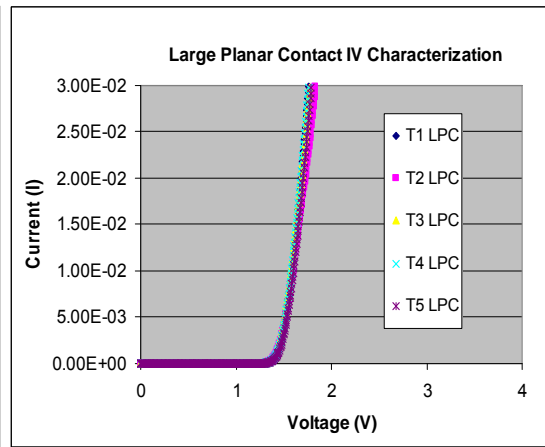
(1)



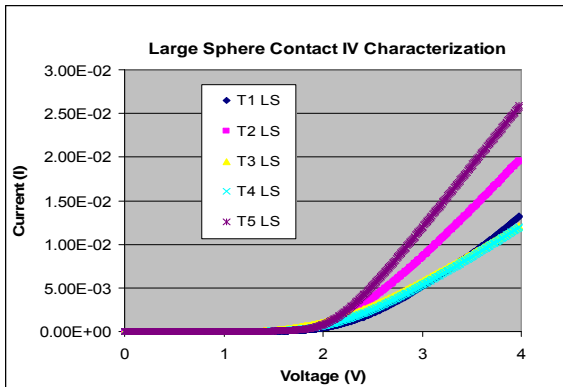
(2)



(3)



(4)



(5)

Figure 48: I-V measurements for diode contacts for various construction geometries.

4.3 Analysis of Varied Contact Geometries in Forward Bias

The evaluation of the forward bias performance of Schottky diode construction types will compare the parameters of series on resistance, Schottky barrier height, and ideality factor. Two data samples from the set of five will be chosen for analysis, the two samples are those with the highest and lowest series on resistance. These diodes were chosen for analysis because they represent the upper and lower boundaries of our data set. The series on resistance will be calculated by the slope at the linear part of the I-V curve. Two voltage and two current measurements will be taken at the end points of the slope so that a resistance may be approximated.

$$R_s = \frac{\Delta V}{\Delta I} = \frac{V_2 - V_1}{I_2 - I_1} \quad (4.3)$$

The Schottky barrier height may be solved for with the manipulation of the Schottky diode equation to form equation 4.4. The value for the initial current when zero volts is applied $I_F(0)$ is determined by the slope intercept point from log plot analysis. This value is then substituted into the equation to determine the SBH.

$$\phi_b = \left(\ln(A_c A^* T^2) - \ln(I_{f(0)}) \right) \times \frac{kT}{q} \quad (4.4)$$

The ideality factor is a measure of diode quality in comparison to a diode of ideal behavior to its actual performance. The slope determined from log plot analysis will be substituted into the equation to determine n and therefore indicate a measure of how close the test sample diode performs relative to ideal diode behavior.

$$n = \frac{q}{kT} \times \frac{1}{(slope)} \quad (4.5)$$

The calculations and analysis conducted with the aid of equations 4.3 to 4.5 has been appended to this document. The results are shown in Figures 49 and 50. A clear contrast can be seen in the different Schottky contact constructions as they vary in ideality factor, Schottky barrier height, and contact resistance.

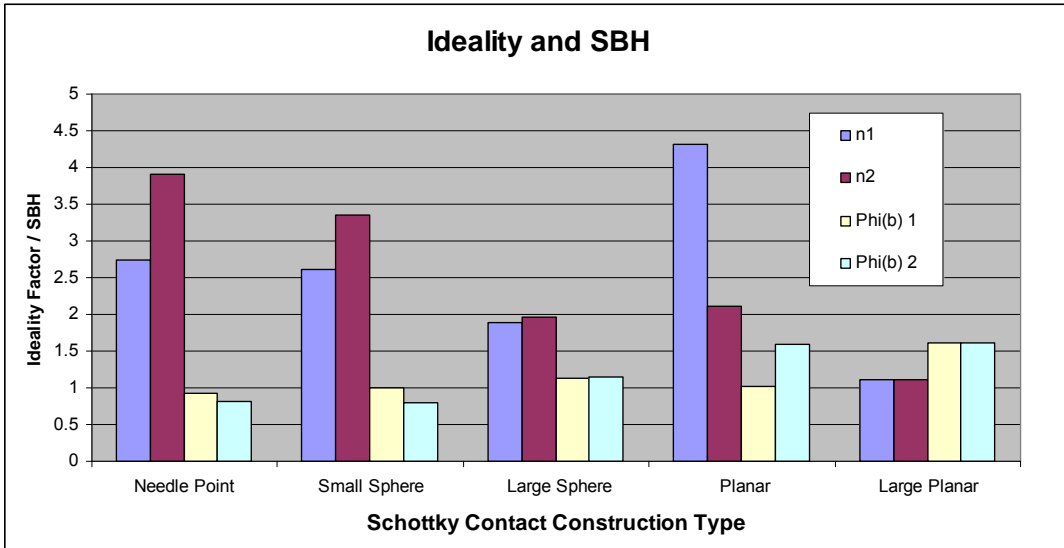


Figure 49: Ideality and SBH for varied contact terminal constructions.

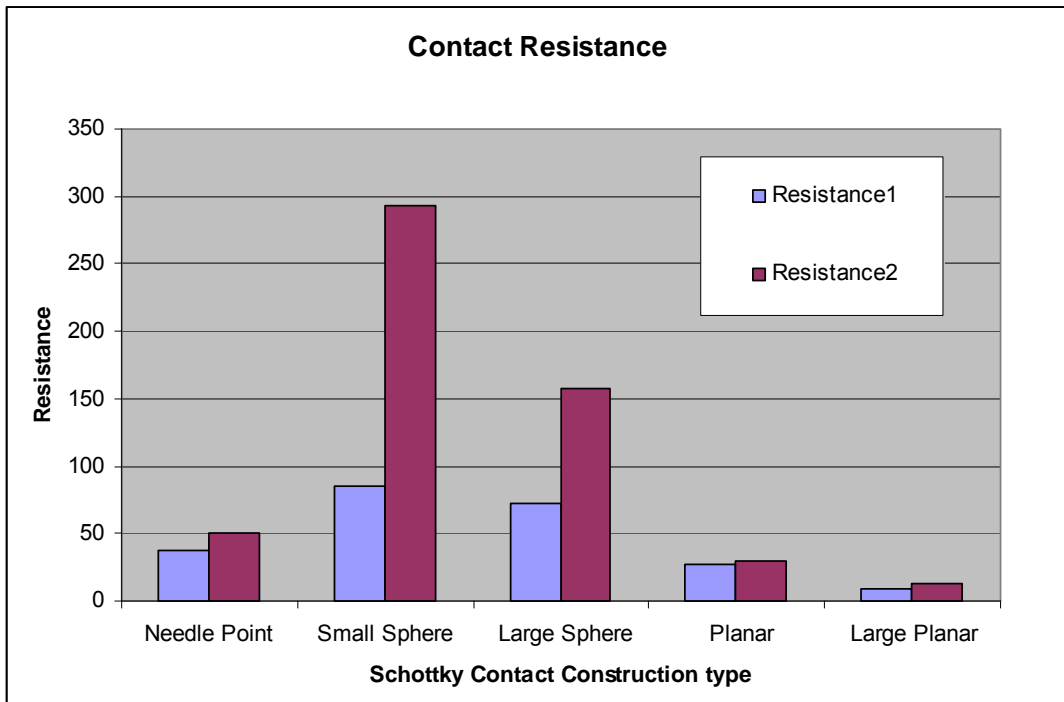


Figure 50: Contact resistance for the varied contact terminal constructions.

4.4 Measurement and Analysis of the Contacts in Reverse Bias

The modification of metal-semiconductor contact terminal construction was anticipated to have the best results for contact terminals with reduced electric field stress at edge termination as per simulations results (i.e. the large spherical contact). The reverse voltage break down potential for SiC with a specified doping concentration may be predicted by the equation (1.9) of the first chapter. When these values are substituted into the equation the SiC samples with an ideal infinite planar contact should breakdown at a voltage potential of 1350 volts.

$$V_{RB} \approx \frac{\epsilon_o \epsilon_m (E_c)^2}{2qN_d}$$

V_{RB} = Breakdown voltage at which exponential current flow will occur.

ϵ_o = Free space permittivity (**8.854e-14 F/cm**)

ϵ_m = Relative permittivity of the SiC material (**10.1**)

E_c = Breakdown voltage of the 4H SiC (**2200 kV/cm**)

N_d = Doping concentration of the surface epilayer (**1e16 cm³**)

q = Charge of the electron (**1.602e-19 Coulombs**)

The value of E_c the critical breakdown electric field strength has been modified with the equation for electric field distribution around high voltage discharge terminals. It is anticipated that large radii of curvature will allow that Schottky diode terminal to perform closer to ideal conditions, and or allow for a better estimate of when breakdown will occur. This equation allows for the inverse of the electric field distribution to be multiplied by the electric breakdown field of the material, intern predicting how much the electric field will be reduced by geometry with a given radius of curvature.

$$E_c = \left(\frac{\frac{1}{R} + 1 + \sqrt{\left(\frac{1}{R} + 1\right)^2 + 8}}{4} \right)^{-1} \times \frac{2200kV}{1cm} \quad (4.6)$$

From the initial results of Figure 51 this modeling appeared to be successful in the ability to predict approximately when electric breakdown would occur. However it was later found that the Keithley source meter could not bias the diodes to true avalanche reverse breakdown. So a Tektronix curve tracer was utilized.

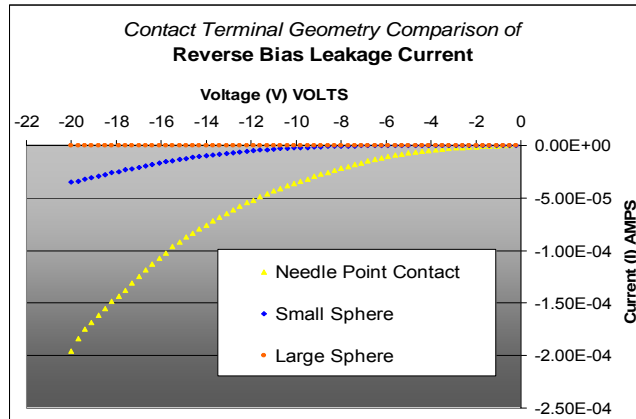


Figure 51: Preliminary reverse bias breakdown with the Keithley/Labview curve tracer.

The Tektronix 576 I-V curve tracer implemented is an instrument that allowed for testing up to 1500 volts and could source much higher currents through the diode that would be comparable to conditions in a typical Schottky diode industrial application.

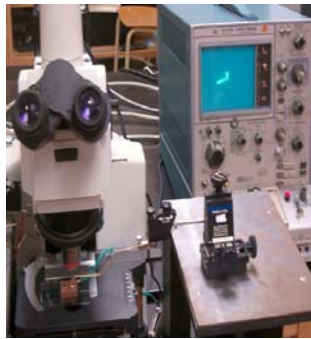


Figure 52: Tektronix 576 I-V curve tracer attached to the probe station.



Figure 53: Tektronix 576 I-V curve tracer attached to the custom diode test rig.

The results of testing with the Tektronix curve tracer are represented in the following Figure 54 oscillograms taken just before permanent device failure. Both the needle point contact and small spherical contact experienced very similar reverse avalanche breakdown potentials. As anticipated the larger spherical contact yields better performance than the other mechanical contacts this is summarized in Figure 55.

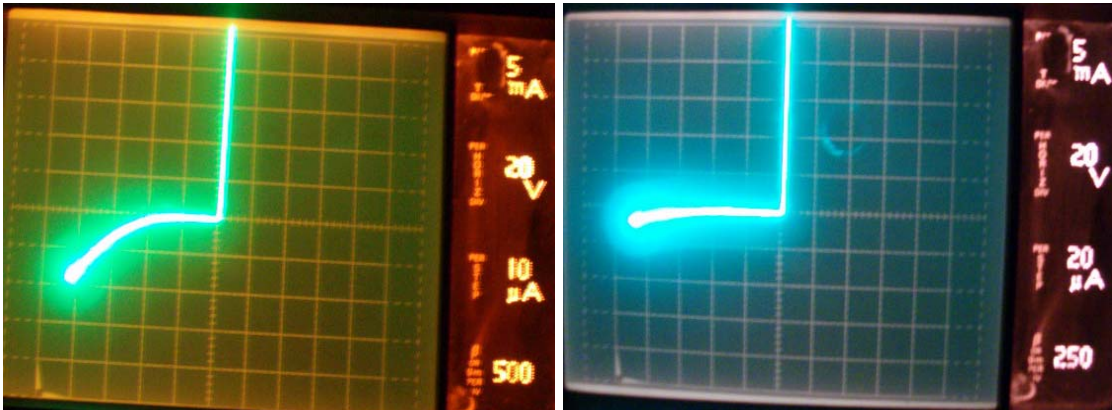


Figure 54: Breakdown for both needle point, small sphere (left) and large sphere (right).

For comparison purposes the data collected in the oscillogram curve traces are drawn in relation to each other in Figure 55. The large spherical contact (1.71mm dia.) was found to have a reverse breakdown voltage of -80 volts. The needle point and small sphere were found to begin breakdown at -40 volts with the needle point contact terminal having greater leakage currents than the spheres.

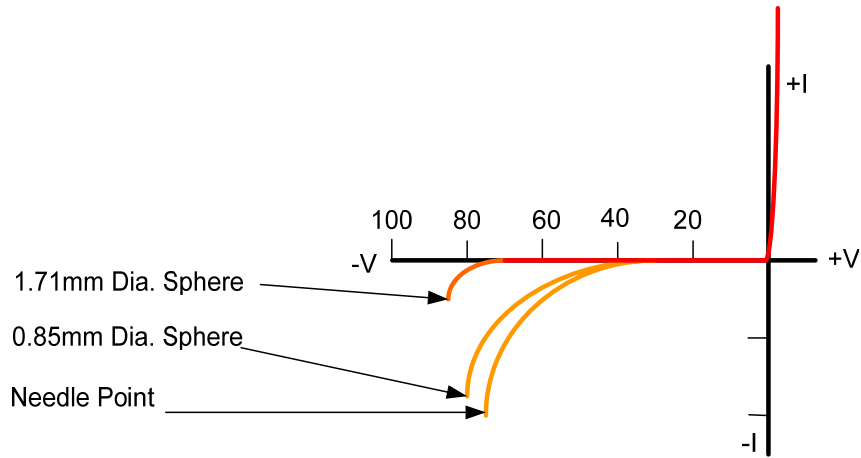
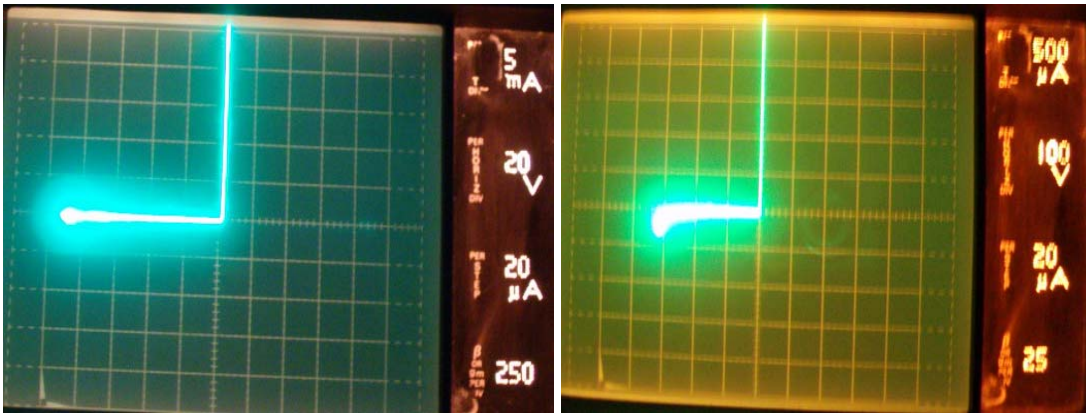


Figure 55: Summary of the mechanical contact reverse breakdown data.

Because the large spherical contact had a radius of curvature much greater than that found at the edge terminations of planar contacts. Modeling and corona discharge experiments also suggested that the larger planar contact terminals (0.5mm dia.) would have more leakage current than that of the smaller planar contacts (0.125mm dia.) However an observation counter intuitive to the simulations was made.



Figures 56: Breakdown for 0.125 planar contacts (left) and 0.5mm planar contacts (right).

The planar contacts were found to have higher reverse breakdown voltages than the spheres. For comparison purposes the curve traces are drawn in relation to each other in Figure 57 below. The large planar contact (0.5mm dia.) was found to have a breakdown voltage of -325 volts. The planar contact (0.125mm dia.) was found to have a breakdown voltage of -150 volts, twice that of the large spherical contact with a breakdown of -80V.

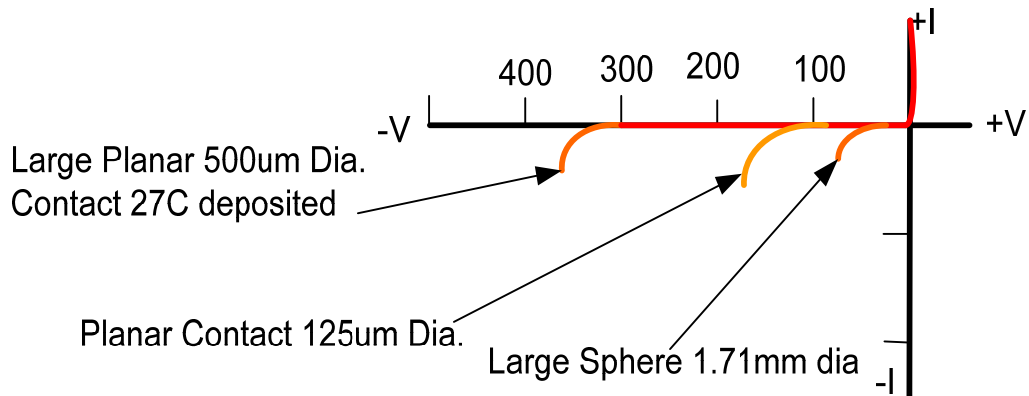


Figure 57: Summary of the planar and large sphere contact reverse breakdown data.

CHAPTER FIVE

EFFECTS OF TEMPERATURE PROCESSES

Two kinds of large planar 500 μ m diameter Schottky contact terminals were tested to investigate the variation of high temperature metal sputter deposition on diode performance. Post 600°C and 27°C metal deposit processes the diodes are tested and then thermally annealed at temperatures from 200°C to 600°C in nitrogen atmosphere to investigate how the diodes react to high temperature exposure. Points of concern are the effects generated by depositing diode material at different temperatures and how will this deposition process affect further exposures to high temperatures in the future life of the device. For each test of a diode the probe was placed on top of a random diode contact in the center of the 5x5mm sample. There were in total six separate collections of diode measurements taken post deposition, the first as deposited, the second at 200°C, third at 300°C, and so on to the last heating and test after exposure to 600°C. All heating treatments were performed in an ultra pure nitrogen atmosphere with the rapid thermal processor. Figure 58 shows a 10 second preheat to 200°C then a 10 second ramp up to the temperature of interest, followed by 10 minutes of exposure to that temperature, with a large period of cool down allowed.

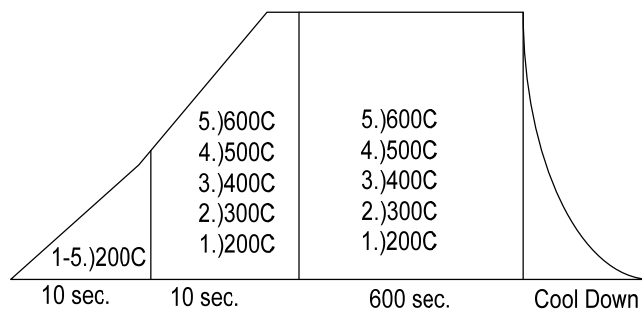


Figure 58: Thermal profile set for the Rapid Thermal Processor (RTP)

In regard to testing and analysis of the diodes, 5 diodes were tested at each of the 6 steps in the planned experiment. However one noticeable effect of heating was that some diodes exposed to high temperatures developed parasitic Schottky diode barriers. This is believed to be due to metal semiconductor compounds formed with exposure to these temperatures, this could be a topic investigated during future research.

5.1 Forward Bias I-V Measurements across Temperatures

The first set of testing was done after initial metal sputter deposit; there is a clearly observable difference shown in Figure 59 between the room temperature and high temperature deposit contacts in both the coloration of the metal and a “halo” effect that appeared around perimeter of the high temperature deposited contacts.

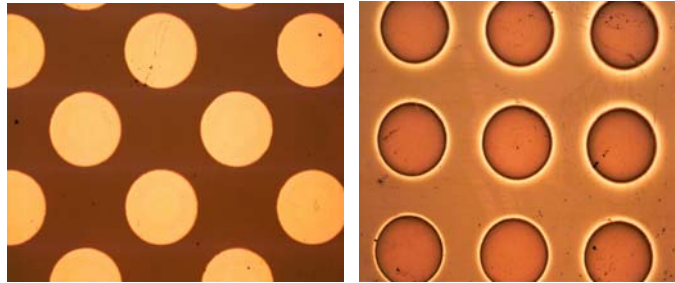


Figure 59: 27°C deposited nickel contact and 600°C deposited nickel contacts.

No Annealing

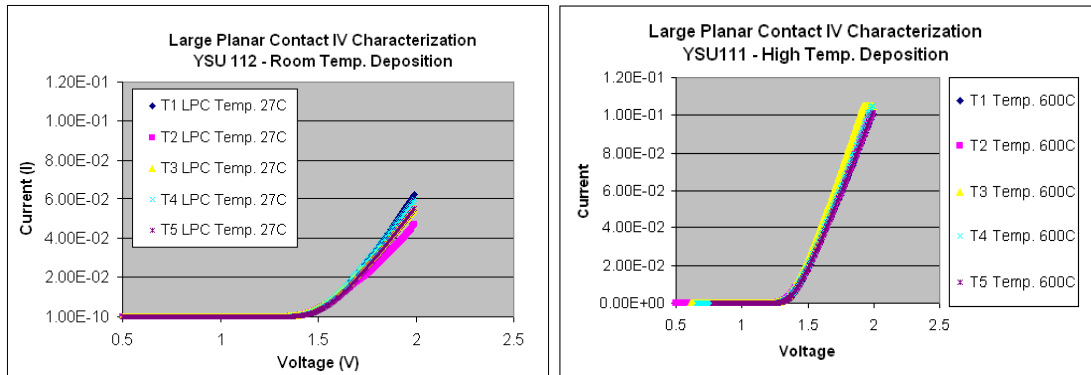
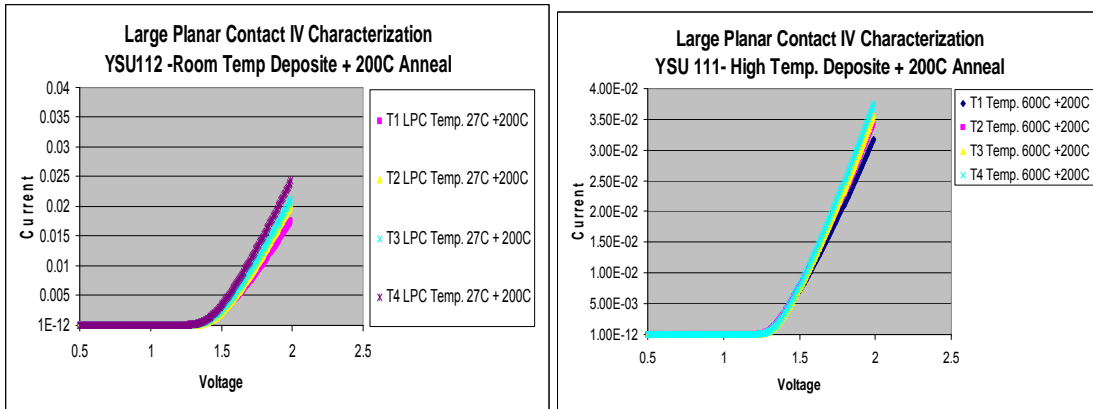


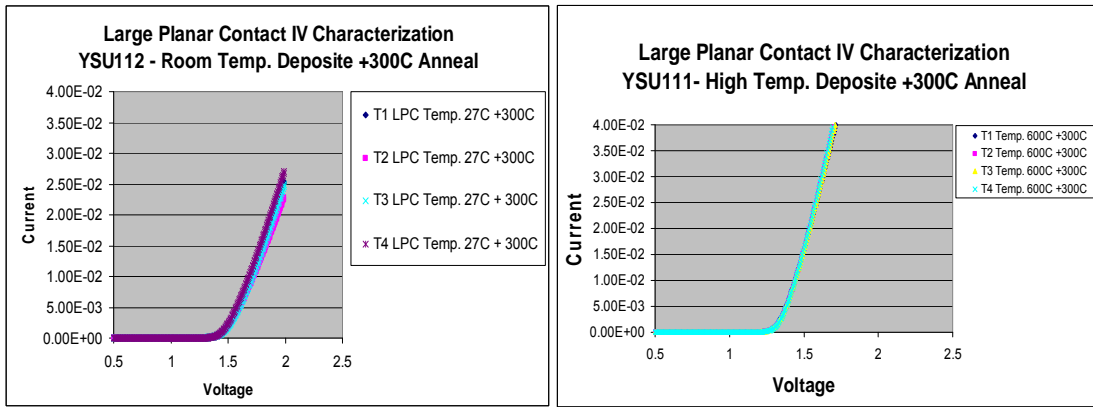
Figure 60: I-V data post deposition no annealing for samples YSU111 and YSU112.

I-V measurements before any annealing heat treatment show that the high temperature deposit contacts have a lower on-resistance. (Figure 60) The second set of testing was done after the 200°C RTP annealing process, the third set of testing was done after the 300°C RTP annealing process, and the fourth set of testing was done after the 400°C RTP annealing process (Figure 61). In all cases there is a clearly observable difference in the room temperature deposition and the high temperature deposition on-resistance.

200°C Anneal



300°C Anneal



400°C Anneal

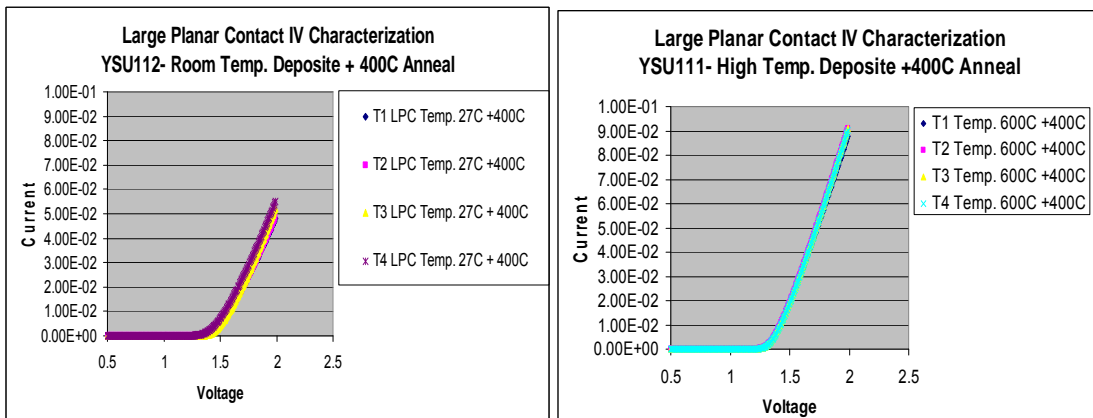


Figure 61: I-V data for 200°C, 300°C and 400°C for samples YSU111 and YSU112.

500°C Anneal

The fifth set of testing was done after the 500°C RTP annealing process. A noticeable discoloration in the 27°C deposited contacts has occurred, while the high temperature contacts continue to be visually unaffected by the heat treatments of the RTP, shown in Figure 62. From the I-V curves plotted in Figure 63 it is shown that there is now a drop in on resistance for the room temperature deposit contacts making their resistance very comparable to the low on resistance of high temperature deposited. The results of annealing the material at 500°C have shown that this temperature appears to be a critical point where interaction between the nickel contacts and SiC substrate will begin to occur.

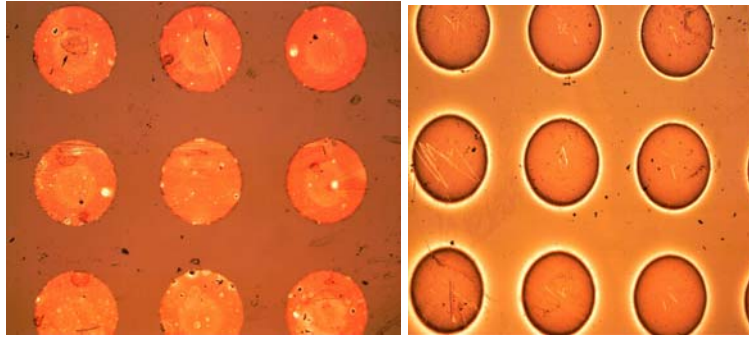


Figure 62: Discolored 27°C and 600°C deposit contact respectively post 500°C anneal.

The resistance of both room and high temperature of the Schottky contacts has become comparable at the annealing temperature of 500°C.

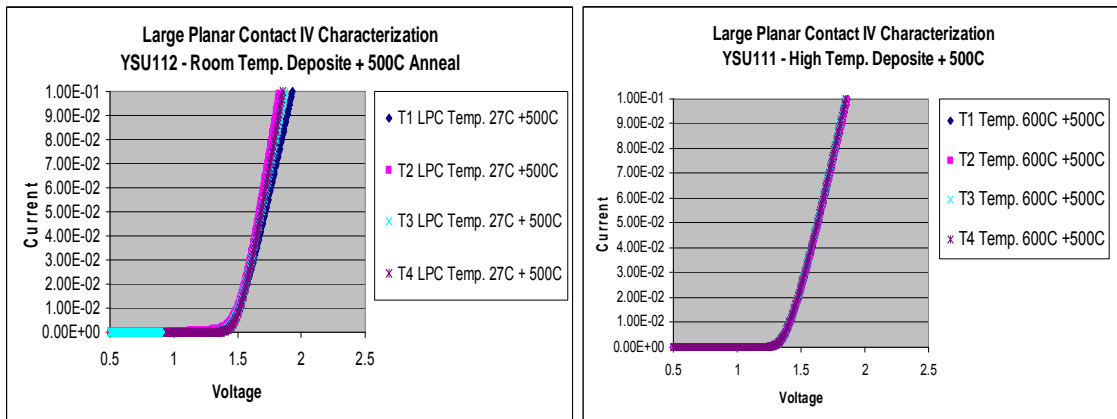


Figure 63: Data for 27°C and 600°C deposited contacts respectively post 500°C anneal.

600°C Anneal

The sixth set of testing was done after the 600°C RTP annealing process. Again noticeable darkening in color of the nickel metal to a deep blue was observed with the 27°C deposited contacts. Meanwhile the high temperature contacts continue to be unaffected by the heat treatments of the RTP shown in Figure 64. From the I-V data plotted for the diodes it is shown that the initial drop in on-resistance for 27°C deposition contacts at 500°C appears to have returned to its original resistance value. The on-resistance of the high temperature deposited diode was not affected by the exposure to the 600°C anneal. The results of annealing the diodes at 600°C illustrate how the different diode deposition temperatures will affect how a diode will handle exposure to high temperatures.

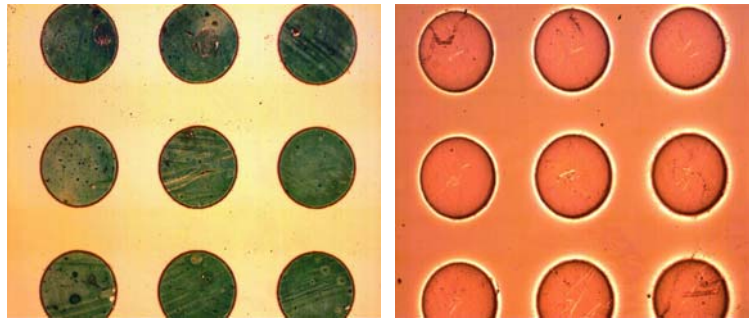


Figure 64: Color change of 27°C and 600°C unaffected contacts post 600°C anneal.

An interesting deviation in resistance occurs at 600°C in which the room temperature contact resistance noticeably increases unlike that of high temperature deposited Schottky contact diodes shown in Figure 65.

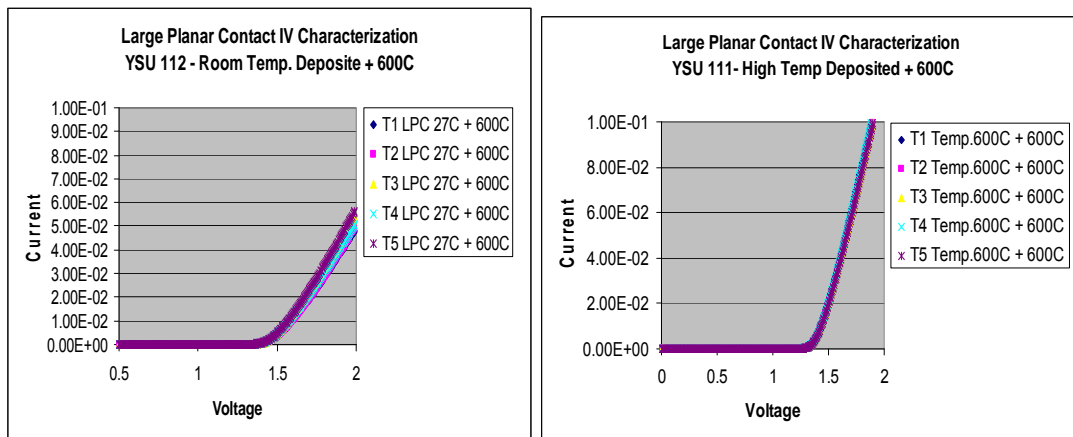


Figure 65: I-V data for the 27°C and 600°C deposited contacts post 600°C anneal.

5.2 Analysis of Temperature Effects in Forward Bias

The calculations and analysis conducted with the aid of equations 4.3 to 4.5 has been appended to this document. The results are shown in Figures 66, 67, and 68. A clear contrast can be seen between the two Schottky contact sputter deposit temperatures. The diodes differ in contact resistance, ideality factor, and Schottky barrier height. In all test cases expect for 27°C deposited contacts had a higher contact resistance except for post 500°C annealing where a drop to 3.6 ohms was recorded. At the temperature of 500°C the first discoloration of the 27°C deposited contacts was noticed. This temperature range from 400°C to 600°C may be of interest in future nickel on silicon carbide contacts.

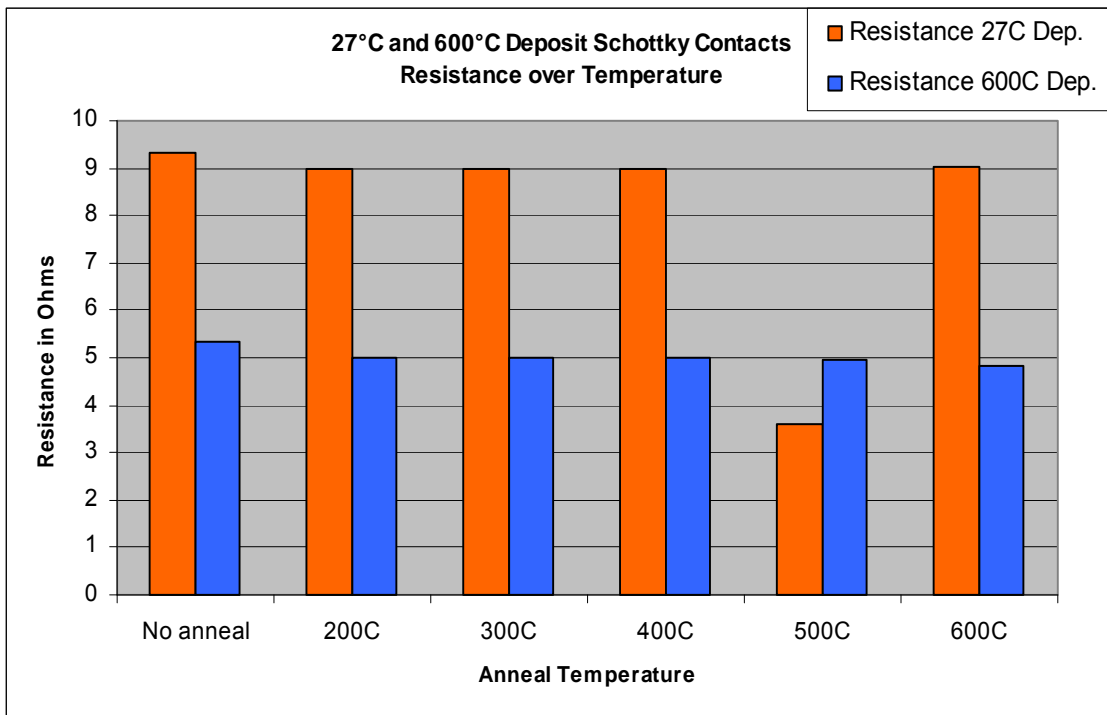


Figure 66: On-resistance verses anneal temperature for 27°C and 600°C deposit contacts.

Notable changes occurred in Schottky barrier height over the range of anneal temperatures. As the 27°C contact was heated up to 600°C the data indicates a rise in Schottky barrier height, while the ideality factor became closer to one. The 600°C deposited contact varied in value slightly but performance was consistent.

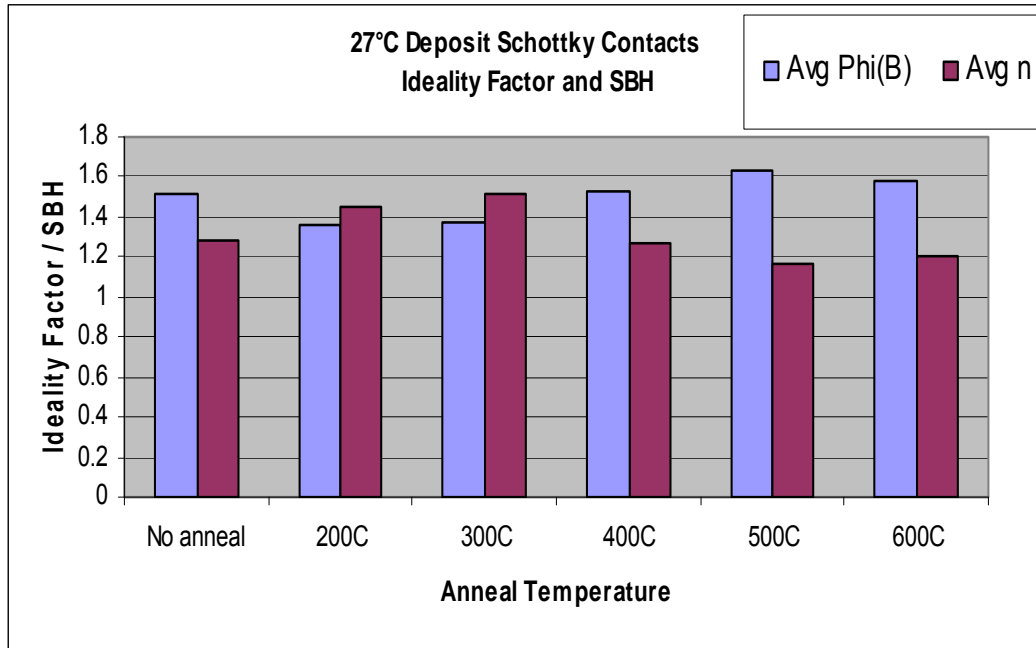


Figure 67: SBH and ideality factor verses anneal temperature for 27°C deposit contacts.

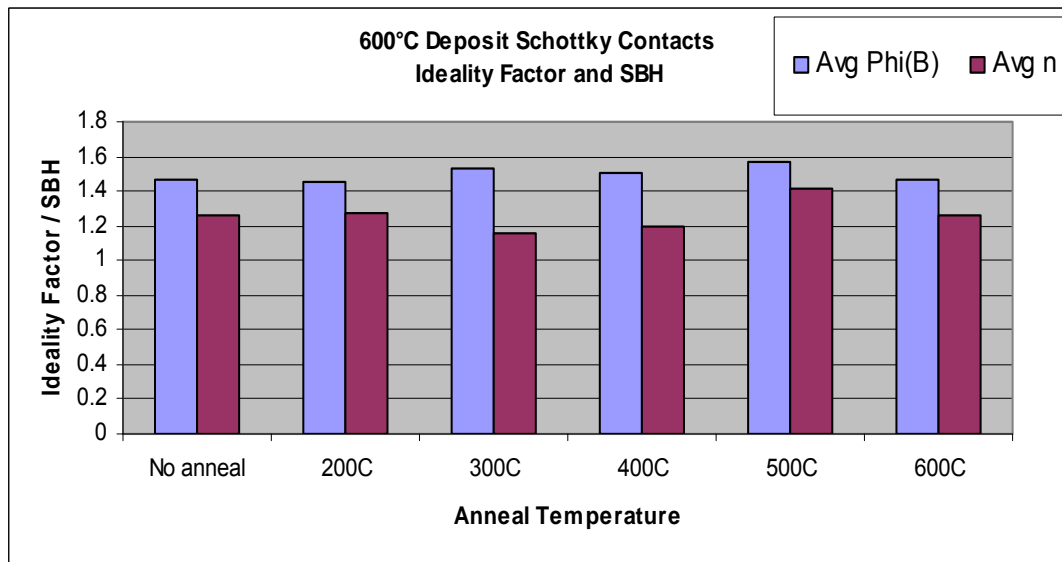


Figure 68: SBH and ideality factor verses anneal temperature for 600°C deposit contacts.

5.3 Reverse Bias I-V Measurement for Temperature Processes

The reverse voltage break down potential for the 500 μ m diameter planar nickel metal room temperature (27 $^{\circ}$ C) sputtered Schottky contact diodes on SiC were evaluated in the previous chapter. The large planar contacts deposited at with different temperatures process are contrasted in reverse breakdown voltage. Then reverse breakdown voltages of 27 $^{\circ}$ C and 600 $^{\circ}$ C diode fabrication processes are contrasted again after 300 $^{\circ}$ C annealing and finally tested after 600 $^{\circ}$ C anneal. The Tektronix I-V curve tracer is employed to measure the high voltage breakdown of the device.

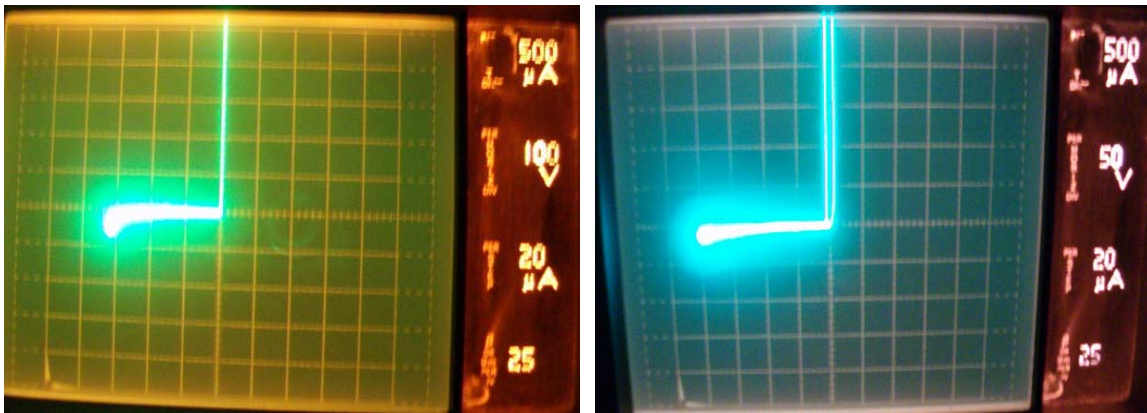


Figure 69: Breakdown 27 $^{\circ}$ C and 600 $^{\circ}$ C deposited contacts -325V and -200V respective.

Because the Tektronix curve tracer could not capture multiple I-V data points for the results shown in Figure 69 they have been drawn in Figure 70. Tests on three diodes from both 27 $^{\circ}$ C and 600 $^{\circ}$ C deposited contacts composed the data sample of Figure 70 and all six diodes for both samples measured consistently.

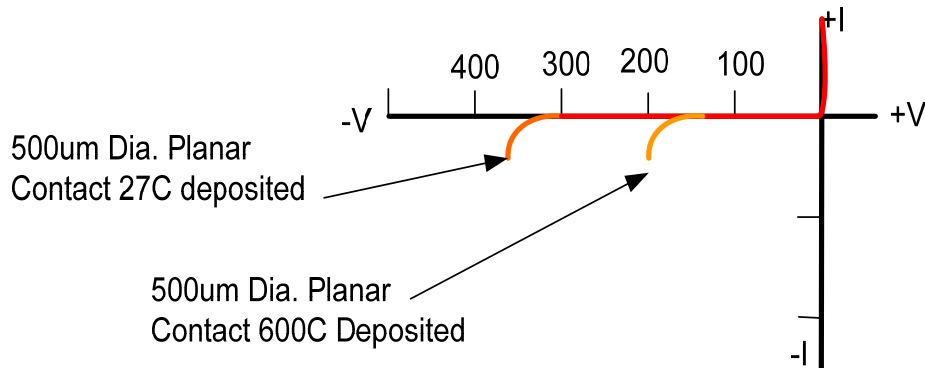
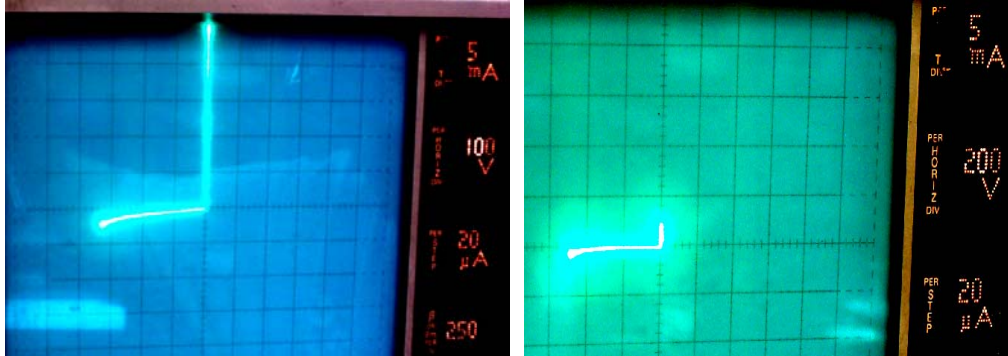


Figure 70: Summary of breakdown voltage for 27 $^{\circ}$ C and 600 $^{\circ}$ C contacts no annealing.

Diode samples were then annealed at 200°C and again at 300°C, after 300°C annealing the breakdown voltage measurements were again taken. Three breakdown measurements from each SiC sample of two different sputter deposit temperatures.



Figures 71: Post 300°C breakdown voltages planar 27°C and 600°C plasma sputter deposit contacts with -325V and -325V respectively single -500V anomaly found.

The 300°C anneal in nitrogen atmosphere has appeared to raise the breakdown voltage of the high temperature (600°C) deposited contacts, while no contacts in the room temperature (27°C) deposited contact sample appeared to greatly change their breakdown voltage. There was also one anomalous diode from the 600°C deposited sample that had a breakdown voltage of around -500 volts.

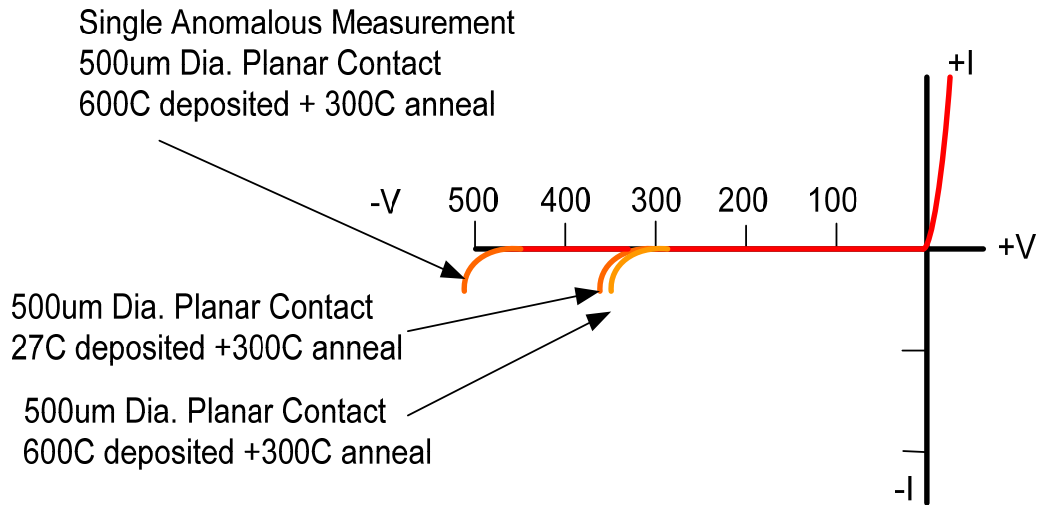
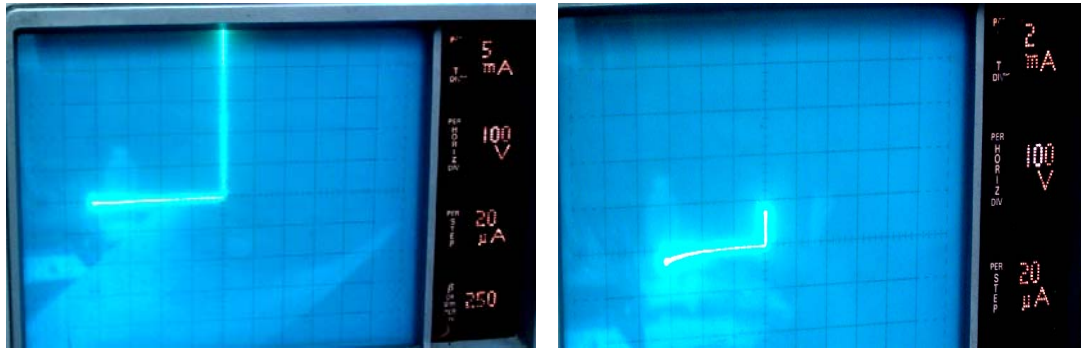


Figure 72: Summary of breakdown voltages for 27°C and 600°C contacts post 300°C.

Both diode samples were then annealed at 400°C, 500°C (some discoloration for room temperature deposition contacts), and finally at 600°C. After the final anneal the last reverse breakdown voltage measurements were taken. Again 3 measurements from each SiC sample of two different sputter deposition temperatures taken.



Figures 73: Oscillographs of 27°C deposit contact with -600V breakdown and 600°C deposit contact with -325V breakdown shown respectively, post 600°C anneal process.

The 600°C anneal process in nitrogen atmosphere markedly improved the reverse voltage breakdown of the Schottky diodes deposited at room temperature (27°C) these diodes were able to resist voltage breakdown up to -600 volts across all three test samples. This was also marked by a darkening of the metal contact terminals. The 600°C deposited contacts after 600°C anneal did not discolor or change in appearance and maintained the voltage breakdown of -325 volts that was experienced after the 300°C anneal process.

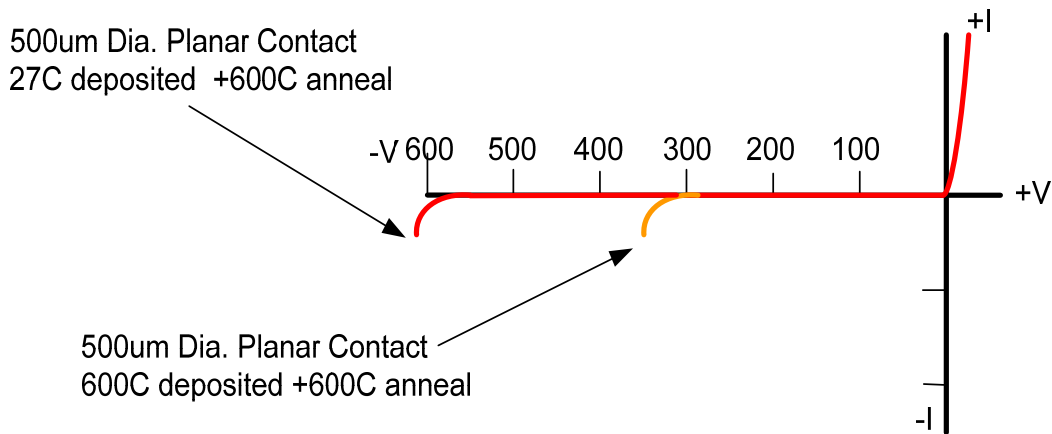


Figure 74: Summary of breakdown voltages for 27°C and 600°C contacts post 600°C.

CHAPTER SIX

CONCLUSION

Six different types of methods for producing Schottky diodes with metal-semiconductor contact terminals i.e., three mechanical contacts (needle point, small sphere, and large sphere) and three planar sputter deposition contacts (125 μm 27°C, 500 μm 27°C, and 500 μm 600°C deposit). Each different diode type was fabricated, modeled, and tested. Fabrication included the machining of test fixtures, plasma bead electro coat/polish process, vacuum chamber metal sputter deposition, and high temperature annealing processes. The modeling include predictions made by Schottky diode equations, Hertz's model for contacting sphere/plane interface, and finite element models of electric field distributions around contact terminal electrodes. Testing of the diodes involved the analysis of the devices based on their current/voltage relationships through/across the device under forward and reverse biases. The results of the research produced a contrast both qualitatively and quantitatively in the way a technique of producing a nickel on silicon carbide diode will affect the way a device will perform. Depending on the specifics of an application there may be one advantage in using a certain type of device architecture verses another. In typical power electronics applications desirable diodes have low "knee" or turn on voltages, low on resistance, and high reverse bias voltage breakdown. The mechanical contacts had low "knee" voltages but higher on resistance and lower reverse voltage breakdown. While the sputter contacts had a higher "knee" voltage but lower resistance and higher reverse breakdown.

The variation of contact geometry does make a difference in how the device will respond to applied voltage, and a larger radius of curvature was an improvement over the other mechanical contacts. Spherical contacts did not have higher reverse breakdown voltages compared to the planar contacts as was originally anticipated. It was also discovered that planar 0.5mm diameter contacts sputtered at 27°C and then annealed at 600°C had higher reverse breakdown voltages than the same 0.5mm planar contacts sputtered at 600°C then annealed at 600°C. This change in diode performance was also not anticipated.

6.1 Conclusions on Varied Fabrication Temperature Processes

The initial measurements of the room temperature 27°C deposition and the high temperature 600°C deposition shows a clear contrast in on resistance and reverse voltage breakdown. It was anticipated that as the room temperature deposited diodes were exposed to high temperatures up to 600°C that their characteristics would look more like the characteristics of those deposited at 600°C. The initial measurements and anticipated changes are illustrated qualitatively in Figure 75.

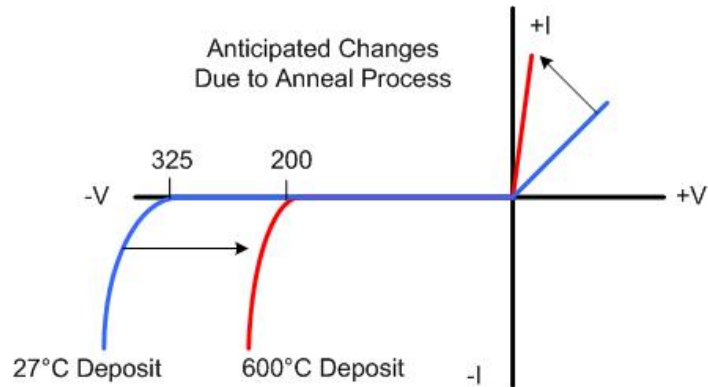


Figure 75: Initial measurements and anticipated changes due to thermal process.

Actual measured results are found to be different than what was anticipated. Upon heating the 27°C deposited contacts dramatically lower and later regain their resistance value while achieving reliable breakdown voltages of -600 volts. The 600°C deposited contacts also experienced a gain in reverse breakdown voltage post depositing annealing. These changes may be due to temperature and/or the nitrogen atmosphere surrounding the SiC sample during the anneal process.

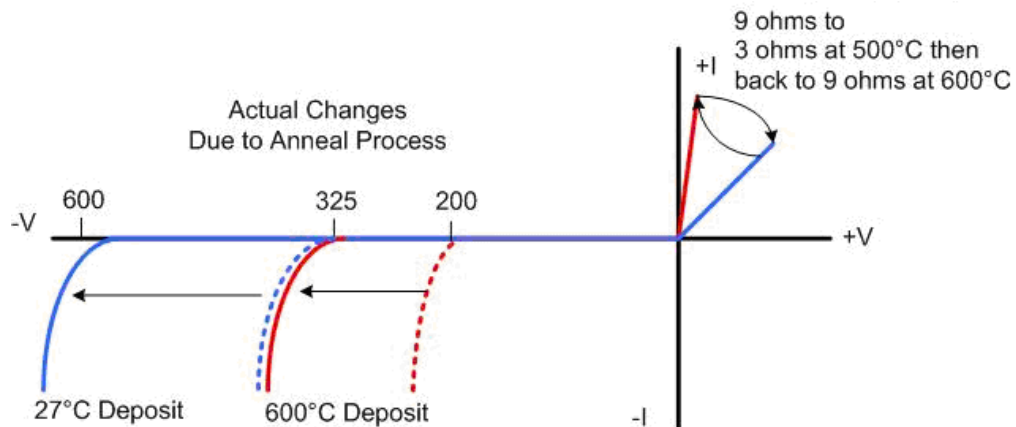


Figure 76: Initial measurements (dotted) and actual changes due to thermal process.

A summary of numerical results from the testing of temperature process effects are depicted in Table 1. These values were used to generate the depicted graphical relationships show in Figures 77 and 78.

Table 1: Summary of 27°C vs. 600°C sputter deposit contacts over anneal temperatures.

Type	0.5mm Dia. Diode						
Parameters	Temperature Exposure						
27C Sputter Deposition	No Anneal	200C	300C	400C	500C	600C	
Avg. On Resistance	9.34 Ohms	NC*	NC*	NC*	3.6 Ohms	9.0 Ohms	
Breakdown Voltage	- 325 Volts	NT*	325 Volts	NT*	NT*	600 Volts	
Avg. SBH	1.505eV	1.363eV	1.373eV	1.529eV	1.634eV	1.583eV	
Avg. n	1.27	1.45	1.51	1.26	1.16	1.12	

	Temperature Exposure						
600C Sputter Deposition	No Anneal	200C	300C	400C	500C	600C	
Avg. On Resistance	5.34 Ohms	NC*	NC*	NC*	4.9 Ohms	4.8 Ohms	
Breakdown Voltage	- 200 Volts	NT*	325 Volts*	NT*	NT*	325 Volts	
Avg. SBH	1.464eV	1.452eV	1.532eV	1.506eV	1.567eV	1.465eV	
Avg. n	1.26	1.27	1.15	1.19	1.42	1.26	

NC* - No Change no numerical value recorded
 NT* - Not Tested
 Volts*- one outlying measurement ignored

The first relationship that was not anticipated is the abrupt drop in resistance experienced by the 27°C deposited diode at 500°C. This occurred when the first sign of metal discoloration was experienced. While the 600°C deposited diodes experienced slight decreases in resistance over annealing temperatures. This resistance phenomenon may be a point of interest in the future and further analysis of the material's physical and chemical properties at this point may be studied. In all figures dots refer to points where numerical values were recorded, lines represent approximate trends.

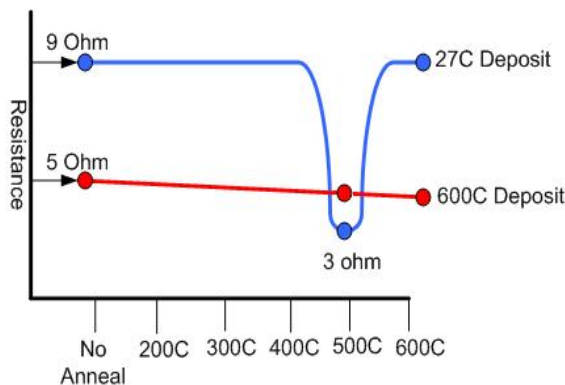
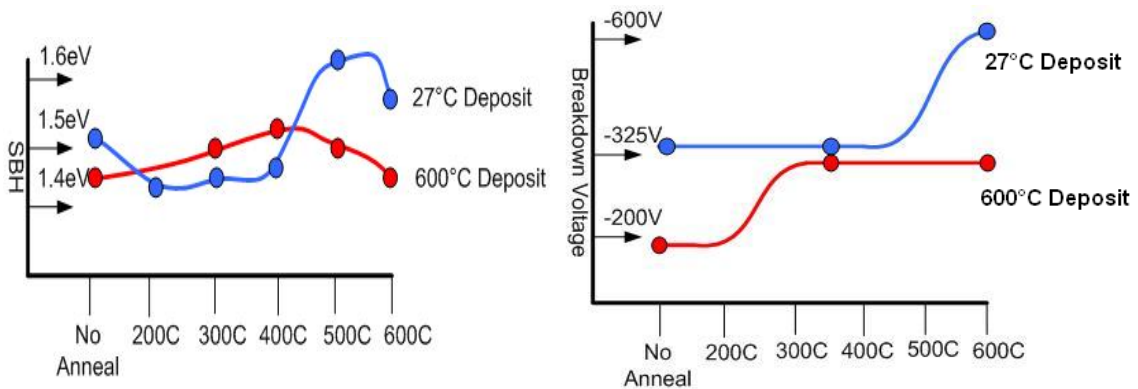


Figure 77: Changes in resistance of the samples over the annealing process.

The Schottky barrier height of a sample diode proved difficult to measure with development of parasitic secondary Schottky barriers at high temperatures. Small deviations in the experimental setup can also make it difficult to discern the accuracy of measurements. After averaging several SBH values for multiple values a trend did emerge. The SBH of the 600°C deposited diodes tended to stay around the 1.5 eV level. There did appear to be a definite increase in SBH as the 27°C deposited contacts were annealed over the range of temperatures. A maximum measured value of 1.667eV for the 27°C deposited diodes was recorded after 500°C anneal. The most dramatic contrasting observation of the temperature process experiments was the significant increase in breakdown voltage experienced by the two SiC samples. The 600°C deposited contact experienced an increase in reverse breakdown voltage after annealing at 300°C, however at this test interval one anomalous diode that with stood -600 volts breakdown was recorded. The 27°C deposited diodes maintain a -325 volt breakdown voltage until tested after 600°C (Note: No reverse breakdown voltage measurements were taken at 500°C when discoloration was first observed). After 600°C anneal the nickel metal contacts had turned a deep blue color and consistently tested to have breakdown voltages of -600volts. Figure 78 qualitatively illustrate the changes above. It may also be interesting to thermally process mechanical (pressure) contacts to see if changes in measurement consistency, on resistance, SBH, and reverse voltage breakdown would be experienced.



Figures 78: Changes in SBH and reverse breakdown voltage with annealing respectively.

6.2 Conclusions on Varied Contact Terminal Geometry

A comparison of the various diode construction types are shown in Table 2 with the various parameters of diode operation. The mechanical contacts typically have high resistances compared to the sputtered planar contacts, this is attributed to the fact that the mechanical contacts have smaller contact areas and are only resting on the surface of the substrate. The SBH was also much lower and the depletion region was of a lesser volume for the mechanical contacts than for planar contacts, this is related to the inconsistency of the metal-semiconductor contact and interface area. The observations made about reverse breakdown voltage had a discrepancy in what was predicted to be a better contact with electric field simulation. It was anticipated that contact terminal experiments would mimic the results from the corona discharge experiment.

Table 2: Summary of data collected on Schottky contact diode terminal construction.

	Diode Construction Types				
	<i>Needle Point</i>	<i>Small Sphere</i>	<i>Large Sphere</i>	<i>Planar</i>	<i>Lg. Planar</i>
Avg. On Resistance	43 ohms	189 Ohms	114 Ohms	28 Ohms	10 Ohms
Breakdown Voltage	-40 Volts	-40 Volts	-80 Volts	-150 Volt	-325Volts
Avg. SBH	0.86eV	0.89eV	1.13eV	1.42eV	1.61eV
Avg. n	3.3	2.9	1.9	3.2	1.1

It is suspected that the inconsistent quality of the mechanical contact reduced the depletion region that forms beneath the metal, leading to a considerably smaller volume of unknown geometric configuration. The planar contact with a larger area and uniform metal-semiconductor contact interface develops a defined depletion region which has the ability to with stand much higher voltages, despite electrical stress at edge terminations.

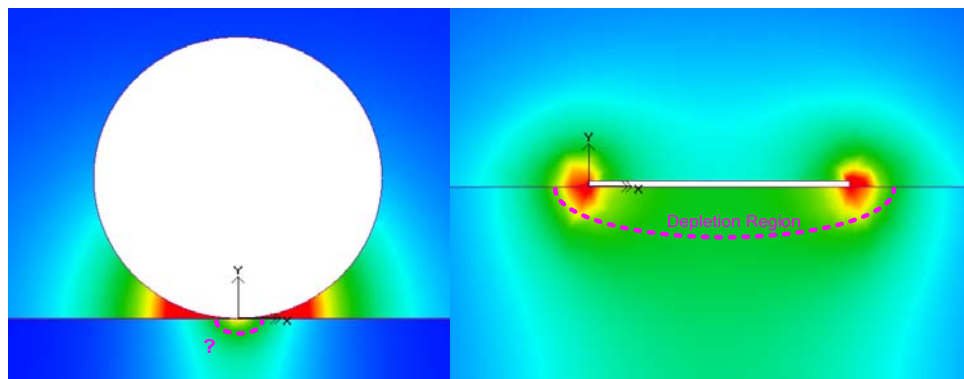


Figure 79: Simulations with dotted line show a questionable volume of depletion region.

6.3 Recommendations for Further Studies

An untested method for the manufacturing of spherical Schottky contacts based on this research may achieve the performance anticipated in simulations see Figure 80. By utilizing the following design, the geometry of the depletion region that forms around the contact may be engineered in shape. Spherical Schottky contacts could regain their proven beneficial corona discharge performance once the depletion region is designed to withstand greater than 3kV/mm electric field stress. The processes of Figure 80 are hybrid designs that combine the benefits of spherical and planar contacts of the research. By etching the semiconductor substrate and sputter depositing metal, the metal-semiconductor interface would be far more controlled. This allows for the geometry of the depletion region around the spherical contact to be engineered with specific dimensions. A secondary method that would have an advantageous geometry would be to create a hemispherical etched substrate depositing metal on top. Further research would combine the improvements demonstrated during temperature processes with the proposed contact terminal designs. Experiments would be vary temperature processing while sputter depositing metal on the etched spherical contacts and anneal the proposed contacts post deposition. Having the metal contact deposited inside a well or on top of a hemispherical substrate could result in some side effects from the unusual thermal profile. The mechanisms of how temperature processes result in higher reverse breakdown voltage should also be a topic to further investigate.

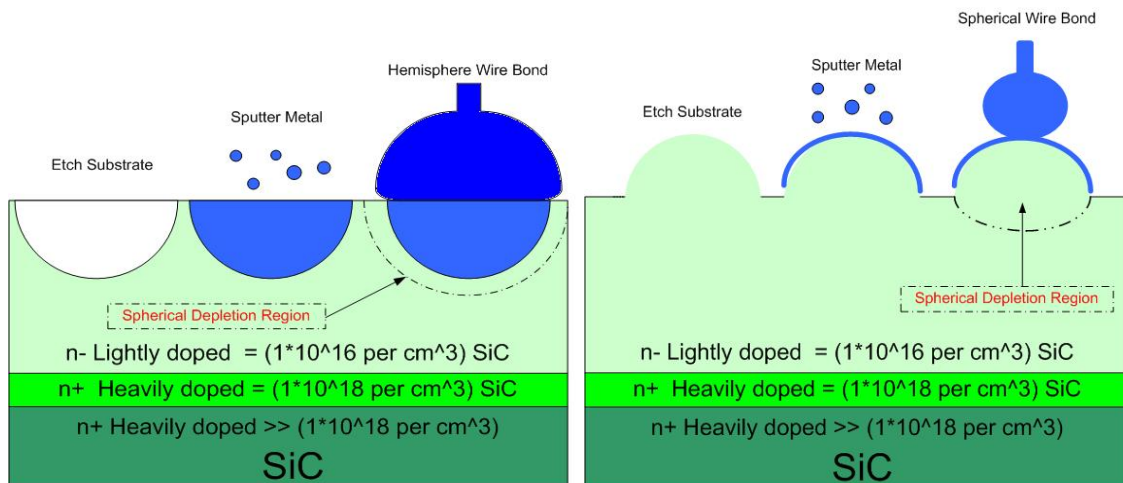


Figure80: Untested design concept for spherical metal–semiconductor contacts.

REFERENCES

- [1] B. Ozpeneci, L.M. Tolbert, "Comparison of Wide –Bandgap Semiconductors for Power Electronics Applications" Oakridge National Laboratory, pg. 6-10 December 12, 2003
- [2] Hyperphysics "Fermi Levels" Copyright 2005 Georgia State, Retrieved: June 1, 2007 <http://hyperphysics.phy-astr.gsu.edu/hbase/solids/fermi.html>
- [3] Tesfaye Ayalew "Dissertation Tesfaye Ayalew - 3.1.6.2 Schottky Contact," Retrieved: June 1, 2007 <http://www.iue.tuwien.ac.at/phd/ayalew/node56.html>
- [4] "Chapter 3: Metal Semiconductor Junctions" Retrived: June 1, 2007 Copyright 2004 B. Van Zeghbroeck http://ece-www.colorado.edu/~bart/book/book/chapter3/ch3_3.htm
- [5] Ben G Streetman "Solid State Electronic Devices" 3rd Edition, Prentice Hall Series in Solid State Physical Electronics. ISBN 0-13-822941-4 Date: pg. 200 -205 December 1990
- [6] Tesfaye Ayalew, "Dissertation Tesfaye Ayalew - 2.1.2 Electrical Properties" Retrieved: June 1, 2007 <http://www.iue.tuwien.ac.at/phd/ayalew/node21.html>
- [7] Seong- Jin Kim "Breakdown Voltage Characteristics of SiC Schottky Barrier Diode with Aluminum Deposition Edge Termination" Woosuk University Jounel of the Korean Physical Society pp. S768 – S773 Vol 49 December 2006
- [8] B. Van Zeghbroeck "Chapter 4: PN Junctions 4.5.1 General Bearkdown Characteristics" Retrived: June 1, 2007 Copyright 2004 http://ecewww.colorado.edu/~bart/book/book/chapter4/ch4_5.htm
- [9] Ravi K. Chilukuri and B. Jayant Balagia, "High Voltage Ni/4H-SiC Schottky Rectifiers" North Carolina State University. pg. 161-164 IEEE article 1999
- [10] Marc C. Tarplee "Design Rules for Field Plate Edge Termination in SiC Schottky Diodes" IEEE Transactions on Electron Devices Vol 48. No. 12, pg. 2659-2654 December 2001
- [11] L. Scaltrito, S. Porro "Correlation between defects and electrical properties of 4H-SiC based Schottky diodes", Department of Physics at the University of Bologna, Italy. pg. 1-3
- [12] Q. Zhang and T.S. Sudarshan, "The Influence of High Temperature Annealing on SiC Schottky Diode Characteristics" Journal of Electronic Materials pg 1446 Vol. 30 No. 11 2001
- [13] D.J. Twitchen, and A.J. Whitehead, "High Voltage Single-Crystal Diamond Diodes" IEEE Transactions On Electron Devices pg 826-828 Vol. 51 No. 5 May 2004.
- [14] Gheorghe Brezeanu, Marian Badila and research associates, "Accurate Modeling and Parameter Extraction for 6H-SiC Schottky Barrier Diodes (SBDs) with Nearly Ideal Breakdown Voltage" IEEE Transactions On Electron Devices pg 2148-2153 Vol 48 No. 9 September 2001
- [15] North, William "High Power Microwave Tube Transmitters Chapter 7" Los Alamos National Laboratory pg 58-60 1994.
- [16] "MIT Physic Lecture Electricity and Magnetism -06- High Voltage Breakdown" Google Video Retrieved: July1, 2007 <http://video.google.com/videoplay?docid=2984712352012344369>

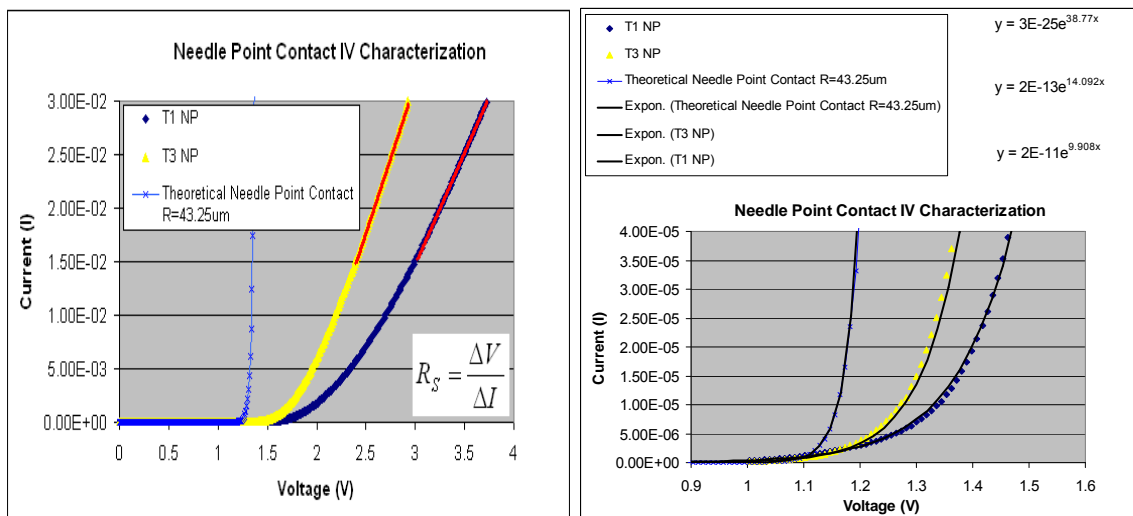
- [17] F. Yang N.E. Jewell-Larsen, D.L. Brown K. Pendergrass, D.A. Parker, I.A. Krichtafovitch*, A.V. Mamishev "Corona Driven Propulsion for Cooling Electronics" University of Washington, Seattle, WA 98105, USA, pg 1-4 2003
- [18] A. Monnier B. Froidurot , C. Jarrige , R. Meyer, P. Teste "A mechanical, electrical, and thermal coupled-field simulation of a sphere-plane electrical contact" pg 224-230 IEEE 2005.
- [19] Ch. Poulain, L. Boyerl, Ph. Sainsot, M.H. Maitournamd, F. Houz, M. Leclercqz., J.P. GuCry, J.P. Charpentier "Experimental and Theoretical Study of Creep Effects in electrical Contacts" pg 147-151 IEEE 1995
- [20] Dr. T. N. Oder, "Wide Band Gap Semiconductor Group at YSU"
Retrived: July 1, 2007 <http://www.ysu.edu/physics/toder/LAB/index.html>
- [21] Tipler, Paul A. and Llewellyn, Ralph A., Modern Physics, 3rd Ed., W.H. Freeman, 1999.
- [22] Fanny Dahlquist. "Junction Barrier Schottky Rectifiers in Silicon Carbide," KTH, Royal Institute of Technology, Department of Microelectronics and Information Technology Stockholm, 2002 pg 20-22

APPENDIX

APPENDED CHAPTER FOUR ANALYSIS

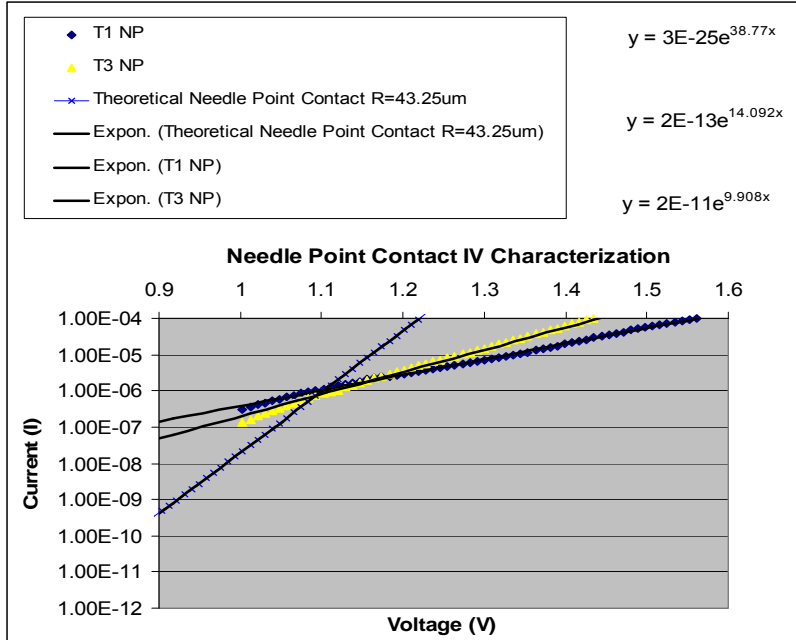
1. Needle Point Contact

From the linear slopes of the IV curves the on resistance for the needle point contact Schottky diodes could be determined. The resistance determined from IV measurements put into equation 4.3 for test diode samples T3 and T1 are shown respectively.



$$R_s^{T3} = \frac{V_2 - V_1}{I_2 - I_1} = \frac{2.929 \text{ V} - 2.407 \text{ V}}{0.029 \text{ A} - 0.015 \text{ A}} = 37.28 \Omega$$

$$R_s^{T1} = \frac{V_2 - V_1}{I_2 - I_1} = \frac{3.721 \text{ V} - 3.019 \text{ V}}{0.029 \text{ A} - 0.015 \text{ A}} = 50.14 \Omega$$



NP Natural Log

T3# $\ln(y) = 14.092 \cdot x - 29.240$

T1# $\ln(y) = 9.908 \cdot x - 24.635$

The exponential curve fits plotted in log scale allow for a slope and intercept point for the diode current to be determined. These values are put into equations 4.4 and 4.5 to determine the Schottky barrier height and the ideality factor for the two contacts show below for contact terminals T3 and T1 of the needle point mechanical Schottky contact.

$$\phi_b^{T3} = \left(\ln(5.8 \times 10^{-5} \cdot 146 \cdot 300^2) + 29.240 \right) \times \frac{kT}{q} = 0.9275 eV$$

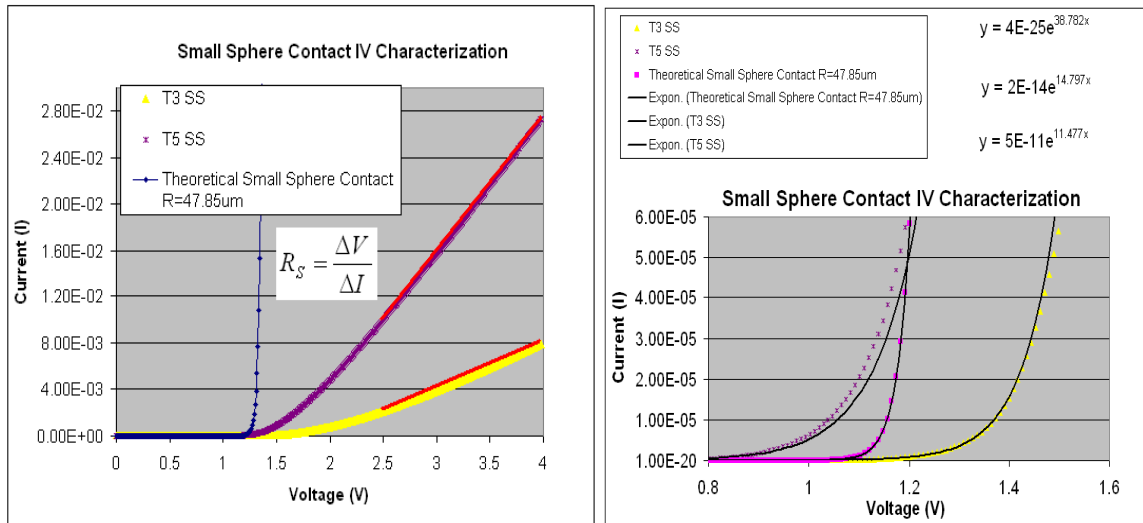
$$n^{T3} = \frac{q}{kT} \times \frac{1}{14.092} = 2.744$$

$$\phi_b^{T1} = \left(\ln(5.8 \times 10^{-5} \cdot 146 \cdot 300^2) + 24.635 \right) \times \frac{kT}{q} = 0.8085 eV$$

$$n^{T1} = \frac{q}{kT} \times \frac{1}{9.908} = 3.903$$

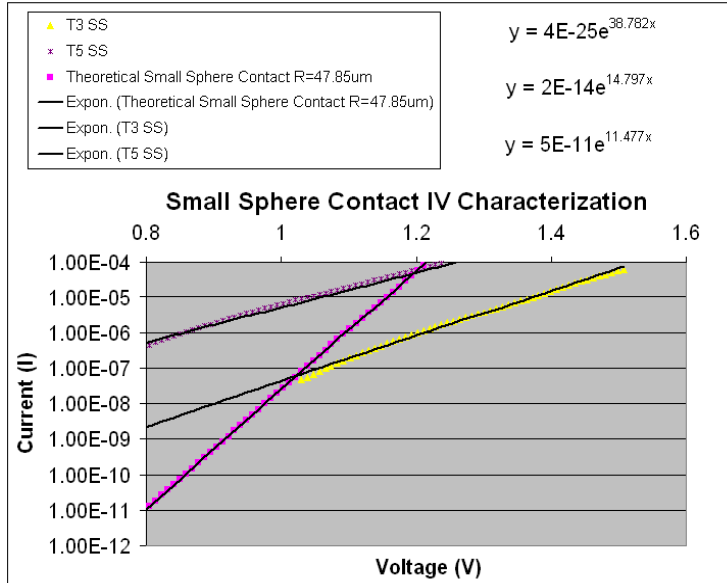
2. Small Sphere Contact (0.82mm dia.)

From the linear slopes of the IV curves the on resistance for the small sphere contact Schottky diodes could be determined. The resistance determined from IV measurements put into equation 4.3 for test diode samples T5 and T3 are shown respectively.



$$R_s^{T5} = \frac{V_2 - V_1}{I_2 - I_1} = \frac{3.982 \text{ V} - 2.488 \text{ V}}{0.027 \text{ A} - 0.009 \text{ A}} = 85 \Omega$$

$$R_s^{T3} = \frac{V_2 - V_1}{I_2 - I_1} = \frac{3.982 \text{ V} - 2.515 \text{ V}}{0.007 \text{ A} - 0.002 \text{ A}} = 293.4 \Omega$$



SS Natural Log

$$T3\# \ln(y) = 14.797 \cdot x - 31.543$$

$$T5\# \ln(y) = 11.477 \cdot x - 23.7189$$

The exponential curve fits plotted in log scale allow for a slope and intercept point for the diode current to be determined. These values are put into equations 4.4 and 4.5 to determine the Schottky barrier height and the ideality factor for the two contacts show below for contact terminals T3 and T5 of the small sphere mechanical Schottky contact.

$$\phi_b^{T3} = (\ln(7.2 \times 10^{-5} \cdot 146 \cdot 300^2) + 31.543) \times \frac{kT}{q} = 0.9927 eV$$

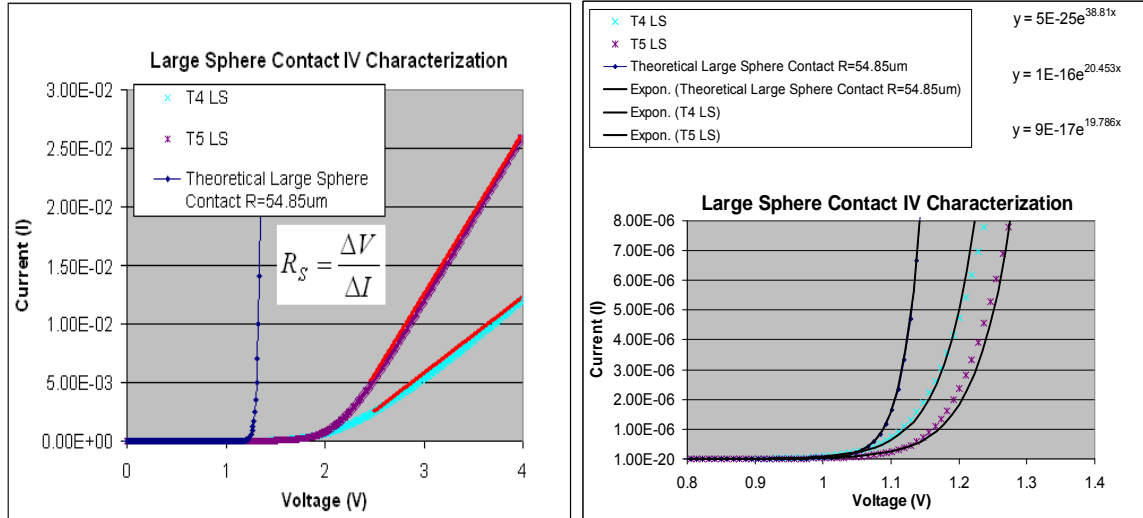
$$n^{T3} = \frac{q}{kT} \times \frac{1}{14.797} = 2.613$$

$$\phi_b^{T5} = (\ln(7.2 \times 10^{-5} \cdot 146 \cdot 300^2) + 23.7189) \times \frac{kT}{q} = 0.7904 eV$$

$$n^{T5} = \frac{q}{kT} \times \frac{1}{11.477} = 3.36$$

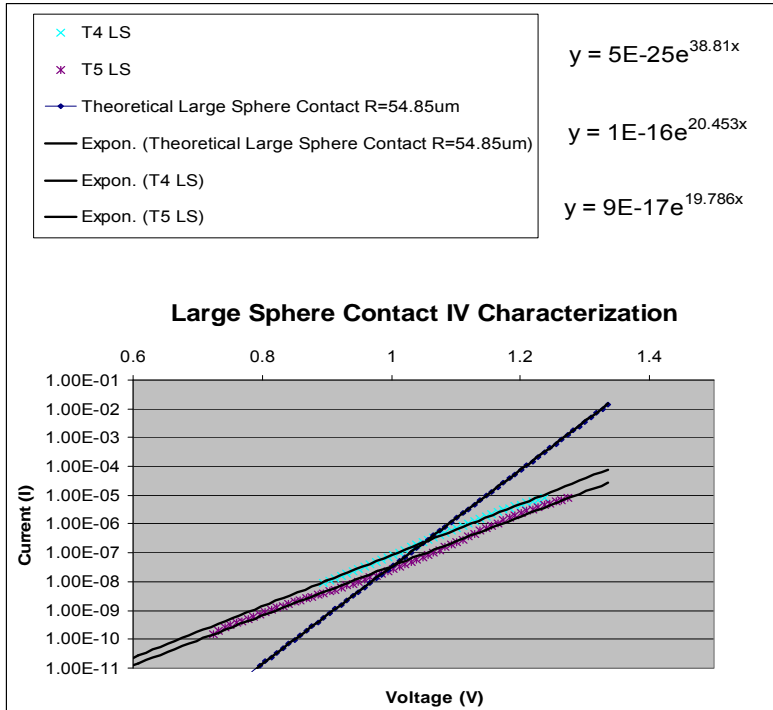
3. Large Sphere Contact (1.71mm dia.)

The resistance is determined from IV measurements substituted into equation 4.3 for test diode samples T5 and T4 are shown below respectively for the large sphere.



$$R_s^{T5} = \frac{V_2 - V_1}{I_2 - I_1} = \frac{3.982 \text{ V} - 2.506 \text{ V}}{0.02589 \text{ A} - 0.00532 \text{ A}} = 71.75 \Omega$$

$$R_s^{T4} = \frac{V_2 - V_1}{I_2 - I_1} = \frac{3.982 \text{ V} - 2.506 \text{ V}}{0.0119 \text{ A} - 0.00254 \text{ A}} = 157.69 \Omega$$



LS Natural Log

$$T4\# \ln(y) = 20.453 \cdot x - 36.841$$

$$T5\# \ln(y) = 19.786 \cdot x - 36.946$$

The exponential curve fits plotted in log scale allow for a slope and intercept point for the diode current to be determined. These values are put into equations 4.4 and 4.5 to determine the Schottky barrier height and the ideality factor for the two contacts show below for contact terminals T4 and T5 of the large sphere mechanical Schottky contact

$$\phi_b^{T4} = \left(\ln(9.4 \times 10^{-5} \cdot 146 \cdot 300^2) + 36.841 \right) \times \frac{kT}{q} = 1.1365 eV$$

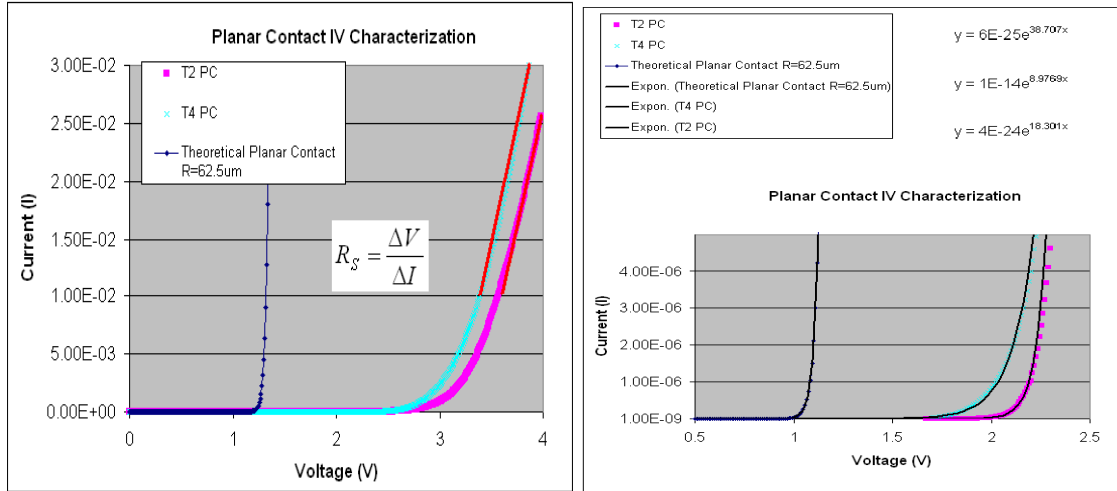
$$n^{T4} = \frac{q}{kT} \times \frac{1}{20.453} = 1.891$$

$$\phi_b^{T5} = \left(\ln(9.4 \times 10^{-5} \cdot 146 \cdot 300^2) + 36.946 \right) \times \frac{kT}{q} = 1.1393 eV$$

$$n^{T5} = \frac{q}{kT} \times \frac{1}{19.786} = 1.954$$

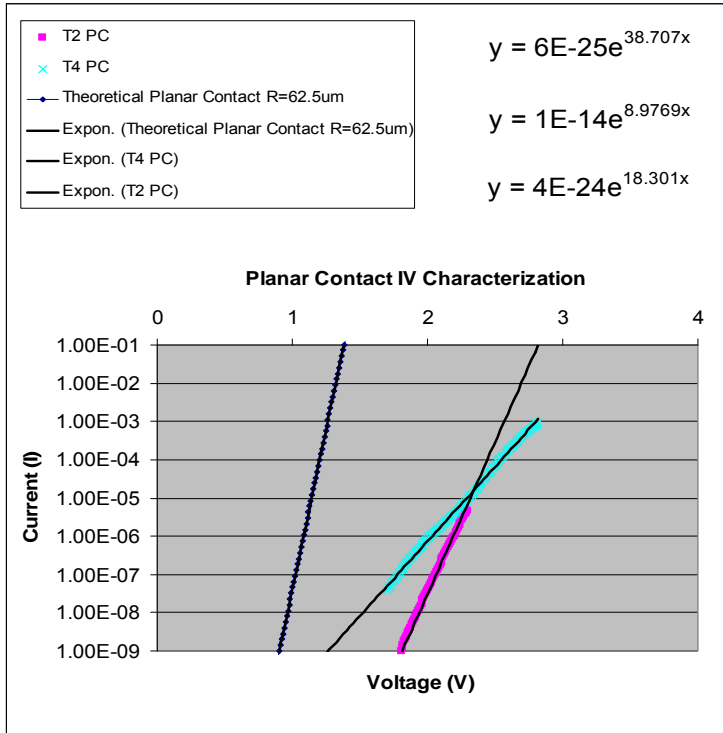
4. Planar Contact (0.125mm dia.)

The resistance is determined from IV measurements substituted into equation 4.3 for test diode samples T4 and T2 are shown below respectively for the planar contact.



$$R_s^{T2} = \frac{V_2 - V_1}{I_2 - I_1} = \frac{3.982 \text{ V} - 3.388 \text{ V}}{0.02563 \text{ A} - 0.00548 \text{ A}} = 29.47 \Omega$$

$$R_s^{T4} = \frac{V_2 - V_1}{I_2 - I_1} = \frac{3.865 \text{ V} - 3.199 \text{ V}}{0.02995 \text{ A} - 0.00539 \text{ A}} = 27.11 \Omega$$



The exponential curve fits plotted in log scale allow for a slope and intercept point for the diode current to be determined. These values are put into equations 4.4 and 4.5 to determine the Schottky barrier height and the ideality factor for the two contacts show below for contact terminals T4 and T2 of the planar Schottky contact.

$$\phi_b^{T4} = (\ln(1.4 \times 10^{-4} \cdot 146 \cdot 300^2) + 32.236) \times \frac{kT}{q} = 1.027 eV$$

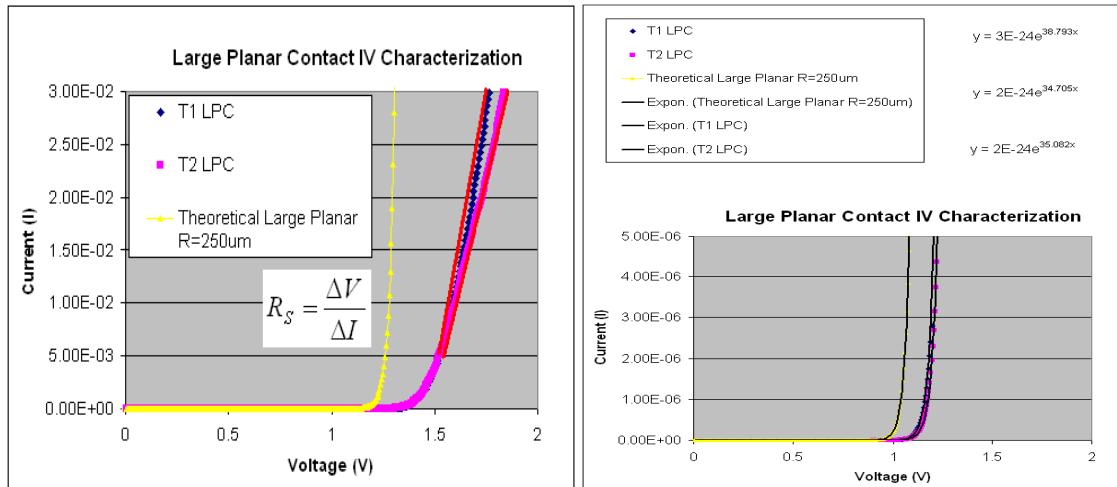
$$n^{T4} = \frac{q}{kT} \times \frac{1}{8.9769} = 4.31$$

$$\phi_b^{T2} = (\ln(1.4 \times 10^{-4} \cdot 146 \cdot 300^2) + 53.875) \times \frac{kT}{q} = 1.587 eV$$

$$n^{T2} = \frac{q}{kT} \times \frac{1}{18.301} = 2.113$$

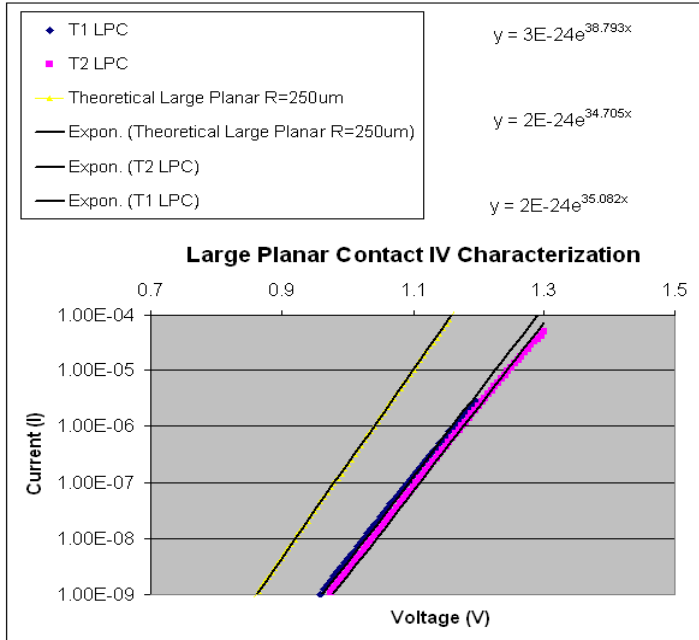
5. Large Planar Contact (0.5mm dia.)

The resistance is determined from IV measurements substituted into equation 4.3 for test diode samples T1 and T2 are shown below respectively for the large planar contact.



$$R_s^{T1} = \frac{V_2 - V_1}{I_2 - I_1} = \frac{1.765 \text{ V} - 1.53 \text{ V}}{0.0299 \text{ A} - 0.00539 \text{ A}} = 9.587 \ \Omega$$

$$R_s^{T2} = \frac{V_2 - V_1}{I_2 - I_1} = \frac{1.835 \text{ V} - 1.53 \text{ V}}{0.0298 \text{ A} - 0.00539 \text{ A}} = 12.494 \ \Omega$$



LPC Natural Log

T1# $\ln(y)=35.082 \cdot x - 54.568$

T2# $\ln(y)=34.705 \cdot x - 54.568$

The exponential curve fits plotted in log scale allow for a slope and intercept point for the diode current to be determined. These values are put into equations 4.4 and 4.5 to determine the Schottky barrier height and the ideality factor for the two contacts show below for contact terminals T1 and T2 of the large planar Schottky contact.

$$\phi_b^{T1} = \left(\ln(6.2 \times 10^{-4} \cdot 146 \cdot 300^2) + 54.568 \right) \times \frac{kT}{q} = 1.617 eV$$

$$n^{T1} = \frac{q}{kT} \times \frac{1}{35.082} = 1.102$$

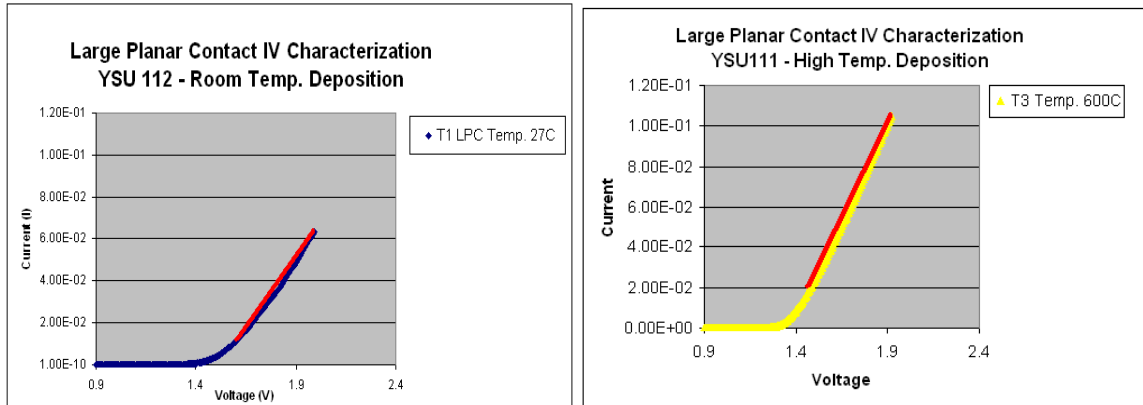
$$\phi_b^{T2} = \left(\ln(6.2 \times 10^{-4} \cdot 146 \cdot 300^2) + 54.568 \right) \times \frac{kT}{q} = 1.617 eV$$

$$n^{T2} = \frac{q}{kT} \times \frac{1}{34.705} = 1.114$$

APPENDED CHAPTER FIVE ANALYSIS

1. No Annealing

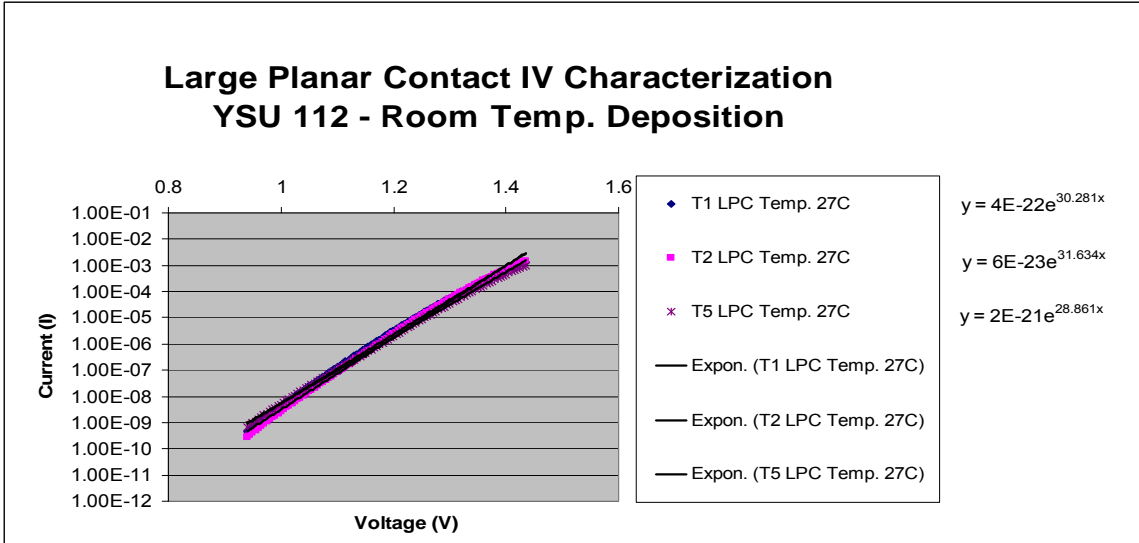
The resistance is determined from IV measurements substituted into the resistance equation for the test diodes. It is clear that the diodes sputter deposited at 600°C have a lower on resistance than room temperature deposited contacts with no post annealing.



$$R_{T1}^{27C} = \frac{V_2 - V_1}{I_2 - I_1} = \frac{1.76V - 1.53V}{0.0299A - 0.0053A} = 9.34 \Omega$$

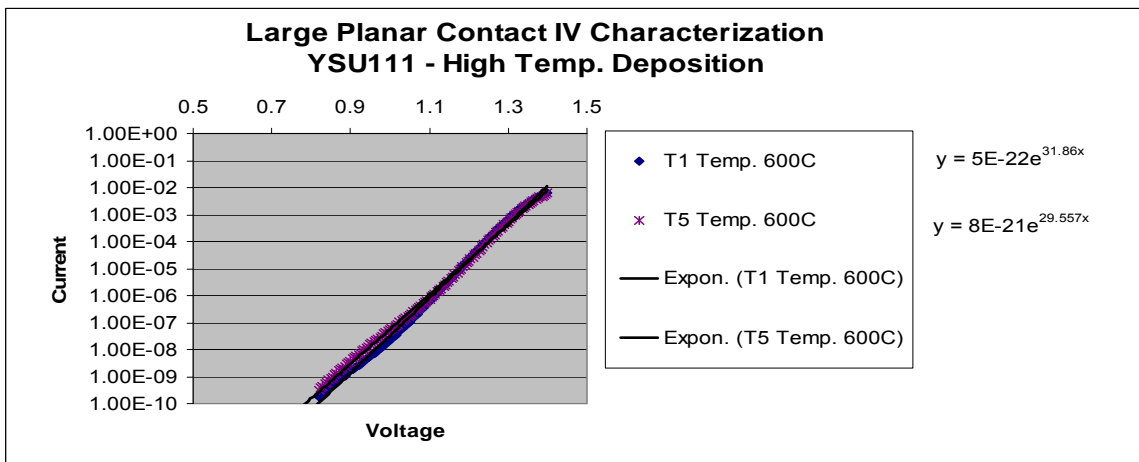
$$R_{T3}^{600C} = \frac{V_2 - V_1}{I_2 - I_1} = \frac{1.94V - 1.49V}{0.105A - 0.021A} = 5.35 \Omega$$

Log scale analysis used to determine the Schottky barrier height and ideality factor for the two different diode fabrication processes with no annealing. The maximum number of test samples without parasitic diodes were used for analysis.



Φ_{T1}	Φ_{T2}	Φ_{T5}
1.506eV	1.555eV	1.465eV

n_{T1}	n_{T2}	n_{T5}
1.27	1.22	1.34

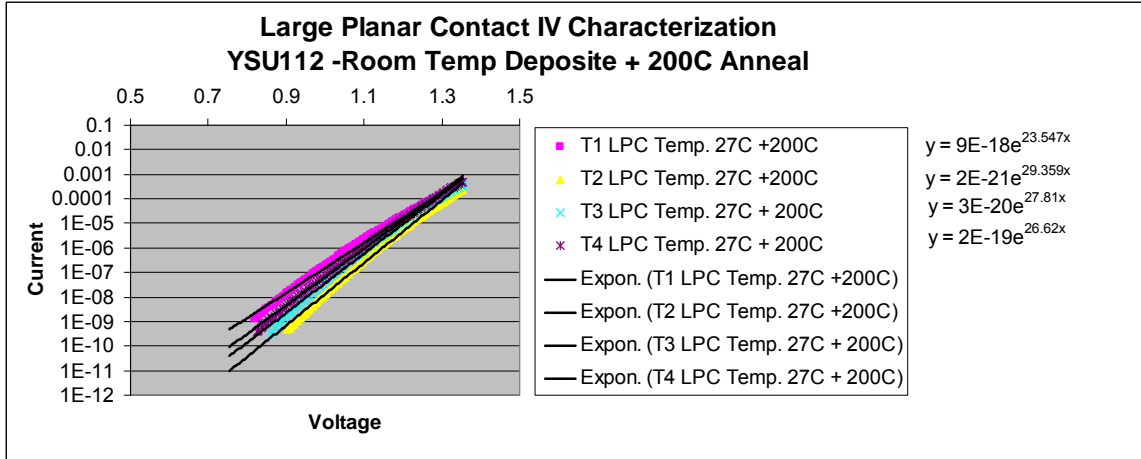


Φ_{T1}	Φ_{T5}
1.500eV	1.429eV

n_{T1}	n_{T5}
1.21	1.31

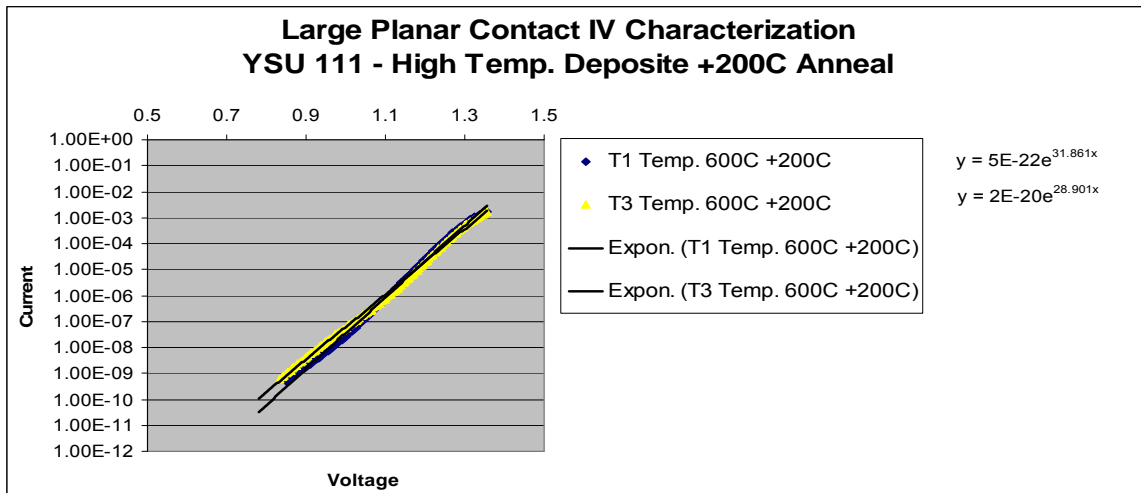
2. 200°C Anneal

Log scale analysis used to again for the two different diode fabrication processes after annealing the samples at 200°C.



Φ_{T1}	Φ_{T2}	Φ_{T3}	Φ_{T4}
1.247eV	1.465eV	1.395eV	1.346eV

n_{T1}	n_{T2}	n_{T3}	n_{T4}
1.64	1.32	1.39	1.45

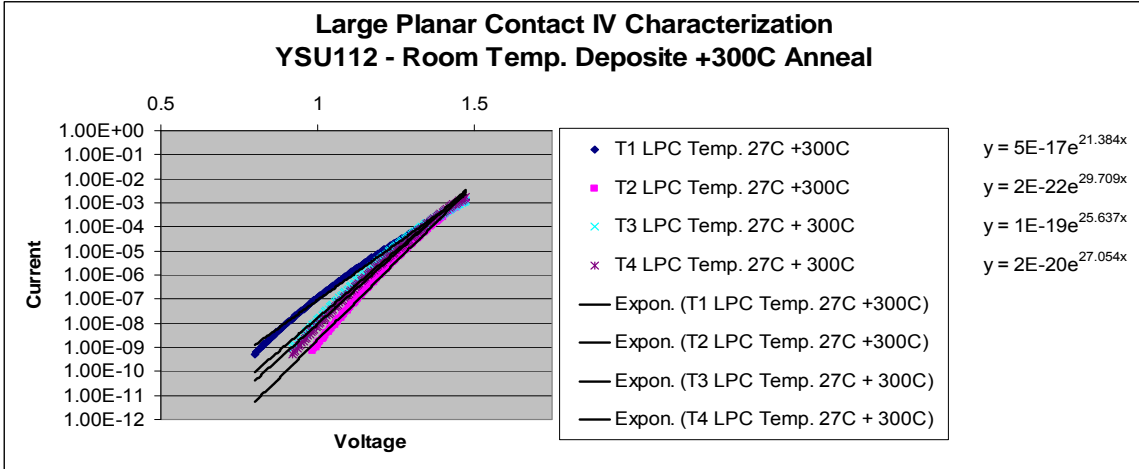


Φ_{T1}	Φ_{T3}
1.500eV	1.405eV

n_{T1}	n_{T3}
1.21	1.33

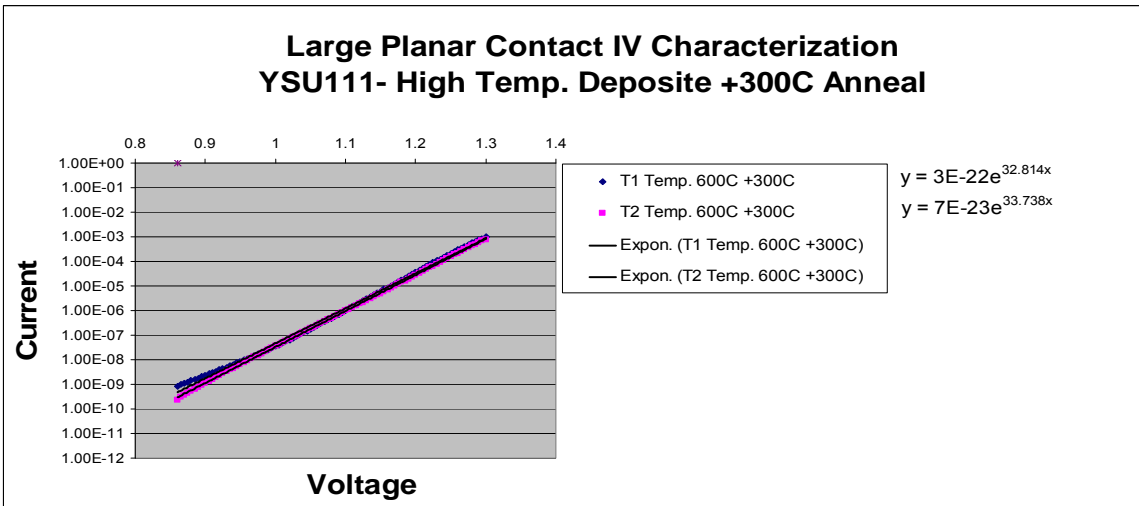
3. 300°C Anneal

Log scale analysis used to again for the two different diode fabrication processes after annealing the samples at 300°C.



Φ_{T1}	Φ_{T2}	Φ_{T3}	Φ_{T4}
1.203eV	1.524eV	1.363eV	1.405eV

n_{T1}	n_{T2}	n_{T3}	n_{T4}
1.81	1.3	1.51	1.42

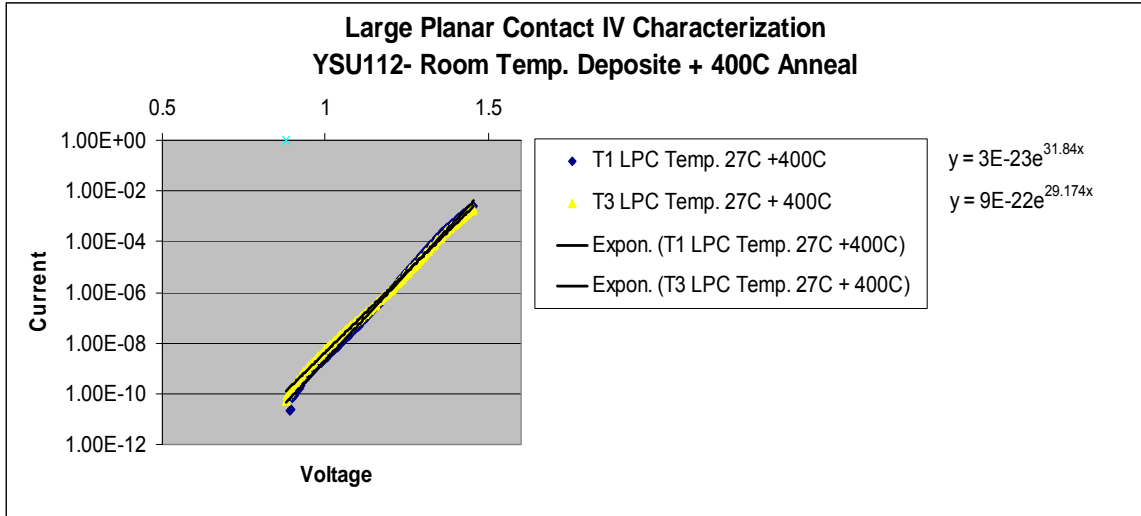


Φ_{T1}	Φ_{T2}
1.514eV	1.551

n_{T1}	n_{T2}
1.17	1.14

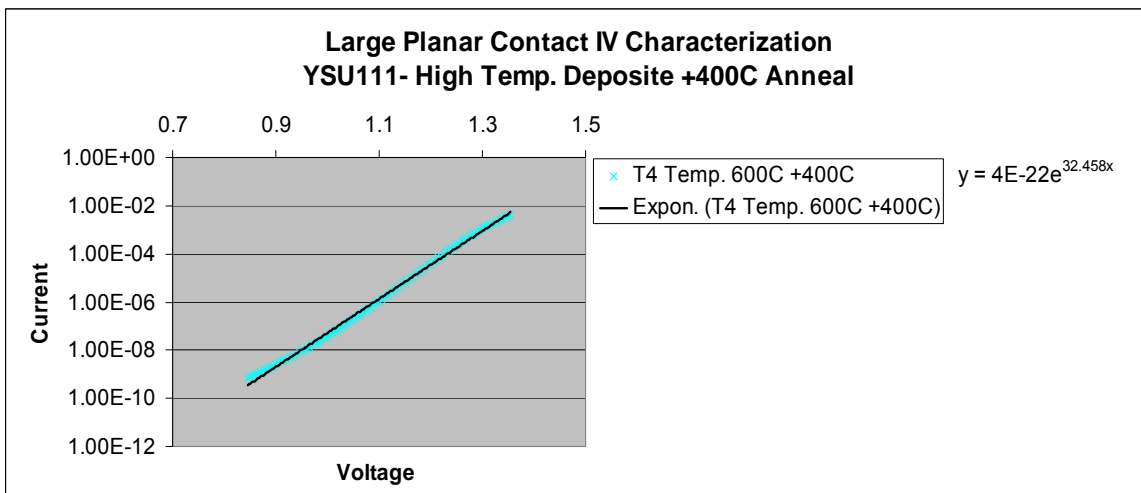
4. 400°C Anneal

Log scale analysis used to again for the two different diode fabrication processes after annealing the samples at 400°C.



Φ_{T1}	Φ_{T3}
1.573eV	1.485eV

n_{T1}	n_{T3}
1.21	1.32

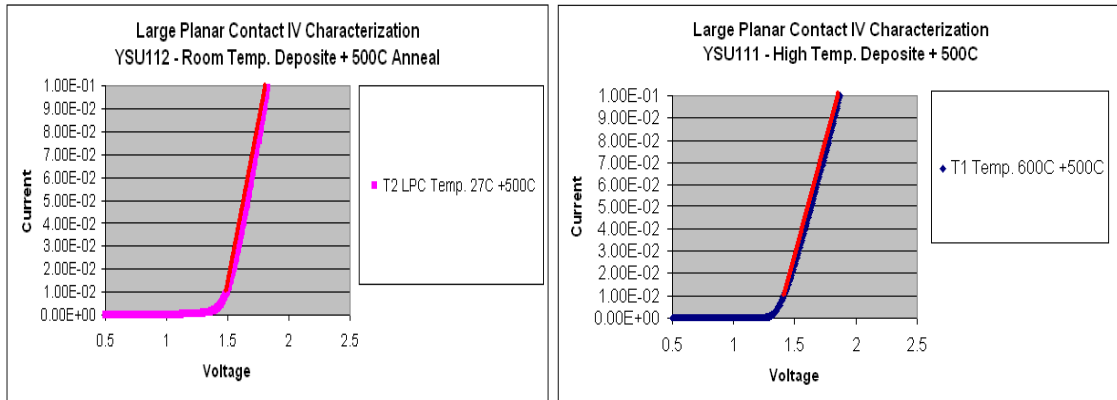


Φ_{T4}
1.506eV

n_{T4}
1.191

5. 500°C Anneal

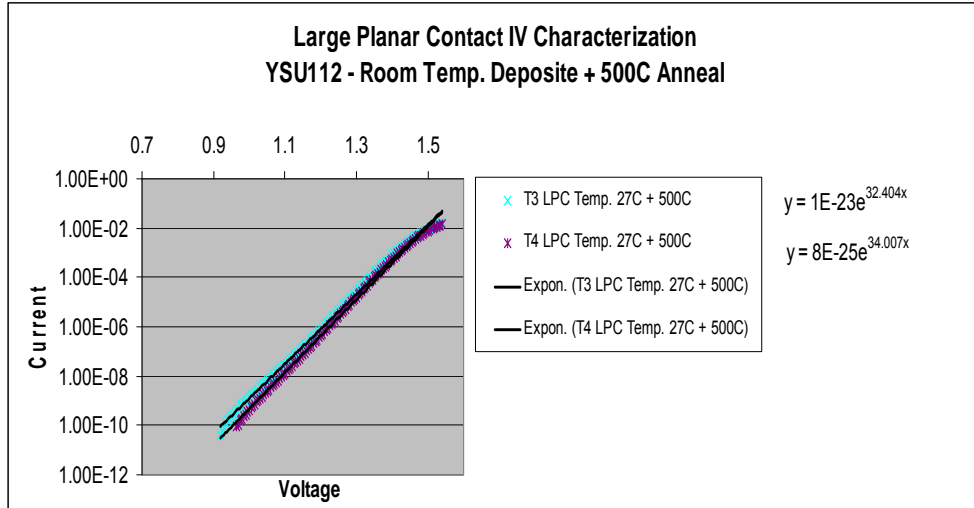
The resistance is determined from IV measurements substituted into the resistance equation for the test sample diodes. This temperature creates a very interesting phenomenon where by the room temperature deposited Schottky diode on resistance drops after an annealing treatment at 500°C for ten minutes. While the 600°C deposited Schottky contacts maintain a consistent on resistance throughout anneal treatments.



$$R_{T2}^{27C} = \frac{V_2 - V_1}{I_2 - I_1} = \frac{1.825 \text{ V} - 1.51 \text{ V}}{0.0989 \text{ A} - 0.0116 \text{ A}} = 3.60 \Omega$$

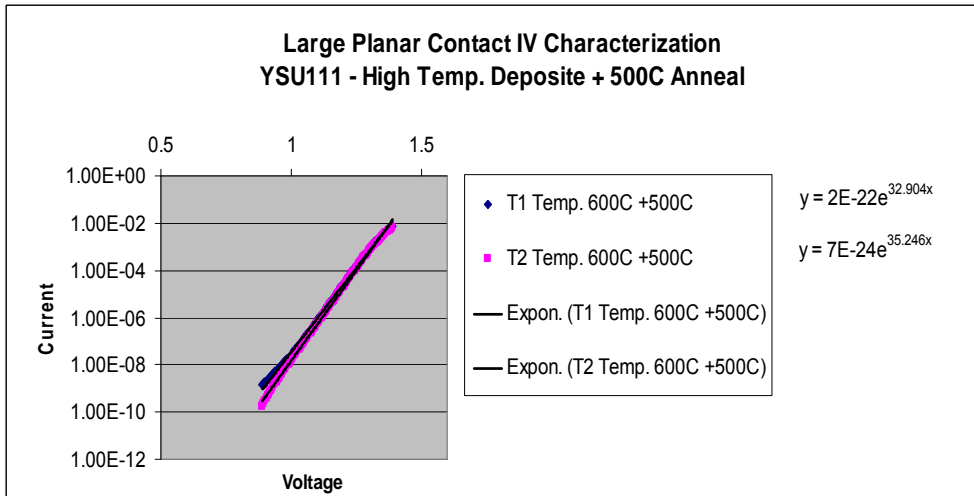
$$R_{T1}^{600C} = \frac{V_2 - V_1}{I_2 - I_1} = \frac{1.865 \text{ V} - 1.43 \text{ V}}{0.0999 \text{ A} - 0.0121 \text{ A}} = 4.95 \Omega$$

Log scale analysis used to determine the Schottky barrier height and ideality factor for the two different diode fabrication processes post at 500°C anneal. The maximum number of test samples without parasitic diodes has now become smaller, it can be seen that high temperatures cause formation of secondary SBH.



Φ_{T3}	Φ_{T4}
1.602eV	1.667

n_{T3}	n_{T4}
1.19	1.13

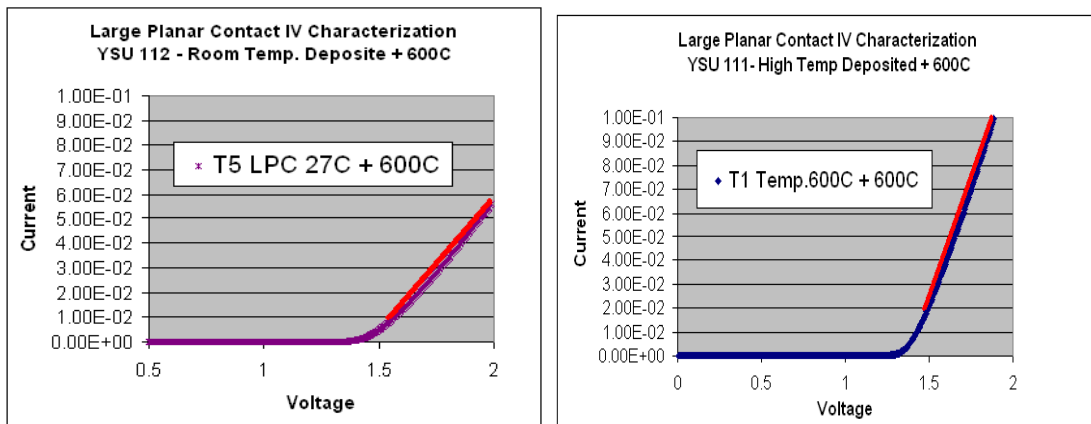


Φ_{T1}	Φ_{T2}
1.524eV	1.611

n_{T1}	n_{T2}
1.75	1.09

6. 600°C Anneal

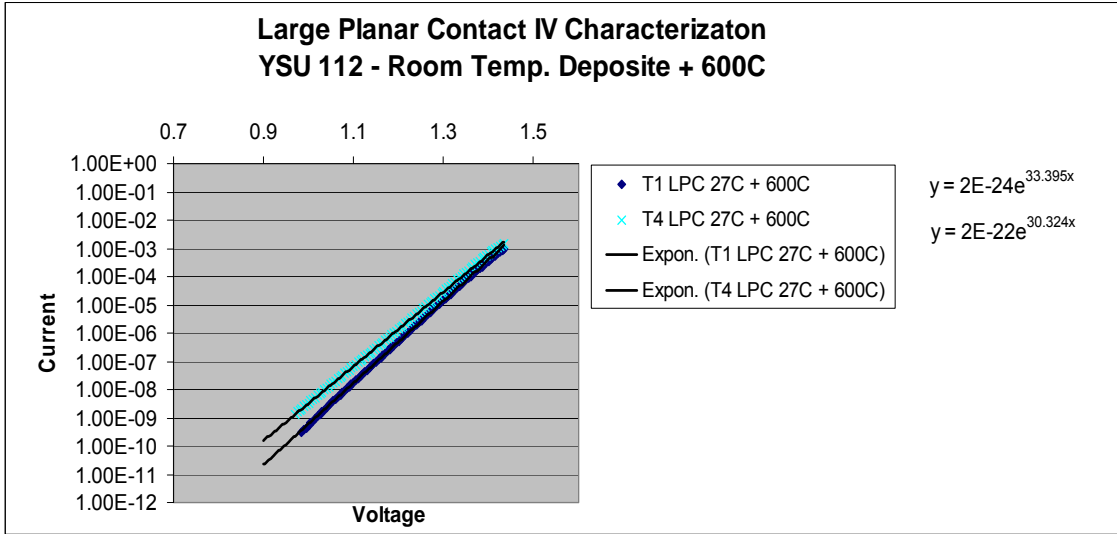
The resistance is determined from IV measurements substituted into the resistance equation for the test sample diodes. It was found that at temperature of 600°C the room temperature deposited Schottky diode on resistance (which was lowered in the previous 500°C anneal) has increased to near its original value of 9 ohms while noticeable discoloration of the contact occurred. However the 600°C deposited Schottky contacts again maintained a consistent on resistance throughout anneal treatments and no discoloration was observed for any diodes in this test set.



$$R_{T5}^{27C} = \frac{V_2 - V_1}{I_2 - I_1} = \frac{1.99 \text{ V} - 1.595 \text{ V}}{0.561 \text{ A} - 0.0125 \text{ A}} = 9.04 \Omega$$

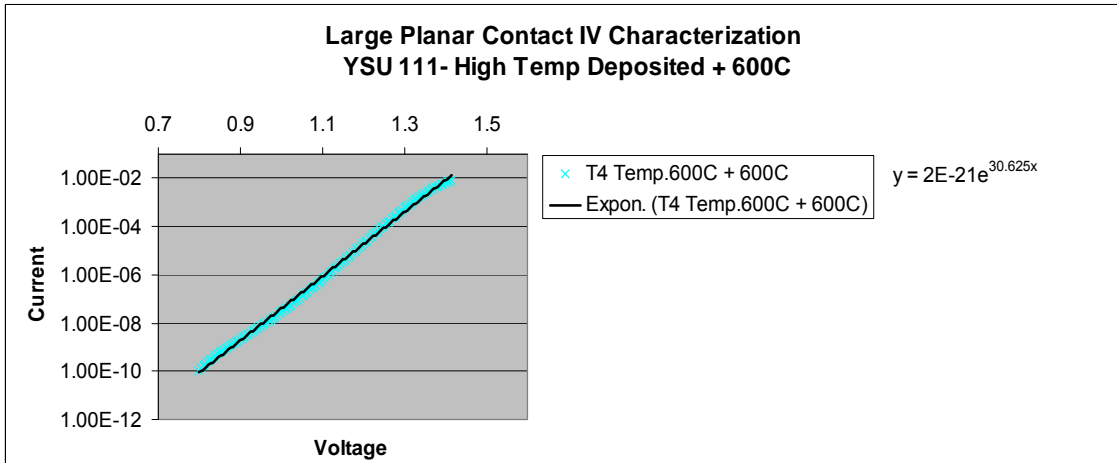
$$R_{T1}^{600C} = \frac{V_2 - V_1}{I_2 - I_1} = \frac{1.94 \text{ V} - 1.49 \text{ V}}{0.105 \text{ A} - 0.021 \text{ A}} = 4.85 \Omega$$

Log scale analysis used to determine the Schottky barrier height and ideality factor for the two different diode fabrication processes post at 600°C anneal. The maximum number of test samples without parasitic diodes is smaller, further illustrating that high temperatures cause formation of secondary SBH.



Φ_{T1}	Φ_{T4}
1.643eV	1.524eV

n_{T1}	n_{T4}
1.15	1.27



Φ_{T4}
1.465eV

n_{T4}
1.26